TABLE DES MATIÈRES

Page

LISTE DES TABLEAUX

Page

LISTE DES FIGURES

Page

LISTE DES ABRÉVIATIONS, SIGLES ET ACRONYMES

Co-Cr	Alliage métallique Cobalt-Chrome
AMF	Alliage à mémoire de forme
Ti-Ni	Alliage titane-nickel
SSD	Système de stabilisation dynamique
PEEK	Polyétheréthercétone
PET	Polythéréphtalate d'éthylène
FDA	Agence américaine des produits alimentaires et médicamenteux (Food and drug administration)

LISTE DES SYMBOLES ET UNITÉS DE MESURE

A_s, °C	Température de début de la transformation martensitique inverse sous contrainte nulle, degrés Celcius
A_f, °C	Température de fin de la transformation martensitique inverse sous contrainte nulle, degrés Celcius
M_s, °C	Température de début de la transformation martensitique directe sous contrainte nulle, degrés Celcius
M_f, °C	Température de fin de la transformation martensitique directe sous contrainte nulle, degrés Celcius
T_{def}, °C	Température de déformation, degrés Celcius

SOMMAIRE

Les opérations visant à stabiliser la colonne vertébrale emploient généralement des implants rigides et solides pour prévenir les bris de l'instrumentation et favoriser la fusion. La rigidité de ces implants engendre cependant des complications fréquentes aux segments adjacents puisque les opérations de révision peuvent concerner 25 % des patients (Gillet, 2003). De nombreux systèmes de stabilisation dynamique ont été proposés pour diminuer ce chiffre, mais leur efficacité n'a pas été prouvée.

Ce projet propose l'utilisation de tiges en alliage à mémoire de forme Ti-Ni aux propriétés mécaniques variables pour la stabilisation de la colonne vertébrale et couvre les aspects de la fabrication des tiges, de la simulation numérique des propriétés variables, ainsi que les résultats d'une étude biomécanique *in-vitro*.

L'introduction générale de ce document présente dans un premier temps la problématique ainsi que certains implants dynamiques disponibles dans le commerce. Par la suite, la solution proposée est décrite et les propriétés mécaniques des alliages à mémoire de forme sont abordées. Les objectifs de recherche, la méthodologie employée ainsi que l'organisation de la thèse sont enfin décrits. Les résultats de ces travaux ont été transcrits dans trois articles scientifiques. Dans le premier article, la technologie de fabrication de tiges aux propriétés variables a été développée. Ensuite, un modèle par élément fini a été construit et validé expérimentalement (article 2). Ce modèle permet de simuler le chauffage local du matériau et l'impact de ce chauffage sur les propriétés variables des tiges. Enfin, l'efficacité de ces tiges a été évaluée *in-vitro* sur spécimens porcins (article 3). Le profil de rigidité des tiges aux propriétés variables a été déterminé grâce aux simulations numériques présentées en annexe I (article 4). La méthodologie développée pour la réalisation de ces essais a été décrite en détail dans un article de conférence présenté en annexe II (article 5).

CHAPITRE 1

INTRODUCTION GÉNÉRALE

1.1 Problématique

Avec l'augmentation de l'espérance de vie, le nombre de problèmes reliés au dos tend à croitre de façon importante. Les pathologies fréquemment observées sont les scolioses, les problèmes lombaires ainsi que les fractures de la colonne vertébrale. Pour pallier à ces problèmes, certains patients doivent subir une intervention chirurgicale pour diverses raisons comme des blessures neurologiques, des instabilités mécaniques, une déformation de la colonne ou encore des douleurs subsistantes malgré un traitement approprié. Une technique courante permettant le traitement de ces symptômes est la fusion osseuse, ou arthrodèse, qui consiste en l'immobilisation d'un segment de colonne afin de faire fusionner plusieurs vertèbres ensemble. Au prix d'une légère perte de mobilité, le patient peut voir ses symptômes diminuer de façon significative. La fusion est provoquée par l'immobilisation du segment concerné à l'aide de vis pédiculaires et de tiges métalliques rigides faites de titane, d'acier inoxydable ou de Co-Cr comme illustré à la Figure 1.1.

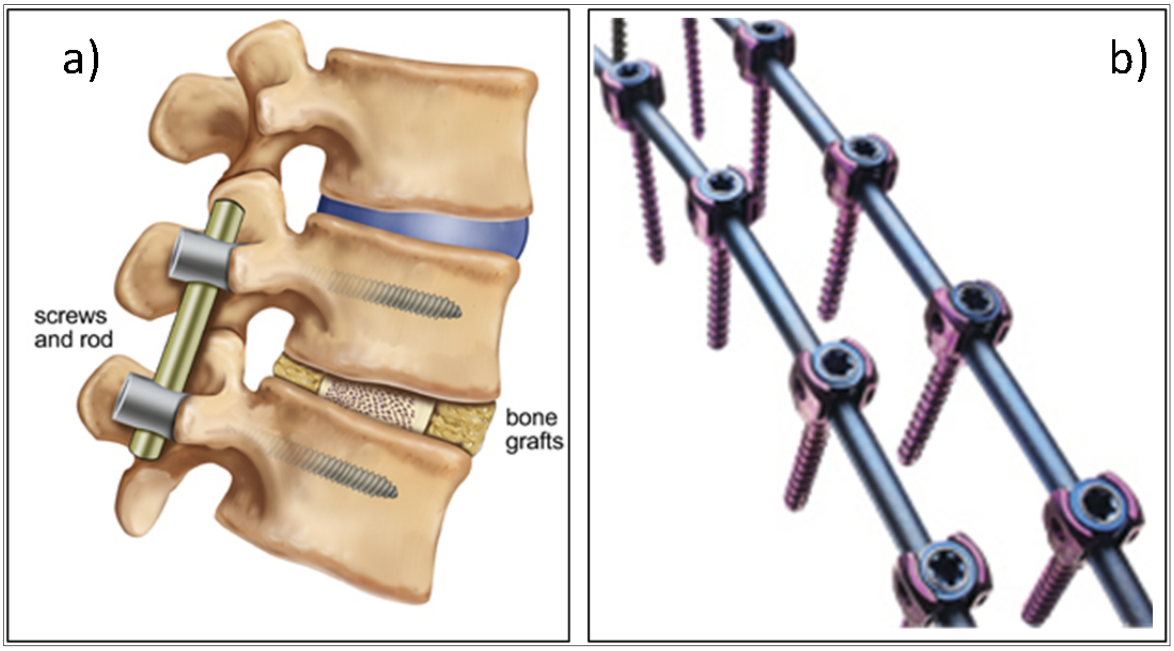

Figure 1.1 a) Segment de colonne instrumenté pour la fusion vertébrale et
b) vue sur le système de fixation
Tirée de a) Lyerlyneuro (2012) et b) Medtronic (2010)

Lors des traitements de fusion vertébrale, l'utilisation de tiges de fixation rigides entraine des taux de fusion importants, certaines techniques approchant les 100% de réussite. Cependant, une fusion réussie n'est pas systématiquement assimilée à un bon résultat clinique (Bono et Lee 2004; Gibson et Waddell, 2005).

Ce type d'instrumentation immobilise totalement le segment traité dans une position définie par le placement des vis et des tiges. La totalité des déplacements se retrouve alors sur le premier segment adjacent à l'instrumentation comme présenté à la Figure 1.2a) ce qui provoque une hypermobilité à ce niveau. Conséquence de ces déplacements, les contraintes sont concentrées à la limite de l'instrumentation, ce qui est à l'origine des dégénérescences et des problèmes rencontrés au niveau des segments adjacents (Cheh et al., 2007; Chou et al., 2002; Dekutoski et al., 1994; Panjabi, 2007). Lors d'une étude clinique sur 215 patients, (Ghiselli et al., 2004) ont observé des problèmes aux segments adjacents sur 27% des patients après 6 ans et 8 mois de suivi. La même tendance a également été observée par Gillet (2003).

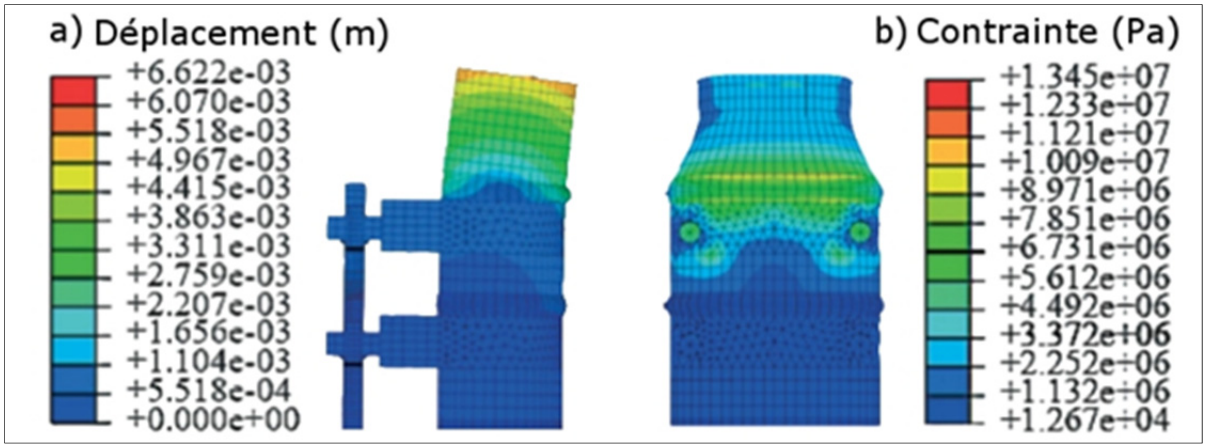

Figure 1.2 Analyse par élément finis d'un segment de colonne instrumenté à l'aide d'un système rigide a) déplacements et b) contraintes
Tirée de Castellvi et al., (2004)

Des systèmes moins rigides, appelés systèmes de stabilisation dynamique (SSD), ont été proposés afin de stabiliser la colonne vertébrale tout en permettant une mobilité controlée. L'avantage principal de tels systèmes est de diminuer les contraintes existantes entre le segment stabilisé et le segment non instrumenté tout en améliorant l'alignement de l'instrumentation avec les segments adjacents (Nockels, 2005). Castellvi et al., (2007) ont comparés numériquement les effets d'une instrumentation rigide et semi-rigide au niveau de la pression sur le disque adjacent à l'instrumentation lors d'une flexion à 45°. Le modèle, ainsi que les résultats, sont présentés à la Figure 1.3. Cette étude montre que la pression maximale subie par le disque est diminuée de 10 % avec l'utilisation d'une instrumentation semi-rigide. Également, les auteurs soulignent que la zone affectée par 80% ou plus de la contrainte maximale est diminuée de presque moitié avec l'utilisation d'un système de stabilisation dynamique.

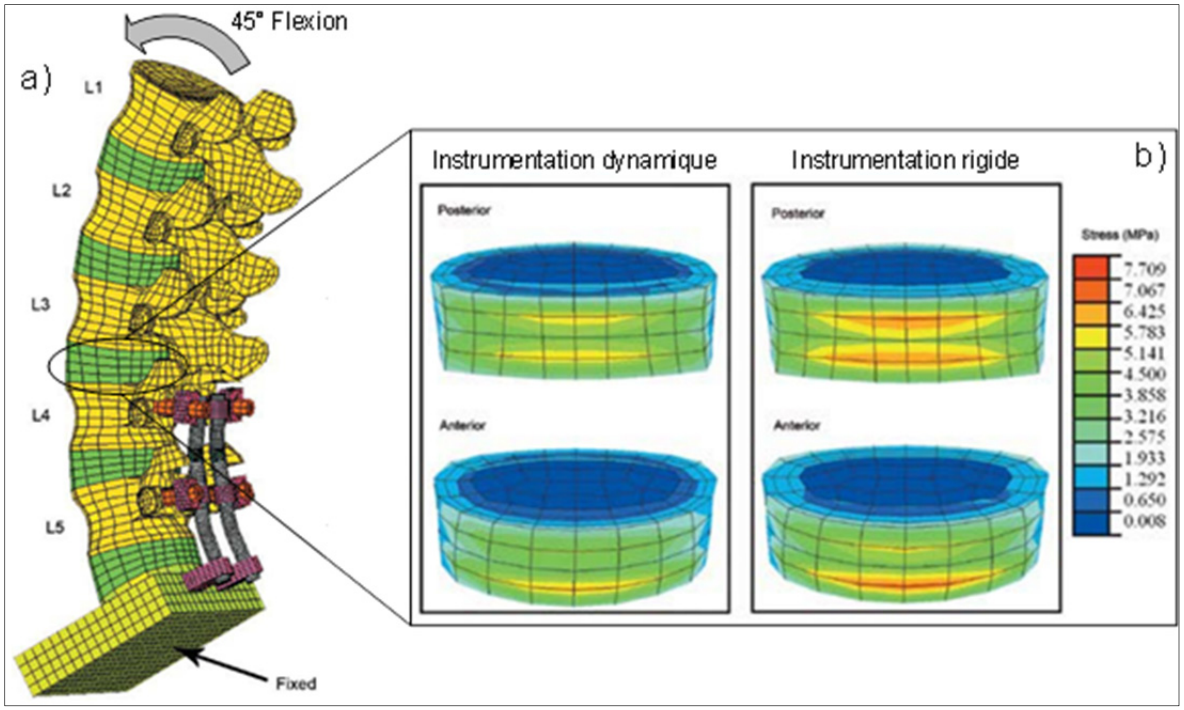

Figure 1.3 a) Vue isométrique du modèle et b) Répartition de la pression dans le disque L3-4 pour les deux types d'instrumentation
Tirée de Castellvi et al., (2007)

Malgré ces résultats numériques prometteurs, de nombreuses études cliniques n'ont pas réussi à démontrer la supériorité des systèmes de stabilisation dynamique (Kelly, Mok et Berven, 2010). La section suivante présente certains systèmes de stabilisation dynamique disponibles dans le commerce ainsi que les résultats d'études cliniques.

1.1.1 Instrumentations dynamiques existantes

Cette section présente certains systèmes de stabilisation dynamique existants sur le marché.

Systèmes polymères PEEK

Ces systèmes utilisent des tiges de polymère polyétheréthercétone (PEEK) à la place des métaux traditionnels. Ce matériau à un module d'élasticité de 3,6 GPa, ce qui en fait un

candidat de choix pour le développement d'instrumentations dynamiques. La tige associée à deux vis pédiculaires est présentée à la Figure 1.4.

Figure 1.4 Tige de PEEK associée à deux vis pédiculaires
Tirée de ORlive (2007)

Highsmith, Tumialan et Rodts (2007) ont présenté des résultats satisfaisants pour 3 patients. Dans une étude de plus grande envergure, Ormond, Albert et Das (2012) ont étudié les cas de 42 patients sur lesquels une fusion a été pratiquée au niveau lombaire à l'aide de tiges en PEEK. Ces auteurs ont conclu que ces tiges ne présentent pas d'avantages par rapport aux tiges métalliques classiques. Ces résultats confirment les observations *in-vitro* de Gornet et al., (2011b) qui n'ont pas perçu de différence entre les tiges polymères et les tiges métalliques en termes de mobilité lorsque des vis pédiculaires sont utilisées comme ancrages.

Dynesys Dynamic Stabilization System

Une autre solution proposée par la société Zimmer est le système Dynesys présenté à la Figure 1.5. Le dispositif est composé d'une corde de PET (poly(téréphtalate d'éthylène))

passant à travers un manchon de polyuréthane et fixée à deux vis pédiculaires. Mis en place avec une certaine précontrainte, le système permet des mouvements en flexion, compression ou extension. Une étude clinique menée sur 54 patients montre que l'utilisation de ce système entrainait un fort taux d'échec, notamment, des bris de l'instrumentation, fracture du pédicule ou, encore, de l'instabilité des segments adjacents (Bothmann et al., 2008). Une autre étude a également montré que ce système donnait des résultats controversés, considérant que 47% des patients raportaient des douleurs après 12 mois (Wurgler-Hauri et al., 2008). Il a également été montré qu'après 4 ans, près de la moitié des patients pouvaient montrer des signes de problèmes aux segments adjacents (Schaeren, Broger et Jeanneret, 2008).

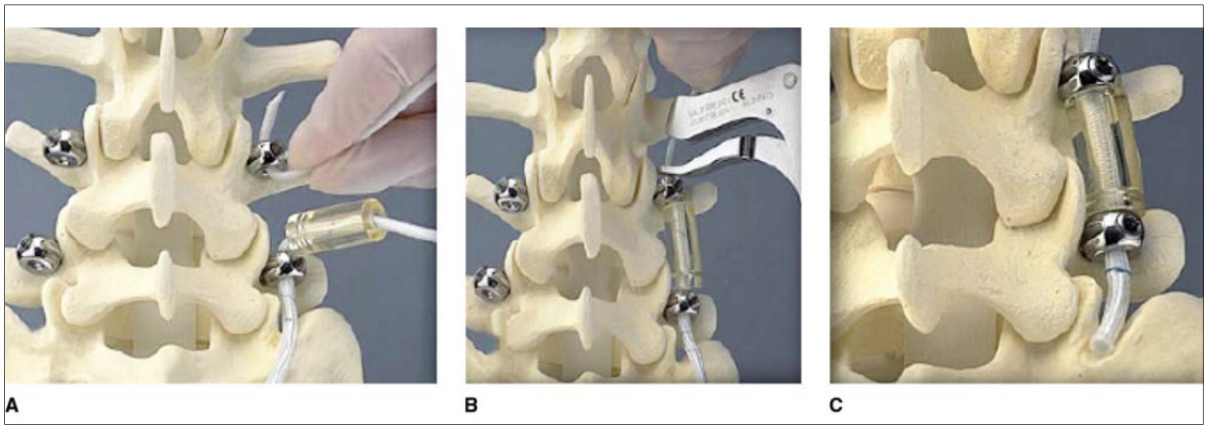

Figure 1.5 Instrumentation Dynesys a) un cordon est inséré à travers les têtes de vis ainsi qu'à travers le manchon b) une tension est appliquée au cordon c) instrumentation en place
Tirée de Lee, Lindsey et Bransford (2010)

Isobar TTL

Le système Isobar TTL de la société Scient'X est conçu pour être utilisé comme système dynamique pour la fusion ou alors comme système de stabilisation avec préservation de mouvement. Cette instrumentation est composée d'une tige de 5,5 mm de diamètre et d'un amortisseur mécanique. L'amortisseur autorise ±2,25° de déplacement angulaire et ±0,4 mm de translation axiale. Ce système autorise également les rotations axiales. L'instrumentation Isobar est présentée à la Figure 1.6.

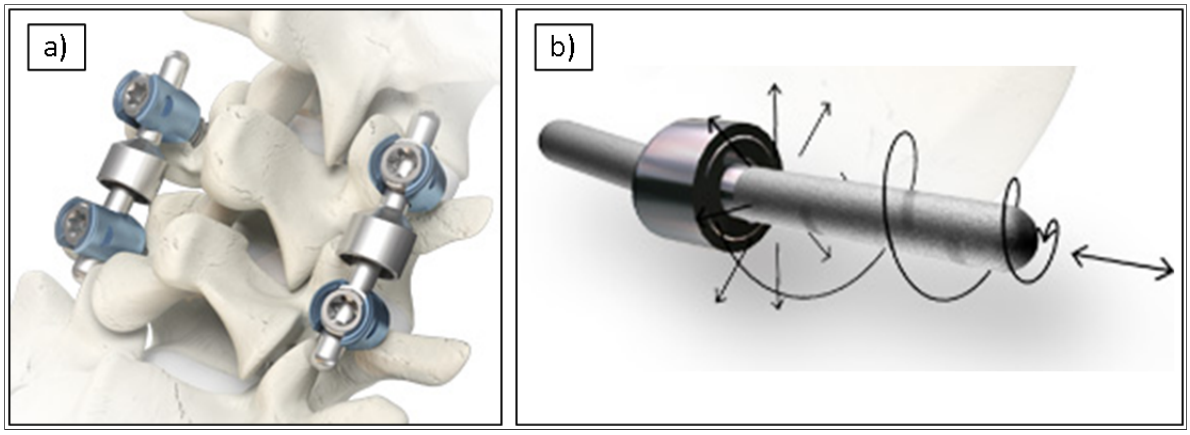

Figure 1.6 a) Système Isobar TTL en place et b) flèches indiquant les mouvements autorisés par l'instrumentation
Tirée de Scientx (2015)

Dans une première étude clinique menée par Li et al., (2013), ce système a été utilisé pour la stabilisation d'un segment avec préservation de mouvement. Les auteurs décrivent des résultats à court terme satisfaisants, mais des problèmes de dégénérescence des segments adjacents sont apparus après 24 mois chez 39 % des patients. Également, un desserrage des vis pédiculaires a été observé sur 11 % des sujets. Les auteurs ont conclu que la supériorité du système comparé à la fusion n'était pas prouvée.

Certains SSD peuvent également être implantés au sein d'instrumentations hybrides. Ce type d'instrumentation est décrit dans la section suivante.

1.1.2 Instrumentations hybrides

Un nouveau type d'instrumentation, les instrumentations hybrides, consistant en la combinaison d'une instrumentation rigide et d'une instrumentation dynamique est en développement. Il s'agit d'une utilisation dite « off label » des implants dynamiques puisque la FDA (Food and Drug Administration) approuve les SSD pour la fusion uniquement. Cependant, des études cliniques sont en cours. Dans le cas du système Dynesis de Zimmer, l'instrumentation dynamique est associée à une tige rigide via une vis de transition. Le système est illustré à la Figure 1.7. La zone rigide procure la stabilité nécessaire pour la

fusion tandis que le système dynamique fait la transition entre la zone de fusion et le segment intact.

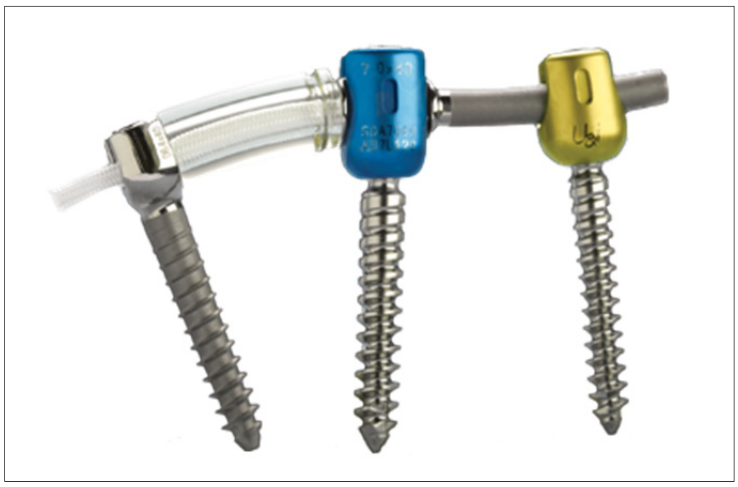

Figure 1.7 Système de stabilisation Dynesys-to-Optima
Tirée de Zimmer (2014)

Des résultats cliniques encourageants ont été décrits par Maserati et al., (2010) après un suivi allant de 1 à 22 mois. Dans une étude similaire, Schwarzenbach, Rohrbach et Berlemann, (2010) ont obtenu des résultats satisfaisants. Les auteurs mettent en évidence le fait que l'instrumentation hybride aide à préserver l'alignement du segment instrumenté, ce qui soulage le segment adjacent. Ces résultats sont cependant à prendre avec précaution puisque, comme le soulignent les auteurs, les suivis sont encore très cours. Également, parmi les complications observées, le desserrage des vis semble être le plus fréquent (Chiu et al., 2011; Ko et al., 2010; Wu et al., 2011).

Dans une autre étude, Hudson et al., (2011) ont implanté une instrumentation hybride utilisant le système Isobar sur 28 patients. Un ou deux niveaux vertébraux ont été fusionnés et le niveau adjacent à la fusion a été stabilisé à l'aide du système Isobar TTL. Bien que le suivi disponible ne soit que de deux ans, les auteurs sont pour l'instant satisfaits des résultats. La Figure 1.8 présente l'instrumentation hybride composée du système Isobar couplé à une tige rigide.

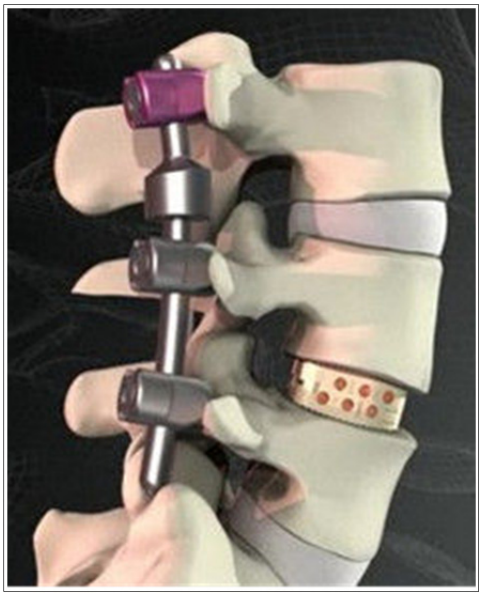

Figure 1.8 Vue sur le système ScientX Isobar utilisé comme instrumentation hybride
Tirée de Scientx (2010)

1.1.3 Influence des ancrages

Tous les systèmes de fixation décrits précédemment utilisent des vis pédiculaires comme liens entre la tige et la colonne vertébrale. Dans cette configuration, l'influence de la rigidité du système de stabilisation semble être limitée. En particulier, il a été démontré que le remplacement d'une tige de titane (100 GPa) par une tige de PEEK (3,6 GPa) ne change pas le comportement d'une paire de vertèbres instrumentées (Gornet et al., 2011a).

En remplacement des vis pédiculaires, les crochets transverses semblent être un moyen d'attache plus permissif qui pourrait potentiellement amplifier l'impact de la rigidité du système de fixation sur la mobilité. Ce moyen d'ancrage est présenté à la Figure 1.9.

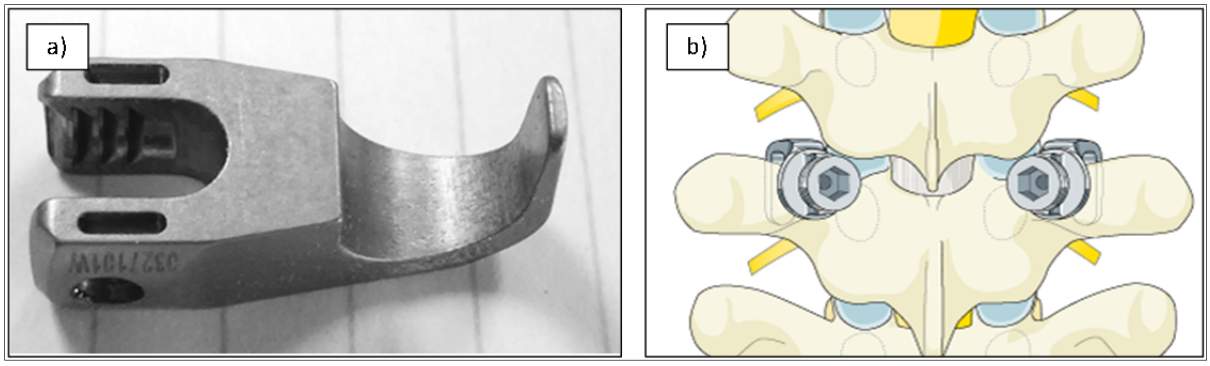

Figure 1.9 a) Photographie d'un crochet transverse et b) crochets en place sur une vertèbre
Tirée de AO Foundation (2015)

Certaines études cliniques ont déjà été faites au sujet de l'utilisation de crochets transverses aux extrémités de la fixation. Hassanzadeh et al., (2013) ont observé une diminution significative des problèmes aux segments adjacents avec l'utilisation de crochets transverses après un suivi de 2 ans. Pour expliquer ces résultats, les auteurs mettent en avant une chirurgie moins invasive et donc une préservation des ligaments ainsi que des contraintes moins importantes générées par le crochet sur le corps vertébral.

Dans le même ordre d'idées, Helgeson et al., (2010) ont précisé que l'utilisation de crochet à l'extrémité de longues instrumentations pourrait réduire la fréquence des problèmes aux segments adjacents.

Ces résultats confirment les observations faites *in-vitro* par Thawrani et al., (2014). Ces auteurs ont démontré que l'utilisation de crochets transverses pouvait créer une transition en termes de mobilité entre le segment immobilisé et le segment intact. Des résultats similaires ont été observés par Hongo et al., (2009). Un inconvénient de telles instrumentations est cependant le risque de fracture des processus transverses, qui se solde par une stabilisation inadéquate (Van Laar et al., 2007).

1.1.4 Résumé

Les systèmes de fixation traditionnels utilisant des tiges métalliques et des vis pédiculaires semblent problématiques puisque jusqu'à 30 % des patients opérés présentent des problèmes aux segments adjacents à moyen terme. Les systèmes de stabilisation dynamique ne semblent pas efficaces pour régler ces problèmes à cause de bris des implants, de desserrage des vis ou encore de problèmes persistants aux segments adjacents. Les systèmes de stabilisation hybrides semblent créer une transition efficace entre la zone de fusion et la zone intacte en termes de mobilité. Les systèmes utilisés pour la stabilisation dynamique de la zone de transition sont cependant mécaniquement complexes et présentent toujours un risque de bris ou de desserrage des vis. Enfin, l'utilisation de crochet à l'extrémité de la fixation semble être prometteuse pour favoriser un bon alignement, malgré les risques de fracture associés à ce type d'ancrage.

1.2 Solution proposée

Il apparait donc nécessaire de développer un nouveau système combinant les avantages des systèmes rigides (fusion osseuse adéquate, solidité du dispositif) avec les avantages des systèmes de stabilisation dynamique (bon alignement et mobilité, réduction des échecs de fixation), tout en gardant un système fiable, simple et peu encombrant.

Dans le cadre de ce projet, l'utilisation des alliages à mémoire de forme (AMF) est proposée pour le développement d'un nouveau type d'instrumentation monolithique à rigidité variable. La Figure 1.10 présente les profils de mobilité d'un segment de colonne instrumentée dans différents cas. Pour un segment de colonne intacte, la désorientation entre chaque paire de vertèbres lors d'un mouvement est relativement constante sur un cours segment. Dans le cas d'une instrumentation très rigide, la mobilité est théoriquement nulle dans la zone instrumentée. Cette immobilité est compensée par de grandes rotations au segment adjacent, ce qui provoque les problèmes décrits précédemment. Idéalement, la zone de fusion devrait être immobile et la transition devrait être progressive à l'extrémité de la fixation pour se rapprocher du comportement de la colonne intacte.

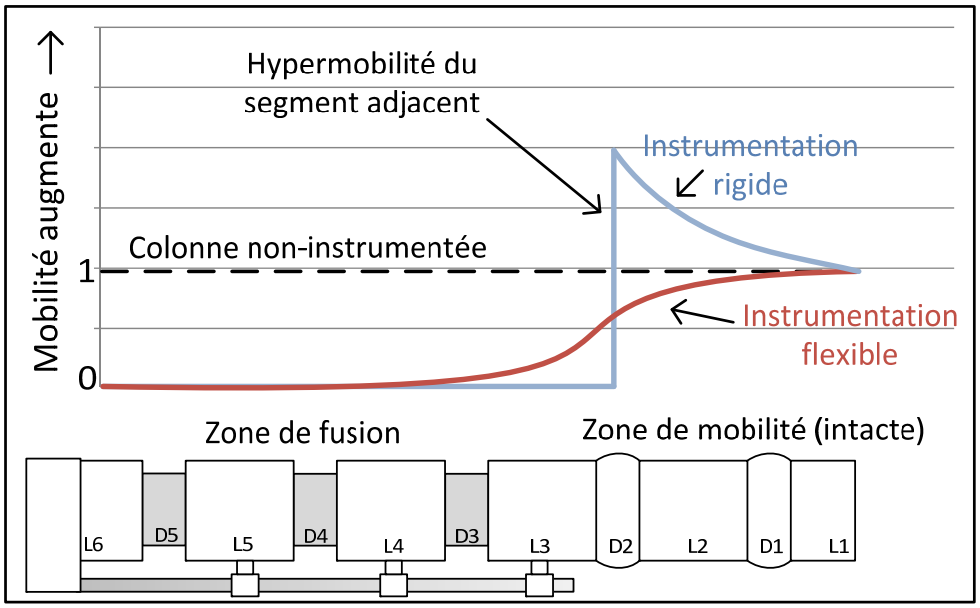

Figure 1.10 Profils de mobilité en fonction de l'instrumentation utilisée

Les tiges vertébrales devraient donc présenter une grande rigidité dans la zone de fusion tout en permettant un cintrage facile pour que le praticien adapte la tige à la courbure de la colonne. L'extrémité de la tige, quant à elle, devrait présenter une plus faible rigidité pour favoriser une transition progressive de mobilité vers le segment intact.

Un concept similaire a été étudié numériquement par Cahill et al., (2012). Il s'agit d'une instrumentation à section variable comme montrée à la Figure 1.11. L'idée est d'allonger l'implant d'un segment à l'aide d'une section plus faible ce qui revient à diminuer la rigidité en flexion de l'extrémité de la tige.

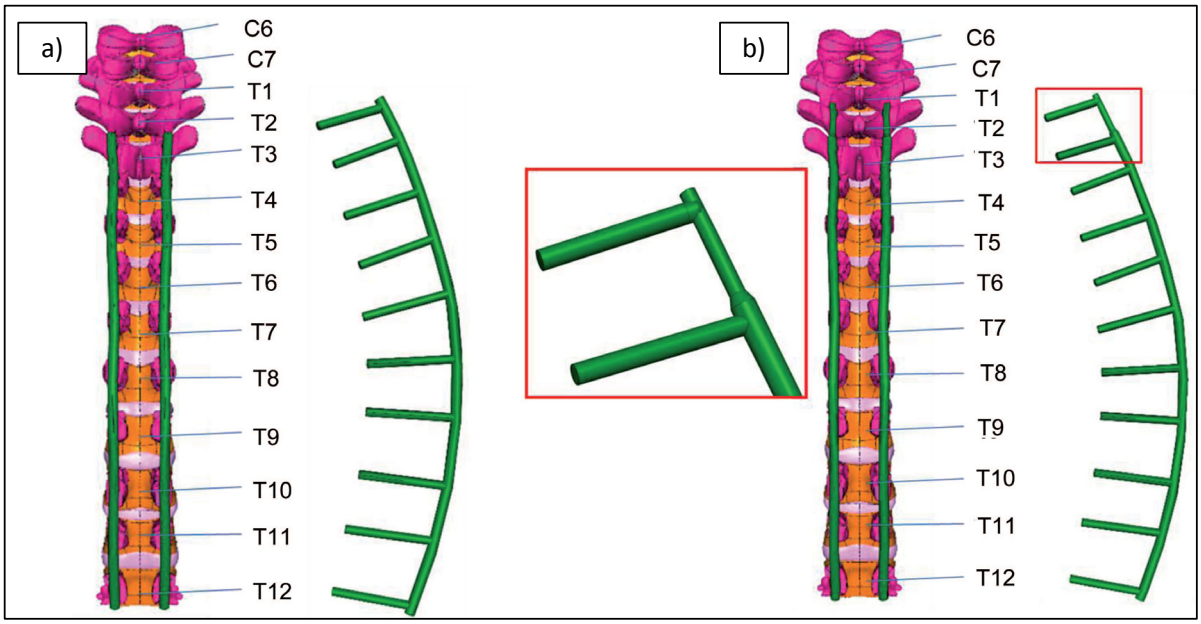

Figure 1.11 Modèle de la colonne avec a) implant classique et
b) implant étendu à section variable
Tirée de Cahill et al., (2012)

Les calculs effectués par les auteurs montrent que l'extension de la tige à l'aide d'une section plus faible permet de diminuer les pressions intradiscales au segment adjacent autant en déplacements qu'en force contrôlées. Également, lors de l'application d'un moment, les déplacements de ce même segment sont diminués d'environ 20 % par rapport à une instrumentation classique.

1.3 Alliage à mémoire de forme : Comportement mécanique et choix du matériau

Les alliages à mémoire de forme sont des matériaux présentant des propriétés mécaniques particulières telles que l'effet mémoire de forme et la superélasticité. Cette section présente les bases théoriques permettant la compréhension de ces différents comportements. Également, l'influence des traitements thermomécaniques sur les propriétés mécaniques est abordée.

Mécanismes de transformation et de déformation

Par définition, la transformation martensitique est dite displacive, ce qui signifie que lors du changement de phase, les mouvements des atomes sont très faibles, de l'ordre d'un dixième de distance interatomique. Le passage d'une phase à l'autre se fait alors par cisaillement du réseau cristallin sous l'influence de la température ou de la contrainte. Cette transformation est donc responsable d'une déformation homogène du réseau qui cependant ne se retrouve pas toujours à l'échelle macroscopique. En effet, lors de la transformation directe, de l'austénite vers la martensite, la déformation du réseau est compensée par la formation de macles, ce qui se traduit par une absence de déformation à l'échelle macroscopique. Ces macles vont en effet permettre à la nouvelle phase de s'accommoder de l'espace disponible pour créer des plaquettes de martensite orientées de façon totalement aléatoire. On parle alors de martensite autoaccommodante. Lors du retour en phase austénitique, sous chauffage, les macles disparaissent. La Figure 1.12 permet d'illustrer schématiquement les différentes transformations à l'échelle atomique.

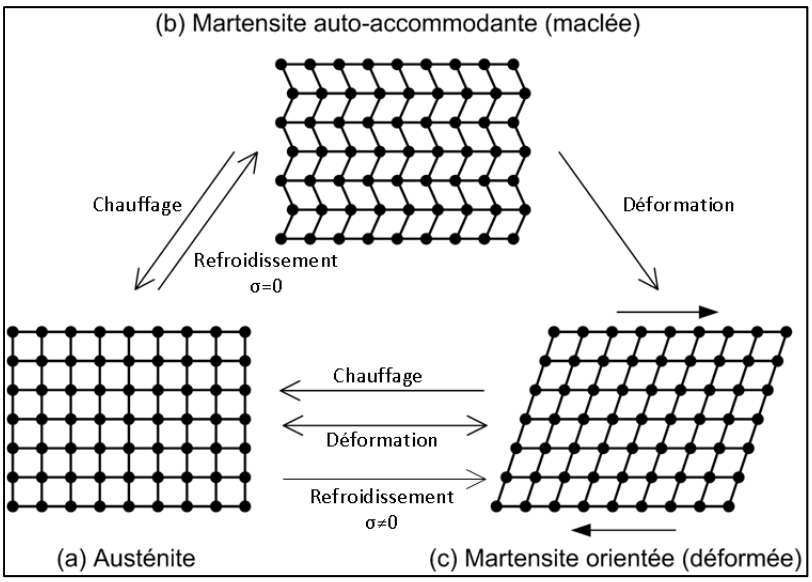

Figure 1.12 Représentation schématique de la transformation martensitique à l'échelle atomique
Adaptée de Brailovski et al., (2003)

Partant d'un état complètement austénitique (Figure 1.12, a), un refroidissement sous contrainte nulle engendre l'apparition de martensite autoaccommodante ou maclée, ce qui n'entraine pas de déformation à l'échelle macroscopique (Figure 1.12, a → b). Cette transformation est totalement réversible puisqu'un chauffage de la martensite maclée va entrainer l'apparition à nouveau de la phase austénitique (Figure 1.12, b → a). Partant de la martensite autoaccommodante, une déformation macroscopique de cette phase va se traduire par une orientation préférentielle des aiguilles de martensite selon la direction de la contrainte (Figure 1.12, b → c). Il est alors question de martensite orientée. Un refroidissement sous contrainte va également orienter la martensite dans une direction préférentielle (Figure 1.12, a → c). Un chauffage de cette martensite orientée à une température supérieure à A_f va entrainer un retour en phase austénitique provoquant le retour du matériau à sa forme initiale (Figure 1.12, c → a). Une déformation de l'austénite (Figure 1.12, a → c) entraînera quant à elle la formation de martensite orientée ce qui provoque l'effet superélastique.

Transformation martensitique

La transformation martensitique est à l'origine des comportements particuliers des AMF et consiste en un changement de phase accompagnant un changement de température ou de contrainte mécanique. Ce phénomène permet à un spécimen préalablement déformé de retrouver, sous chauffage, sa forme initiale. Par analogie aux aciers, la phase basse température est appelée « martensite » tandis que la phase haute température est appelée « austénite ». Grâce au caractère réversible de cette transformation, cette famille d'alliage présente des propriétés de mémoire de forme et de superélasticité. La Figure 1.13 présente le diagramme d'état contrainte-température d'un alliage à mémoire de forme Ti-Ni.

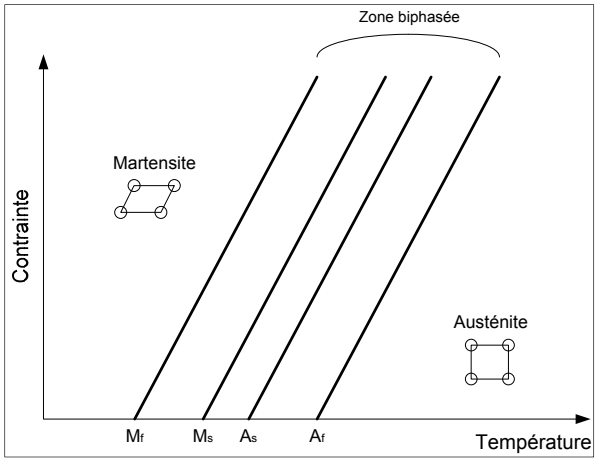

Figure 1.13 État de phase d'un matériau
présentant une transformation martensitique
Tirée de Brailovski et al., (2003)

Ce type de diagramme permet de prévoir l'état de phase du matériau en fonction de la température et de son état de contrainte. Il est alors constatable que pour des températures inférieures à M_f, le matériau sera dans un état martensitique quel que soit la contrainte appliquée. Pour des températures supérieures à A_f, le matériau est à l'état austénitique à contrainte nulle. Sous l'application d'une force, il apparaît qu'un changement de phase va intervenir, l'austénite se transformant en martensite. Cette transformation de phase sous charge est à l'origine de l'effet superélastique.

Effet superélastique

La Figure 1.14 propose une représentation détaillée de l'effet superélastique sur le diagramme d'état et sur un diagramme contrainte-déformation. Il apparaît alors sur le diagramme d'état qu'à partir de l'austénite (A), une contrainte appliquée engendre la transformation de l'austénite en martensite (A → C). Au relâchement de la contrainte, la martensite retourne spontanément à un état austénitique qui est l'état d'équilibre à cette température (C → A). Le même « trajet » est représenté sur le diagramme contrainte – déformation où apparaît le plateau de déformation (B → C) ainsi que le retour à l'état initial après chargement (C → A). Ce graphe montre également la présence d'un comportement

hystérétique ce qui implique une dissipation d'énergie entre le chargement et le déchargement mécanique.

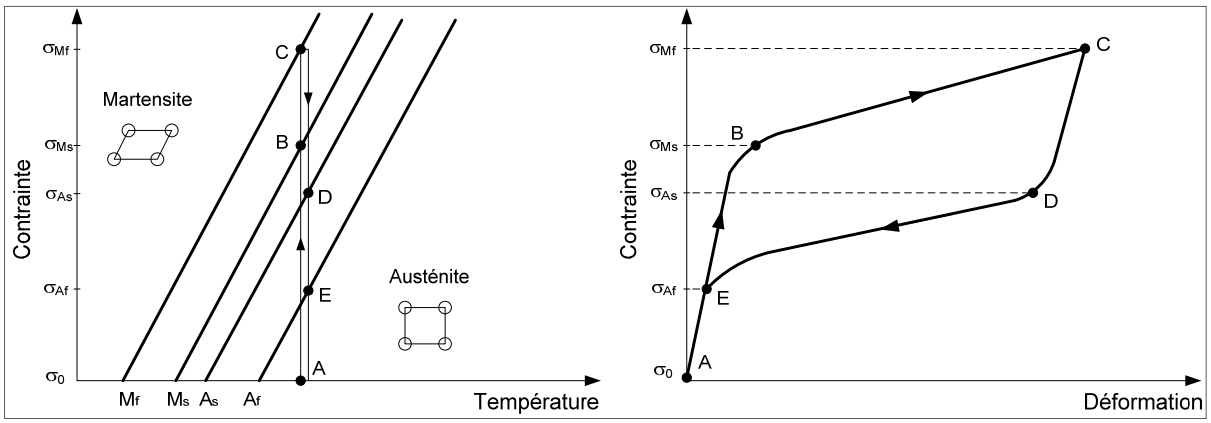

Figure 1.14 Chargement thermomécanique permettant d'obtenir l'effet superélastique
Adaptée de Brailovski et al., (2003)

L'observation de l'effet superélastique pour une application à une température donnée T implique donc d'ajuster les températures de transformation de l'alliage pour que A_f soit inférieure à T. Également, la Figure 1.15 présente l'influence de la température d'utilisation sur la réponse mécanique du matériau.

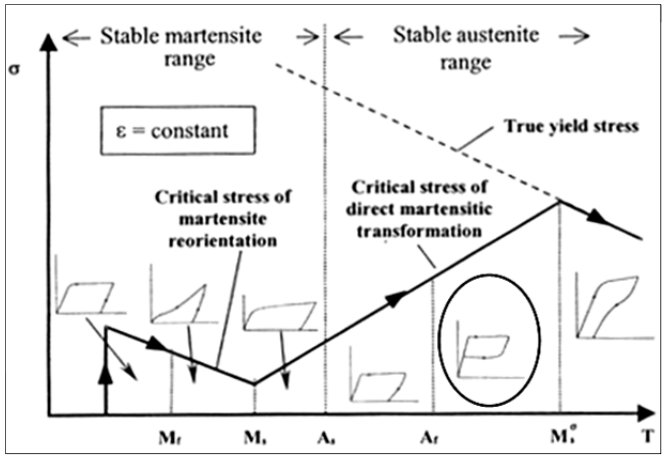

Figure 1.15 Diagramme d'état d'un alliage à
mémoire de forme Ti-Ni
Comportement superélastique encerclé
Tirée de Brailovski et al., (2003)

Pour des déformations effectuées à des températures où la martensite est stable, la réorientation de cette martensite est observée, ce qui se traduit par un changement de forme de l'échantillon et une absence d'effet superélastique. Si la température de déformation est élevée au-delà de A_f, l'alliage change de comportement et présente des propriétés superélastiques. Dans cette zone, la Figure 1.15 montre que plus la température de transformation est proche de la température d'utilisation, moins la force nécessaire pour déformer l'échantillon est grande. C'est cette propriété qui pourrait être utilisée pour la partie souple de la tige puisqu'elle permet d'obtenir de grandes déformations à partir de faibles forces.

Influence du taux d'écrouissage

Pour les alliages à mémoire de forme, un taux d'écrouissage élevé peut bloquer la transformation martensitique et donc supprimer l'effet superélastique. La Figure 1.16 décrit le comportement en traction de l'alliage Ti-50.8 at.% Ni pour deux niveaux de travail à froid et trois temps de traitement thermique.

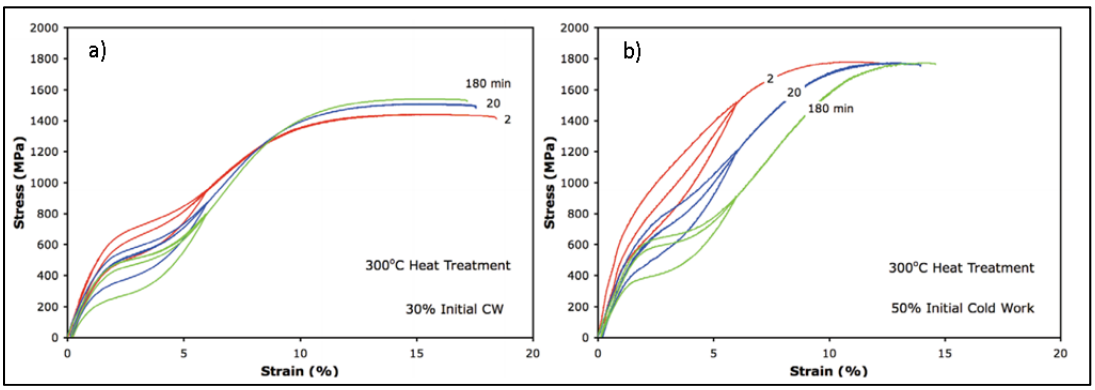

Figure 1.16 Essais de traction isotherme d'un alliage Ti-50.8 at.% Ni, déformation à 6%, relâchement et traction à la rupture
a) 30% de travail à froid initial et b) 50 % de travail à froid initial
Tirée de Drexel, Selvaduray et Peltan, (2008)

Ces résultats montrent que des taux d'écrouissages plus élevés ((b), 2min) permettent bien de bloquer la transformation martensitique alors que le recuit permet au contraire d'abaisser la

courbe de traction, de restaurer l'effet superélastique et, également, de réduire le module d'élasticité. Les courbes de tractions du matériau non traité thermiquement (absente sur la Figure 1.16) ne présentent pas de boucle caractéristique du comportement superélastique, ce qui signifie que le haut taux d'énergie stocké dans le matériau empêche la transformation martensitique d'intervenir (Drexel, Selvaduray et Peltan, 2008).

Traitements thermiques locaux

Les notions sur l'influence du taux d'écrouissage présentées précédemment concernent uniquement des pièces homogènes. Cependant, les traitements thermomécaniques locaux peuvent être utilisés pour fabriquer des pièces aux propriétés variables. Bellouard et al., (1999) ont utilisé les recuits locaux par effet Joule ou par laser pour la fabrication d'un dispositif mécanique monolithique en AMF. L'idée étant de prendre une pièce écrouie et de restaurer les propriétés de mémoire de forme dans une zone restreinte de cette pièce.

Mahmud, Yinong et Tae-hyun (2008) ont étudié l'effet d'un gradient de température sur les propriétés d'un alliage à mémoire de forme Ti-Ni. Il a été constaté qu'un gradient de propriétés mécaniques résultait du gradient de température.

Ces travaux laissent présager qu'il est possible de fabriquer des tiges aux propriétés mécaniques variables en utilisant les recuits locaux par effet Joule. Également, un gradient de propriété devrait apparaitre entre la zone chauffée et la zone non chauffée.

1.4 Objectifs de recherche

L'objectif de ce projet est donc d'appliquer des traitements thermomécaniques localisés sur des tiges de TiNi afin de faire varier localement leurs propriétés mécaniques et d'identifier les éventuels bénéfices de ces tiges pour la stabilisation de la colonne. Ce but global peut être divisé en plusieurs objectifs spécifiques :

Le premier objectif est de développer une technique de fabrication simple, rapide et fiable permettant de produire des tiges en alliage à mémoire de forme Ti-Ni aux propriétés variables.

Le deuxième objectif est de modéliser numériquement le comportement mécanique des tiges aux propriétés variables. Pour cela, un modèle simulant les interactions entre le procédé de fabrication et les propriétés mécaniques de ces tiges doit être développé.

Le troisième objectif est d'identifier l'impact du nouveau type de tiges sur le comportement d'un segment de colonne lombaire porcine. L'effet des crochets transverses placés en fin d'instrumentation sera également évalué.

1.5 Méthodologie

La méthodologie employée lors de ces travaux est présentée sommairement dans les paragraphes suivants. Pour plus de détails, une description complète est fournie dans chaque article.

1.5.1 Matériau utilisé

Trois matériaux sont utilisés dans cette étude. Dans un premier temps, des fils de Ti–50.6 at%Ni, 2 mm de diamètre fourni par SAES Getters (Italie) sont employés pour une étude de faisabilité. Pour la fabrication des tiges de 5,5 mm de diamètre, un alliage à mémoire de forme Ti-50.9at.%Ni fourni par Johnson Mattey Medical (PA, USA) est utilisé. Ces tiges ont été comparées à des tiges de titane (Ti-6Al-4V) fourni par Fort Wayne Metals (IN, USA)

1.5.2 Technologie de fabrication des tiges

Afin de modifier localement les propriétés mécaniques des tiges, deux techniques ont été étudiées: la déformation à froid localisée et les recuits locaux. Ces méthodes sont décrites en

détail dans l'article intitulé « Manufacturing of monolithic superelastic rods with variable properties for spinal correction: Feasibility study » présenté au chapitre 2 de cette thèse.

Écrouissage local : Afin de déformer localement le matériau, un laminoir de précision FENN est utilisé. Cet équipement permet de modifier le taux d'écrouissage d'une tige de façon locale en ne laminant qu'une partie de la pièce.

Recuits locaux : La technique des recuits locaux par effet Joule est choisie. Pour cela, deux sources de courant (Matsusada Precision, Japon, 170A@30V et AMREL, USA, 33A@100V) sont utilisée. Une photo de l'installation est présentée à la Figure 1.17. Le profil de température résultant du chauffage est mesuré par une caméra thermique E60 (FLIR Systems, USA) ou par un thermocouple de type K (TT-K-36-SLE, Omega Eng. Inc, USA)

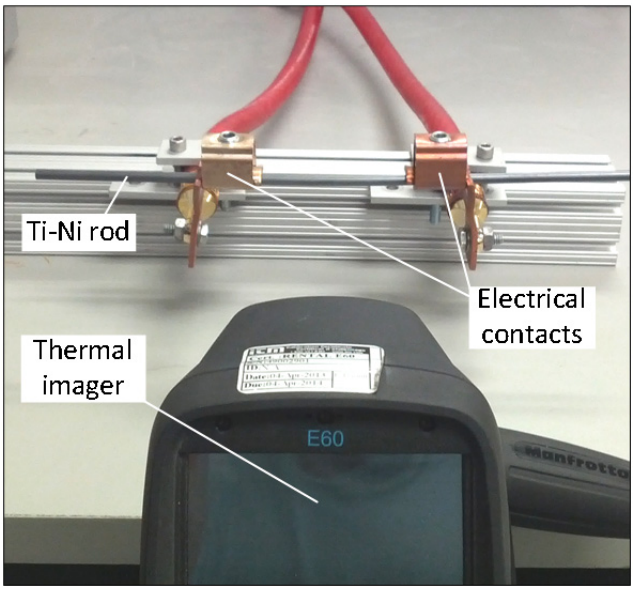

Figure 1.17 Photographie du montage permettant les recuits localisés par effet Joule

Cette méthode permet de chauffer une portion de tige jusqu'à 600°C ce qui engendre des changements de propriété mécanique en quelques minutes seulement.

1.5.3 Modélisation

Un modèle numérique a été développé afin de simuler l'impact du chauffage sur les propriétés mécaniques de la tige. Ce modèle, sa validation ainsi que des exemples d'application sont décrits dans l'article intitulé « Monolithic superelastic rods with variable flexural stiffness for spinal fusion: Modeling of the processing-properties relationship » présenté au chapitre 3. Le modèle est développé à l'aide du logiciel commercial Ansys Workbench 14. Le modèle simule premièrement le chauffage par effet Joule. Ensuite, le profil de température obtenu est utilisé afin de prédire la variabilité des propriétés mécaniques. Le modèle utilise donc deux modules du logiciel Ansys : le module thermique (statique et transitoire) ainsi que le module mécanique statique. Le modèle thermique est validé en comparant les profils de température obtenus numériquement avec les profils expérimentaux mesurés par la caméra thermique. Le modèle mécanique est validé en utilisant des données expérimentales provenant de tests en flexion encastrée. Une photographie de ce test est représentée à la Figure 1.18.

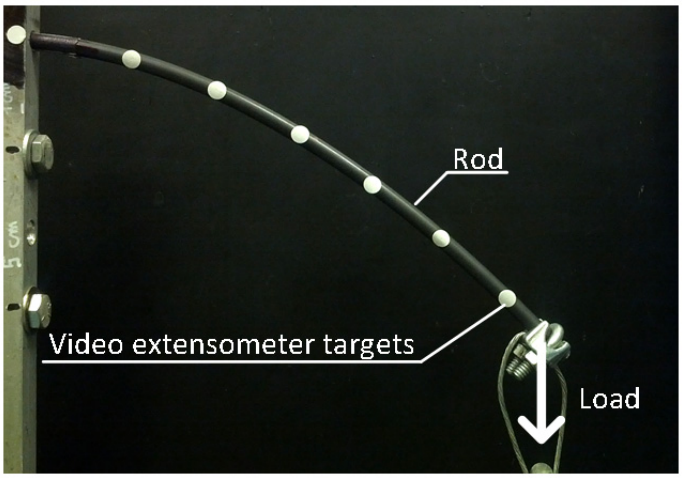

Figure 1.18 Photographie d'un
test de flexion encastrée

1.5.4 Étude biomécanique

Les tests biomécaniques sont réalisés sur spécimens porcins (L1-L6) pour identifier les éventuels bénéfices des tiges aux propriétés variables. Les détails de cette étude expérimentale sont présentés dans l'article intitulé « Biomechanical assessment of the stabilization capability of monolithic spinal rods with variable flexural stiffness » présenté au chapitre 4.

Les spécimens ont été instrumentés avec trois types de tiges : Ti, Ti-Ni entièrement superélastique et Ti-Ni à rigidité variable. Ces tiges sont fixées aux spécimens selon deux configurations d'ancrages : vis pédiculaires uniquement ou alors vis pédiculaires et crochets à l'extrémité des tiges. Les calculs préliminaires présentés en annexe I dans l'Article « Monolithic superelastic rods with variable flexural stiffness for spinal fusion: Simplified finite element analysis of an instrumented spine segment » ont montré que pour diminuer les contraintes aux segments adjacents, la portion souple de la tige variable devrait être située vers la partie non instrumentée du spécimen. Également, la méthodologie développée pour ces tests est décrite et validée dans l'article « In-vitro assessment of the stabilization capacity of monolithic spinal rods with variable flexural stiffness: Methodology and Examples » présenté en annexe II.

Les spécimens ont été chargés en déplacement contrôlé selon trois mouvements : Flexion, extension et inflexion latérale. Durant tous les tests, un « follower load » de 400 N est utilisé. Afin d'appliquer un moment pur, une table de translation est utilisée pour fixer la base des spécimens comme représentée à la Figure 1.19b.

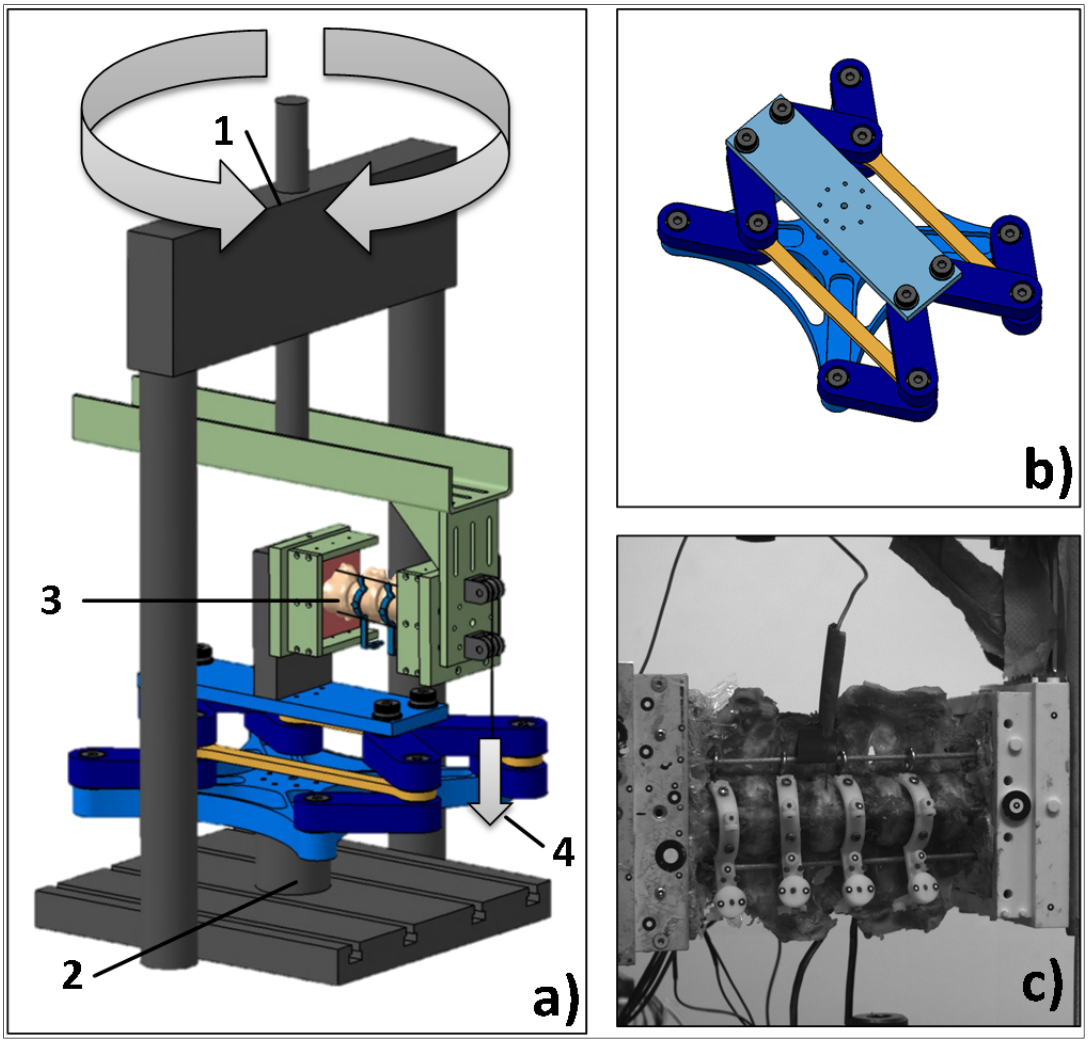

Figure 1.19 a) Description du banc d'essai avec 1) MTS Minibionix 2) Cellule de charge 3) Spécimen en place et 4) Follower load. B) Vue sur la table de translation et c) Photographie d'un spécimen en place

Les paramètres mesurés lors de ces tests sont décrits dans les paragraphes suivants.

Rigidité du spécimen : La rigidité du spécimen (N.m/°) représente le moment de flexion nécessaire pour appliquer une rotation de 18° à la vertèbre L1 du spécimen. Ce moment est mesuré à l'aide de la cellule de charge de la MTS (150 N.m).

Rotation vertébrale : Les caméras du système de corrélation d'images Aramis (GOM, Allemagne) sont utilisées pour filmer des marqueurs fixés aux vertèbres (voir Figure 1.19c). Les rotations de ces marqueurs sont déterminées à l'aide du logiciel Proanalyst (Xcitex, MA, USA) et d'un programme Matlab (MathWork, MA, USA).

Force dans les ancrages : Les moments de flexion appliqués sur les vis pédiculaires sont évalués en appliquant des jauges de déformation proche des têtes polyaxiale des vis selon la méthode décrite par (Freeman, Fahim et Bechtold, 2012). Les crochets transverses sont également munis de jauges. Cependant, à cause de leur géométrie, une seule jauge est utilisée par crochet ce qui ne permet pas de faire la distinction entre effort axial et moment de flexion. Le signal enregistré peut cependant être utilisé pour comparer différents types de tiges. Des photographies de ces ancrages instrumentés sont proposées à la Figure 1.20.

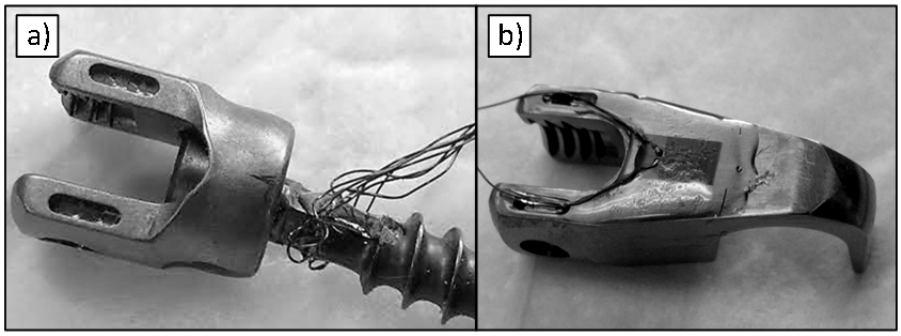

Figure 1.20 Photographies de a) une vis pédiculaire instrumentée
et b) un crochet transverse instrumenté

Pression intradiscale : La pression intradiscale est mesurée au niveau du disque D3 situé à l'extrémité de l'instrumentation (voir Figure 4.1). Pour cela, un capteur de pression miniature de la compagnie Gaeltec pouvant mesurer jusqu'à 30 bars est utilisé.

1.6 Organisation de la thèse

Les résultats obtenus lors de ces travaux ont été présentés dans trois articles de revue et deux articles de conférences. Chaque article est présenté dans son intégralité dans les chapitres 2, 3, 4 et annexes I et II de ce document.

Partie 1 : Développement de la technologie de fabrication des tiges aux propriétés variables.

La technologie de fabrication ainsi que la caractérisation de tiges aux propriétés variables est présentée dans l'article intitulé : *"Manufacturing of monolithic superelastic rods with variable properties for spinal correction: Feasibility study."*Facchinello, Y., V. Brailovski, K. Inaekyan, Y. Petit and J.-M. Mac-Thiong publié dans Journal of the Mechanical Behavior of Biomedical Materials, 2013, 22: 1-11.

Partie 2 : Modélisation du procédé de fabrication et de son impact sur les propriétés mécaniques des tiges.

Le modèle et sa validation ont été décrits dans l'article : *"Monolithic superelastic rods with variable flexural stiffness for spinal fusion: Modeling of the processing-properties relationship. "* par Facchinello, Y., V. Brailovski, Y. Petit and J.-M. Mac-Thiong publié dans Medical Engineering and Physics, 2014 36 (11): 1455-1463.

Partie 3 : Étude biomécanique sur spécimens lombaire porcins.

Une étude expérimentale a été menée dans le but d'identifier les éventuels bénéfices des tiges variables. Le profil de rigidité des tiges variables est justifié par les calculs présentés en annexe I. La méthodologie expérimentale ainsi que sa validation sont présentées en annexe II. Les résultats complets de cette étude biomécanique sont présentés dans l'article intitulé *"Biomechanical assessment of the stabilization capacity of Ti-Ni monolithic spinal rods with different flexural stiffness and anchoring arrangement"* par Facchinello, Y., V. Brailovski, Y. Petit, Brummund M., Tremblay J. and J.-M. Mac-Thiong. Clinical biomechanics, 2015.

CHAPITRE 2

MANUFACTURING OF MONOLITHIC SUPERELASTIC RODS WITH VARIABLE PROPERTIES FOR SPINAL CORRECTION : FEASABILITY STUDY

Yann Facchinello[1,2], Vladimir Brailovski[1,2], Karine Inaekyan[1], Yvan Petit[1,2],
Jean-Marc Mac-Thiong[2,3]
[1]Département de Génie Mécanique, École de technologie supérieure,
1100 Notre-Dame Ouest, Montréal, Québec, Canada H3C 1K3
[2]Centre de recherche, Hôpital du Sacré-Cœur de Montréal,
5400, boul. Gouin Ouest, Montréal, Québec, Canada H4J 1C5
[3]Département de chirurgie, Faculté de médecine, Université de Montréal,
Pavillon Roger-Gaudry, Local: S-749, Montréal, Québec, Canada H3C 3J7

Article publié dans la revue « Journal of the Mechanical Behavior of Biomedical Materials »,
v 22, p 1-11, Juin 2013

2.1 Résumé

Cet article présente le développement de la technologie de fabrication de tiges en alliage à mémoire de forme aux propriétés mécaniques variables. Deux méthodes de fabrication ont été explorées : l'écrouissage local et les traitements thermiques locaux. À partir d'une tige superélastique, l'écrouissage local empêche la transformation martensitique dans la zone déformée et produit donc un matériau élastoplastique conventionnel. À l'inverse, à partir d'une tige écrouie, le traitement thermique local par effet Joule restaure le comportement superélastique dans la zone chauffée. Il a été démontré que les traitements locaux permettaient de modifier drastiquement les propriétés du matériau dans une zone bien définie. De plus, les essais de traction ont montré que la transition entre les différentes propriétés mécaniques était graduelle. Enfin, des essais de fatigue ont prouvé que la zone de transition ne présentait pas une faiblesse du matériau puisque les échantillons hétérogènes n'ont pas une durée de vie inférieure à celle des échantillons homogènes.

2.2 Abstract

A new concept of monolithic spinal rod with variable flexural stiffness is proposed to reduce the risk of adjacent segment degeneration and fracture associated with rigid spinal fixation techniques while providing adequate stability to the spine. The concept is based on the use of Ti-Ni shape memory alloy rods subjected to different processing schedules implying local annealing, cold work, or a combination of both. A feasibility study of the concurrent technological routes is performed by comparing their potential to locally control material microstructure and properties.

2.3 Introduction

Spinal disorders including fractures and deformities can be treated by several means including fusion surgery. Different types of spinal instrumentation exist for such treatments. Metallic rods are widely used because they provide the stability and rigidity needed for fusion. However, two main problems are observed with metallic constructs for spinal fusion, such as implant failure and adjacent (non-instrumented) segment disease (DeWald and Stanley, 2006; Nasser et al., 2010; Park et al., 2004). Implant failure can be reduced by using stronger fixation anchors or rods. Conversely, adjacent segment problems are due to significant stresses observed at the implant's extremities, especially when stronger fixation techniques are used. To lower the stress concentration at the extremities of the implant and to reduce the risk of adjacent segment disease, dynamic stabilization systems have been used (Bono et al., 2009; Kelly et al., 2010). Concerns with such dynamic stabilization systems include eventual mechanical failure and degeneration within the stabilized segments, especially when no fusion is performed. These findings highlight the difficulties associated with the current instrumentation systems for obtaining strong spinal fixation and stabilisation while preventing implant fracture and adjacent segment disease.

The ideal situation would be a type of spinal instrumentation with simultaneous static and dynamic stabilisation capabilities: greater stiffness in zones where stability from rigid

fixation is critical to prevent fixation failure, and lower stiffness in zones where dynamic properties and load-sharing capacity is important (at the rod's extremities, for example).
There are thus two principal ways to convey a different stiffness to different portions of a spinal rod: varying its cross-section geometry, varying its modulus of elasticity, or a combination of both. Several technical solutions exploiting these avenues have already been investigated: a) alternating straight and helix portions (Park, 2010); and b) using a rod-hinge combination (Trieu, 2010) or an assembly of smaller segments made either of different materials (Capozzoli, 2010; Patterson et al., 2008; Petit and Droulout, 2005; Zylber et al., 2011) or having variable cross-section (Gayet and Rideau, 1994). The common limitation of the above-mentioned systems is their bulkiness and complexity, the latter inevitably affecting system reliability. These limitations could however be overturned by using the unique properties of shape memory alloys (SMA).

SMAs, such as nearly equiatomic (approximately 50%-50%) titanium-nickel alloys, demonstrate plateau-like superelastic behaviour, which is much more biomimetic than the linear elastic behaviour of conventional metals and alloys. This feature can result in a better load sharing between the implant and the spine structure, thus decreasing the risk of stress-shielding related complications. A series of patents claim the potential utility of superelastic instrumentation for spinal fusion, for the dynamic stabilization of vertebral implants, and for spine correction (Jeon et al., 2009; Justis and Sherman, 2001, 2004a, b). The drawback of superelasticity is that it allows much larger displacements than conventional materials under the same loads, which can compromise the fixation stability.

It is known that, depending on an alloy's composition, processing and temperature of use, SMAs exhibit either shape memory (SM) or superelastic (SE) behavior, or they behave as conventional elastoplastic metallic materials. Since the properties of the Ti-Ni SMA are extremely sensitive to the alloy's composition (a 1% variation in composition corresponds to ~300 MPa of variation in the onset stress for superelasticity), and the application temperature is constant (the human body), modifying the material processing is the most reliable avenue to modify the alloy's properties.

Processing of SMAs includes a specific sequence of plastic deformation and thermal treatments. Plastic deformation can be performed at room or at elevated temperatures (Brailovski et al., 2004). When this deformation is carried out at room temperature (cold work or CW), the crystallographic structure of the material is severely deformed, thus introducing a large number of defects and suppressing superelasticity (Saburi et al., 1982, 1986; Dayananda and Rao, 2008). A post-deformation annealing (PDA) at a specific temperature is then necessary to restore superelasticity (Otsuka and Wayman, 1999). If no annealing is performed, the deformed alloy behaves as a conventional elastoplastic material.
Different local heating techniques can be applied to a hardened material to locally restore superelasticity or shape memory effect: Joule heating, laser heating, or induction heating (Bellouard et al., 1999; Groh, 2007; Mahmud, 2008; Quiglin, 2012). Alternatively or in combination, starting from an entirely annealed rod, local cold work can be performed to suppress superelasticity in the designated zone of the rod. Different combinations of local cold work and local annealing could also be contemplated. In summary, by modulating -along the rod's length- the cold work intensity and the annealing temperature and duration, gradual variation of the material properties can be obtained, in conformity with the application requirements (Brailovski et al., 2012). The objective of this work is to demonstrate the feasibility of monolithic Ti-Ni rods with properties graded from elastoplastic to superelastic by means of local thermomechanical processing.

2.4 Methodology

Since it is potentially possible to convey different properties to distinctive parts of a single SMA piece by differentiating their processing, as an example, two complementary manufacturing routes conferring different mechanical properties to two parts of a monolithic Ti-Ni rod are illustrated schematically in Figure 2.1.

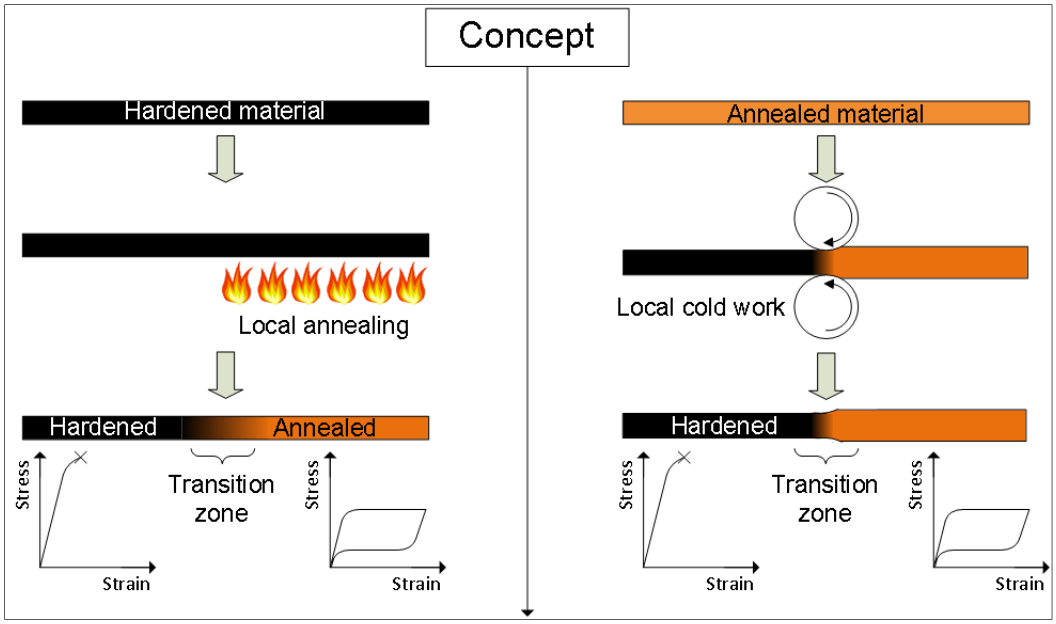

Figure 2.1 Description of the two processing routes used to produce samples with variable properties

As a first step of the study, a detailed thermomechanical characterization of an alloy of a given composition subjected to PDA at different temperatures is performed to assess the property-modification capabilities of PDA. During this step, PDA is carried out using homogeneous furnace heating of the entire rod specimen. Second, among all the stress-strain diagrams potentially available, only the one corresponding to the targeted superelastic behavior is retained. Then, the identical superelastic behavior is obtained using Joule heating of the supplied material, and the Joule-heating conditions (current intensity and time) thus determined are applied to anneal a part of a cold-worked rod, leaving the remaining part non-treated.

The resulting specimen has therefore two parts: cold worked (CW) and cold-worked and annealed (CW+PDA). The difference in static and dynamic stress-strain behavior of the CW and CW+PDA parts of the rod is then assessed. Finally, a combined three-step processing routine consisting of two-step PDA with intermediate CW is conducted to illustrate in more details the potential of using thermomechanical processing to locally modify the Ti-Ni mechanical behavior.

Materials

In this study, local cold work and local post-deformation annealing are used to modify the properties of an as–drawn (CW strain of about 30%) Ti-50.6at.%Ni 2 mm diameter rod supplied by SAES Getters.

Processing

Furnace annealing

To assess the property-modification capabilities of PDA at different temperatures, 10-min furnace annealing of the as-drawn specimens is performed at 300, 400, 450, 500, 600 and 700°C.

Local annealing or combined CW1+PDA1+CW2+PDA2 routine

Joule-heating PDA is performed using an SPS 100-33 (AMREL Power Product Inc, CA, USA) power supply capable of delivering 33 A at 100 V. The temperature of the specimen in the middle of the heated region is measured by a K-type thermocouple (TT-K-36-SLE, Omega Eng. Inc.). The Joule-heating current intensity, duration and control temperature are selected to obtain specimens with the same properties as those that are furnace-annealed. Type I and Type II locally-annealed 110 mm-long specimens are tested (Figure 2.2). Type I specimens are annealed on 1/2 of their entire length, whereas Type II specimens are annealed on 1/3 of their length, in the middle. To assess the influence of a combined thermomechanical routine (Figure 2.2, Type III specimens), the as-supplied CW1 (30%) specimens are initially furnace-annealed: PDA1 (recrystallization annealing at 800°C, 20 min). The specimens are then cold-rolled on 1/2 of their length: CW2 (thickness reduction of 35%). Finally, they are furnace-annealed again: PDA2 (300°C, 10 min).

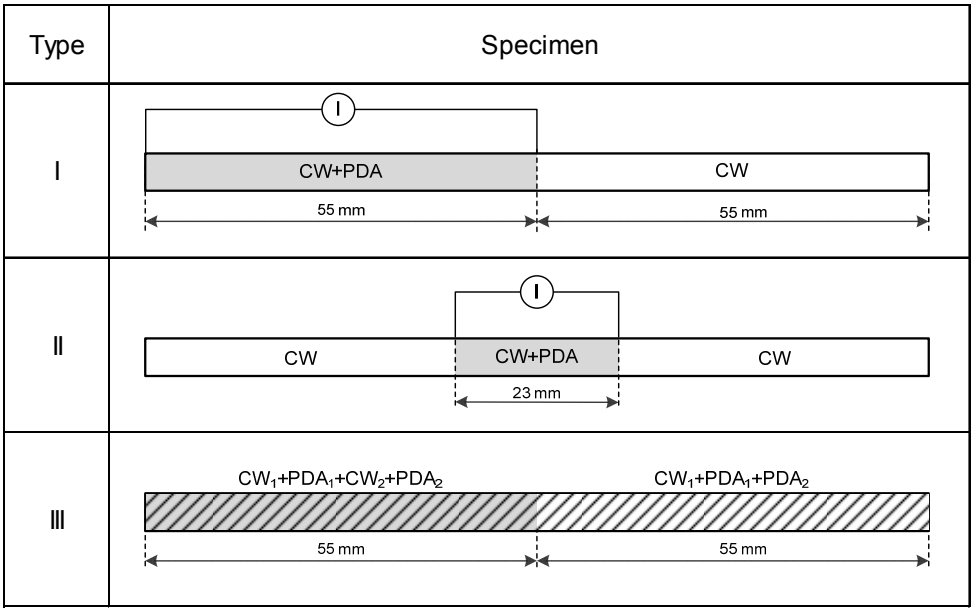

Figure 2.2 Type I, II and III specimens with variable flexural stiffness

Characterization

Differential Scanning Calorimetry (DSC) measurements (Perkin-Elmer Pyris-1 DSC, 10ºC/min heating-cooling rate) are performed on the furnace-annealed specimens to determine the temperature ranges of direct and reverse martensitic transformations – the information required to establish the phase state of the material at a given temperature. DSC measurements of the locally-annealed Type I specimens are also carried out. X-ray diffraction analysis of Type I specimens is performed using a Panalytical X'Pert diffractometer ($\lambda_{CuK\alpha}$ =1.541874 Å).

Tensile testing of all specimens (subjected to either homogeneous or localized processing) is realized at room temperature (RT) using an MTS Minibionix 858 with a crosshead speed of 0.14 mm/sec. 110 mm-long (working length of 70 mm) specimens are strained up to 6%, then released and loaded again to failure. Selected specimens are subjected to two loading-unloading cycles before straining to failure. Such a sequence allows the characterization of both the superelasticity-related and the conventional elastoplastic mechanical behaviour of the material under study.

To measure tensile strain locally, a Multipoint Video Extensometer (Messphysik, Germany) is used. The testing is simultaneously video-recorded using a custom recording system (Camera GRAS-20S4M-C, Point Grey Research, Japan, Labview programming).

The fatigue life of the as-supplied (CW), totally superelastic (CW+PDA) and partially superelastic Type I (1/2(CW) + 1/2(CW+PDA) specimens is evaluated using a custom-made rotary bending fatigue bench (Figure 2.3) inspired by Figueiredo et al., (2009) and Wagner et al., (2004). The position of the bearings controls the radius of curvature of the sample and thus the applied strain from 1 to 4 %. Rotational speed of around 500 rpm is used. Each test is repeated 12 times. Fractography analysis of the fatigue-tested samples is carried out using a Hitachi S3600N SEM with 20 kV of acceleration voltage.

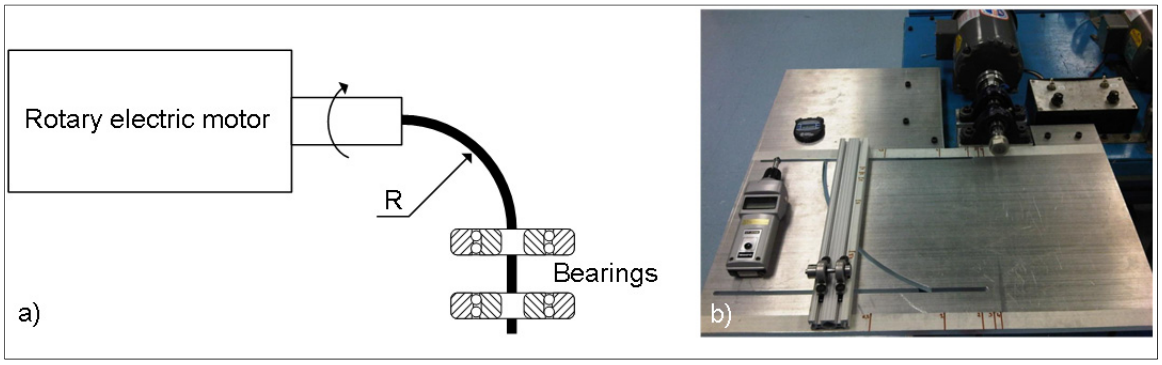

Figure 2.3 Rotary bending fatigue bench: a) Schematic representation and b) Photography of the bench

2.5 Results

Furnace-annealing: assessment of the property-modification capabilities

DSC and tensile tests

In Figure 2.4, the DSC plots and the tensile stress-strain diagrams of specimens subjected to PDA at various temperatures are all indicated. Figure 2.5 a) shows one of the obtained stress-strain curves (400°C PDA) and highlights some key parameters of such a diagram: ε_P and ε_{SE}

refer to the permanent and superelastic recovery strains, respectively; σ_{Cr} corresponds to the transformation yield stress, σ_y, to the true yield stress, and σ_u, to the ultimate tensile strength; E_L and E_U correspond to the loading and unloading Young's moduli, respectively, and δ to the elongation to failure.

Figure 2.5 b)-f) illustrates the evolution of the temperature range of martensitic transformation (TRMT) obtained from the DSC plots and stress-strain diagrams as functions of the PDA temperature. Note that the dotted line of Figure 2.5 separates the PDA conditions leading to superelastic (SE) (left) and mixed SE+SM (shape memory) (right) behavior of the same material at RT. It appears that 400°C (10 min.) furnace annealing perfectly restores the superelastic behaviour of the material and corresponds to the lowest Young's modulus as well as to the greatest difference between σ_{Cr} and σ_y (for a good safety margin). To obtain the same mechanical behavior with a locally-annealed sample, the equivalence must now be established between the furnace-heating and Joule-heating annealing conditions.

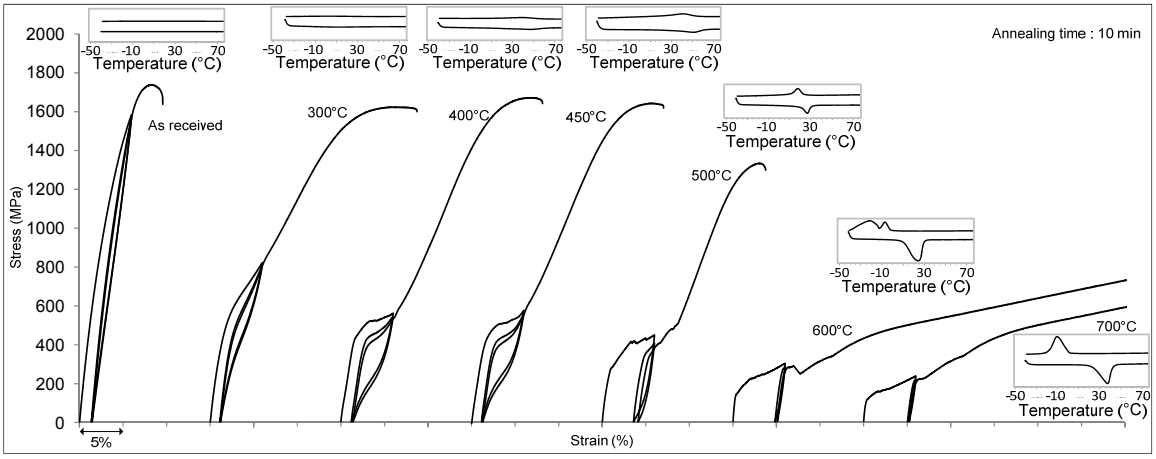

Figure 2.4 DSC curves and stress-strain plots of Ti-50.6 at.%Ni Ø2mm rod annealed at different temperatures

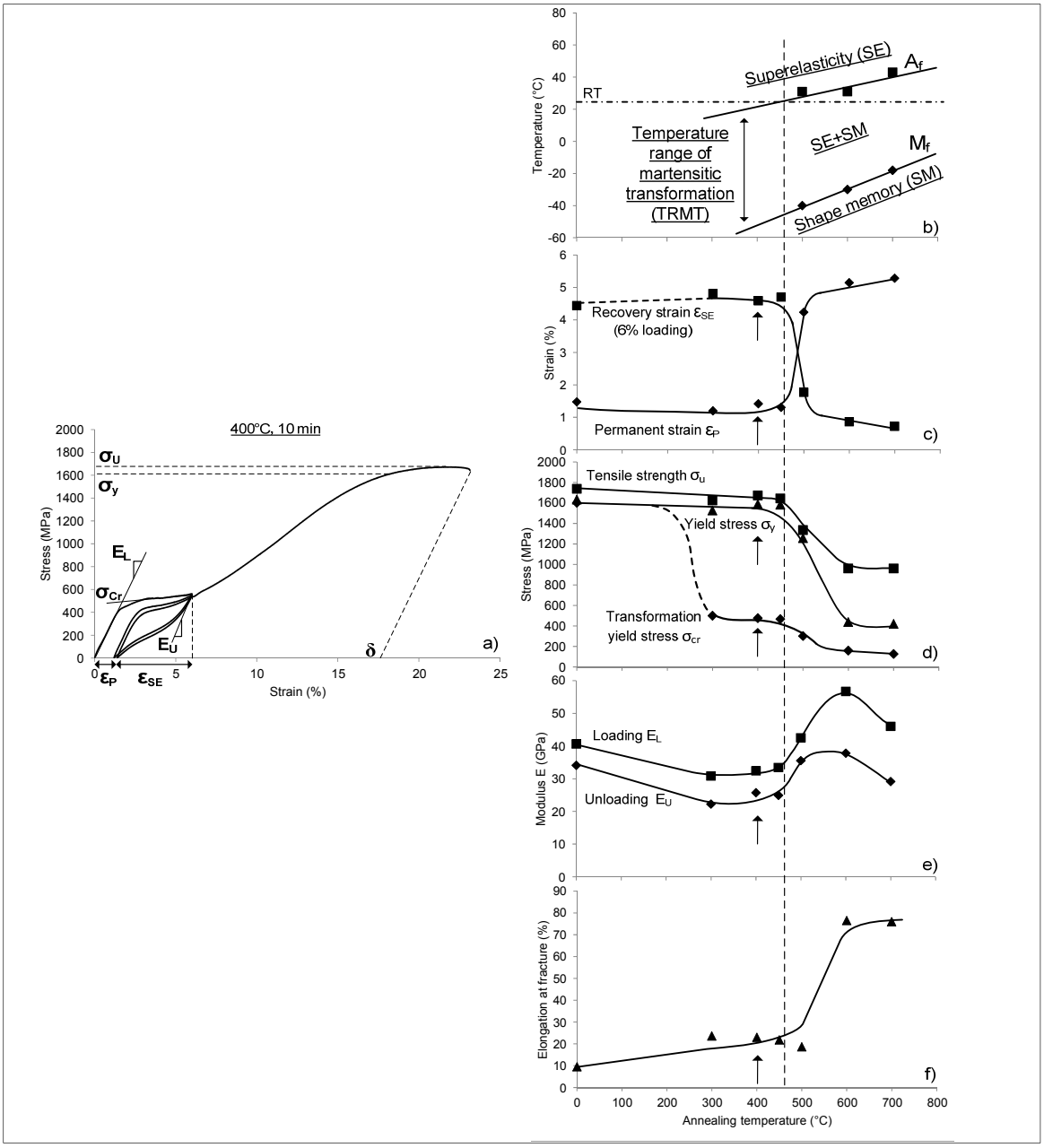

Figure 2.5 Mechanical properties of Ti-50.6at.%Ni Ø2mm rod:
a) stress-strain curve after 400°C PDA (10 min); b) Temperature range of martensitic transformation (TRMT): A_f, (austenite finish) - M_f (martensite finish; c) superelastic recovery (ε_{SE}) and permanent strain (ε_P) d) ultimate tensile strength (σ_u), true (σ_y) and transformation (σ_{cr}) yield stresses, e) modulus under loading (E_L) and unloading (E_U) and f) elongation to failure (δ); arrow correspond to 400°C PDA (10 min); the dotted line separates superelastic (left) and shape memory (right) behavior of the same material

Joule-heating equivalence

Figure 2.6 presents two stress-strain diagrams: the as-drawn specimen (black bold line) exhibits classic elastoplastic behaviour, while after furnace-annealing at 400°C, 10 min (grey bold line), or Joule-heating annealing at 320°C, 10 min (grey dotted line), its behavior becomes superelastic. Given the acceptable equivalence observed between the results of the furnace-annealing and the Joule-heating annealing, in the remaining of this work, local Joule-heating will be performed under these conditions.

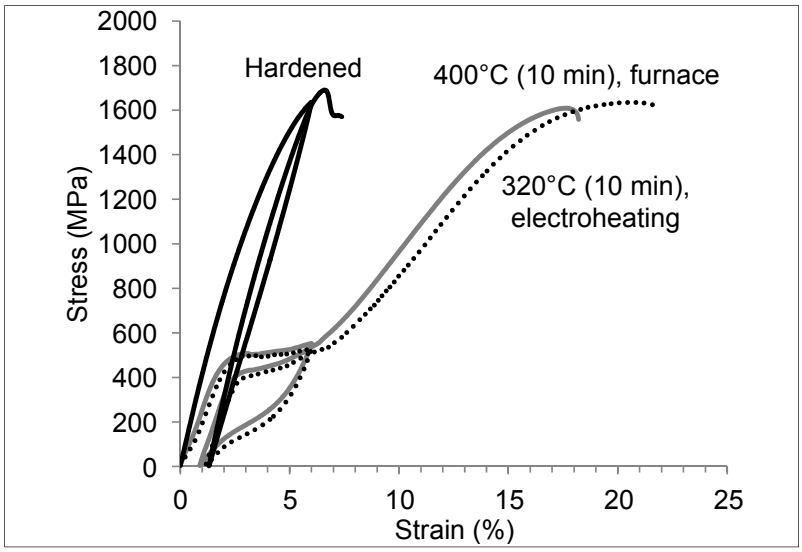

Figure 2.6 Stress strain plots of
Ti-50.6 at.% Ni Ø2 mm rod in as-drawn state
(dark bold line), after furnace annealing (400°C, 10 min),
grey bold line and after Joule-heating at 320°C, 10 min
(grey dotted line)

Local CW+PDA and combined CW1+PDA1+CW2+PDA2 routines

DSC and X-ray

Figure 2.7 shows the DSC and X-ray plots obtained on the Type 1 specimen from four different locations (⊗): one in the CW+PDA zone and three in the CW zone. It appears that

local annealing results in stress relaxation and recovery, which is demonstrated by a significant narrowing of the (110)-austenite peak in the CW+PDA processed zone. In the CW zone, all three measurements resulted in similar X-ray plots (only one is presented in Figure 2.7), thus proving that the material remained strongly hardened even in the close vicinity of the electrical contact (within 10 mm of distance from the electrical contact).

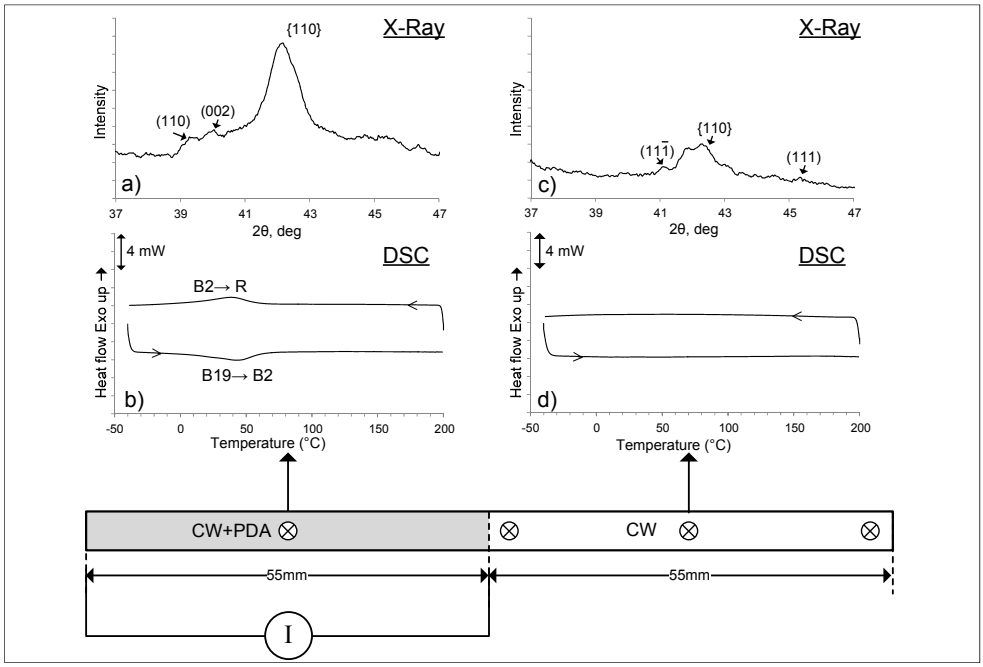

Figure 2.7 Local X-ray (a) and c)) and DSC (b) and d)) tests on Type I specimen: ½ CW – ½ (CW+PDA); locations of DSC and X-ray testing spots are indicated by the symbol ⊗. For three measurements in the CW part, the DSC and X-ray plots of (110) B2-austenite peak are presented for the central testing point only

Multipoint tensile tests

Multipoint tensile tests were carried out on Type I, II and III specimens (see the results obtained for each type in Figure 2.8, Figure 2.9 and Figure 10, respectively). Each figure contains the local stress-strain diagrams, the stress-strain diagram of the entire specimen and the video-recorded displacement of each marker (point). The stress-strain diagrams of Figure 2.8 show that local annealing restores superelasticity on the left half of the specimen. Also,

the transition between the superelastic and elastoplastic behaviour is gradual (Figure 2.8, #4 - #5 and #5 - #6 stress-strain diagrams). The video-recorded data indicate that the fracture occurs in the transition regions between points #5 and #6. The same behaviour is observed in Figure 2.9 for a Type II specimen, but now with two transition zones (#2 - #3 and #5 - #6) given a central location of the annealed region.

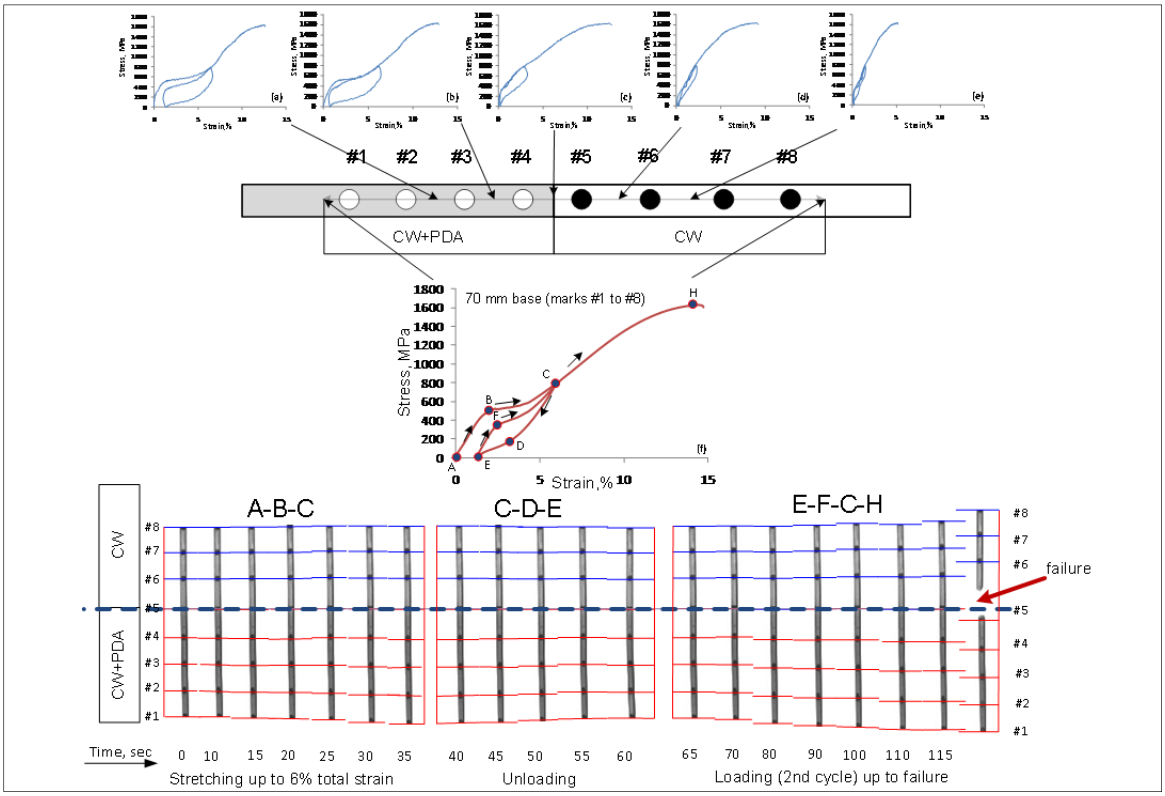

Figure 2.8 Type I specimens: (a)-(e) local stress-strain diagrams,
(f) overall mechanical behavior of the specimen (between points #1 and #8);
A-B-C, C-D-E and E-F-C-H are video-recorded data

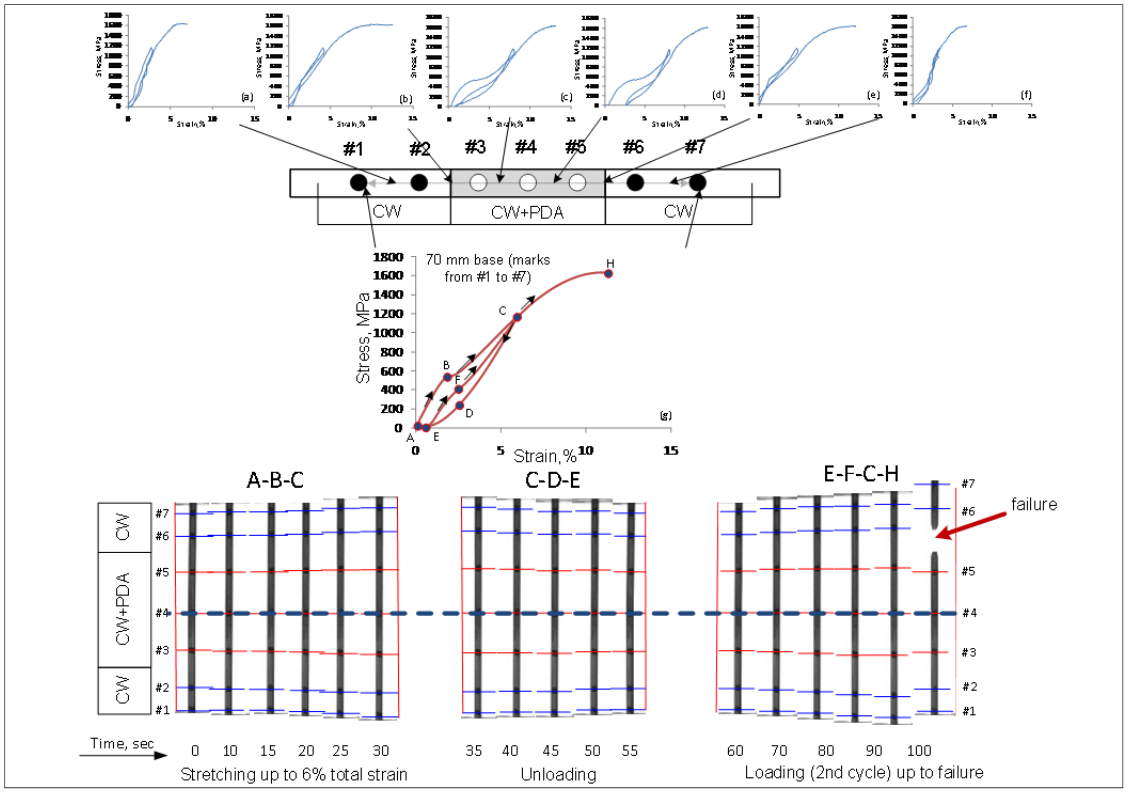

Figure 2.9 Type II specimens: (a)-(f) local stress-strain diagrams,
(g) overall mechanical behavior of the specimen (between points #1 and #7);
A-B-C, C-D-E and E-F-C-H are video-recorded data

Figure 2.10 makes it clear that one half (CW1+PDA1+CW2+PDA2) of the Type III specimen exhibits superelasticy, whereas the other half (CW1+PDA1+PDA2) shows quasi-elastoplastic behavior similar to that observed in Figure 2.4 after PDA at 700°C.

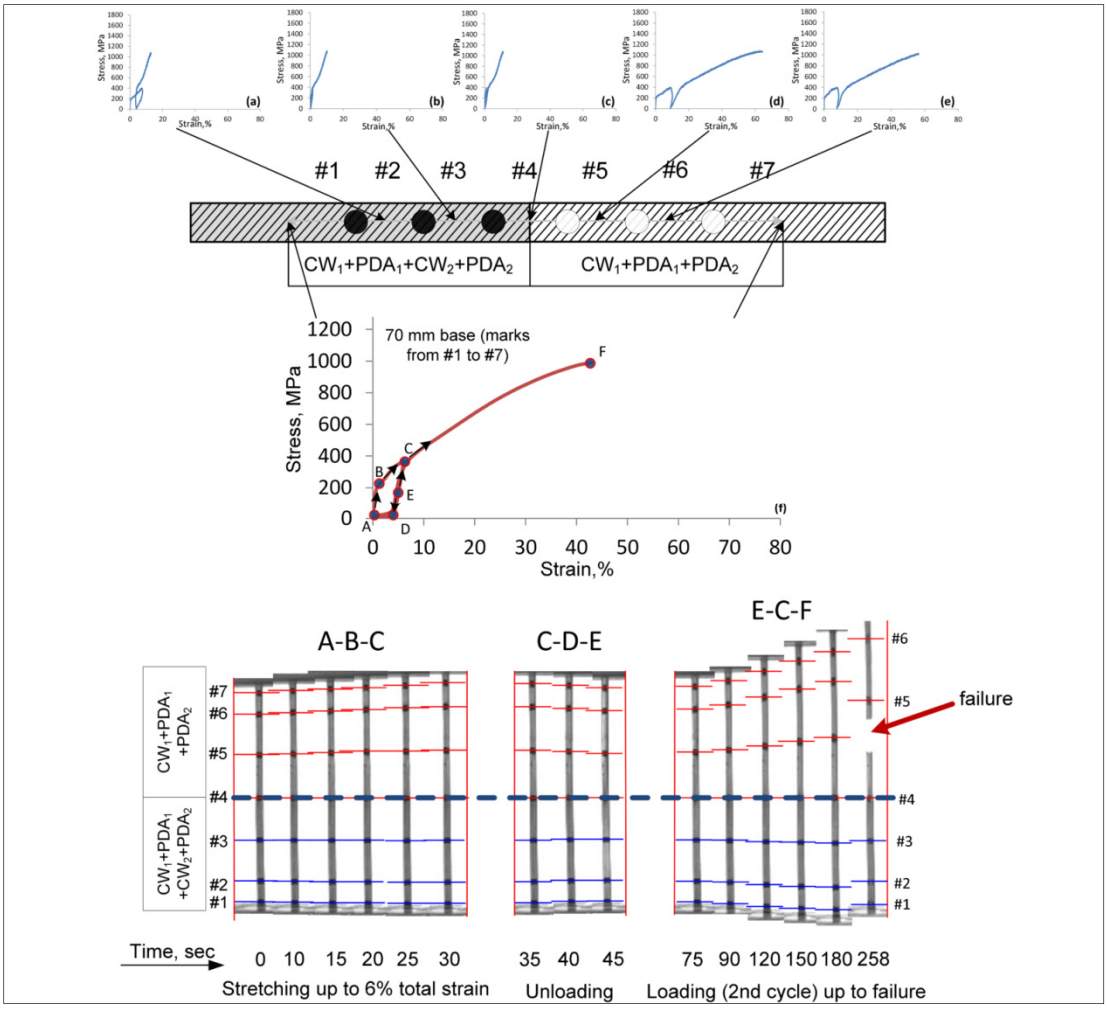

Figure 2.10 Type III specimens: (a)-(e) local stress-strain diagrams,
(f) overall mechanical behavior of the specimen (between points #1 and #7);
A-B-C, C-D-E and E-C-F are video-recorded data

Figure 2.11 presents the variation of the tensile strength σu, true yield stress σ_y, and transformation yield stress σ_{cr} along Type I, II and III specimens. These values are extracted from the multipoint stress-strain curves of Figure 2.8, Figure 2.9 and Figure 2.10, respectively. Note that the overall tensile strength and yield stress for Type I and Type II specimens are affected slightly by the processing conditions (1600 MPa versus 1400…1600 MPa). The transformation yield stress σ_{cr} exhibits the most sensitivity to the processing conditions. For Type I and Type II specimens, it drops significantly in the annealed regions

from over 1400 to about 400 MPa, which is coherent with the observations made with the homogeneous furnace-annealed specimens.

The situation with two-stage annealed Type III specimens is different. In this case, the tensile strength and the transformation yield stress are almost constant along the specimen length regardless of the localised processing ($\sigma_u \cong 1000$ MPa and $\sigma_{tr} \cong 200$ MPa). However, the true yield stress, σ_y, varies significantly along the specimen length. It drops from 900 MPa in the two-time deformed part of the specimen to 400 MPa in the one-time deformed part of the specimen, thus approaching the transformation yield stress measured in this latter part. Note that the observed residual strain on the right part of the Type III specimen (Figure 2.10) is not a true plastic strain, because it can be reversed upon heating due to the shape memory (SM) effect. The difference between the plastic strain and the induced shape memory strain resides in the difference between the underlying deformation mechanisms: irreversible dislocation slip for the former and reversible thermoelastic martensitic transformation for the latter. Since for the contemplated application of the proposed technology, service temperature remains constant (human body temperature), the reversibility of deformation is not relevant.

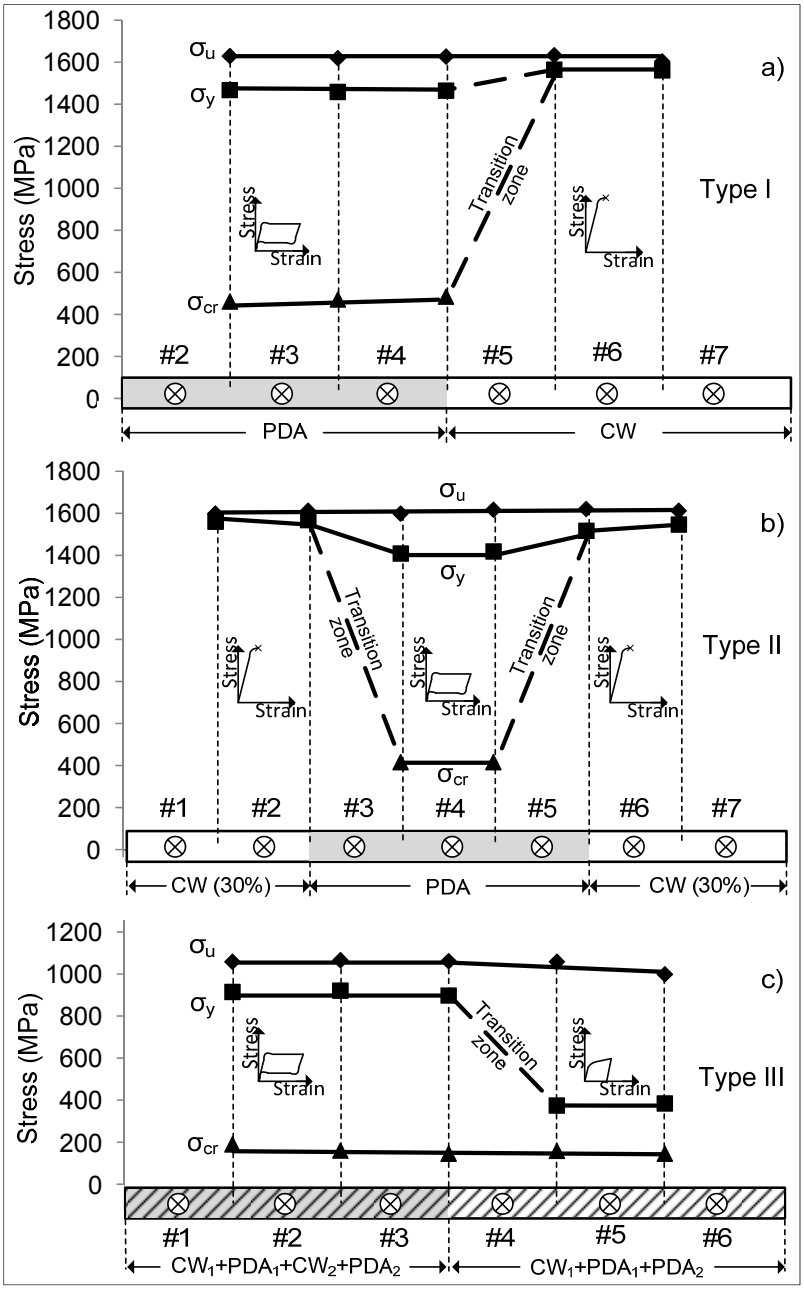

Figure 2.11 Tensile strength σ_u, true yield stress σ_y and transformation yield stress σ_{cr} extracted from multipoint tensile tests and plotted for a a) Type I sample, b) Type II and c) Type III

Fatigue testing

The results of the rotary bending fatigue testing are presented in Figure 2.12 for the completely CW and the CW+PDA specimens and for Type I specimens: ½CW - ½(CW+PDA). These results show that for the highest strain of 4%, all the specimens exhibit a similar fatigue life. For the medium strain of 2%, CW+PDA (entirely superelastic) specimens have the shortest fatigue life and CW specimens have the longest fatigue life, whereas Type I specimens occupy an intermediate position. For the lowest strain of 1%, the superelastic (CW+PDA) and half superelastic/half-hardened specimens (Type I) show relatively high and similar (no significant differences) fatigue lives, as compared to the fatigue life of the completely hardened specimen (CW). In order to complete the fatigue study, SEM fractography of a Type I specimen tested with 2% controlled strain is presented in Figure 2.13. The fracture initiation site (designated by the white arrow) is located at the point where the lines of the pattern converge and is probably coincident with a defect on the specimen surface. Figure 2.13 b) and c) show the difference between the smooth crack propagation zone and the dimpled rupture morphology which indicates a ductile fracture (Luebke et al., 2005).

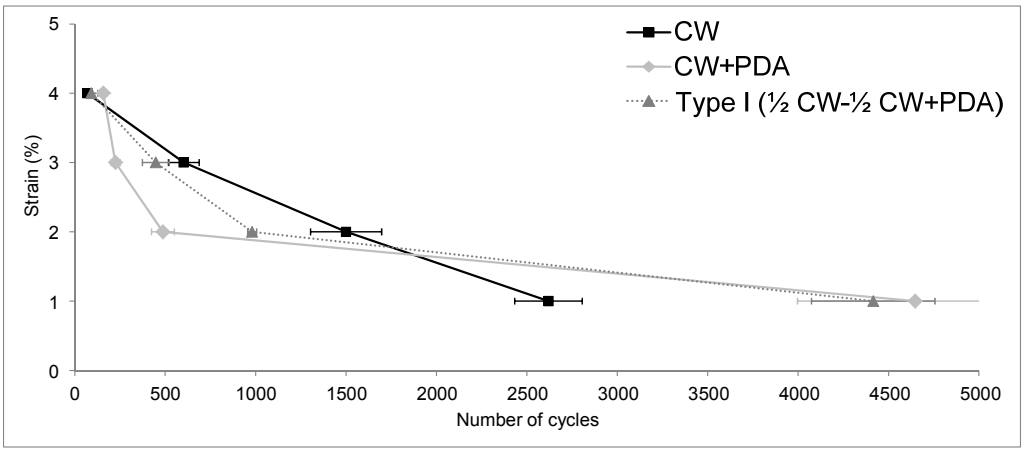

Figure 2.12 Fatigue curve for hardened, annealed (400°C, 1 hour) and type I specimens

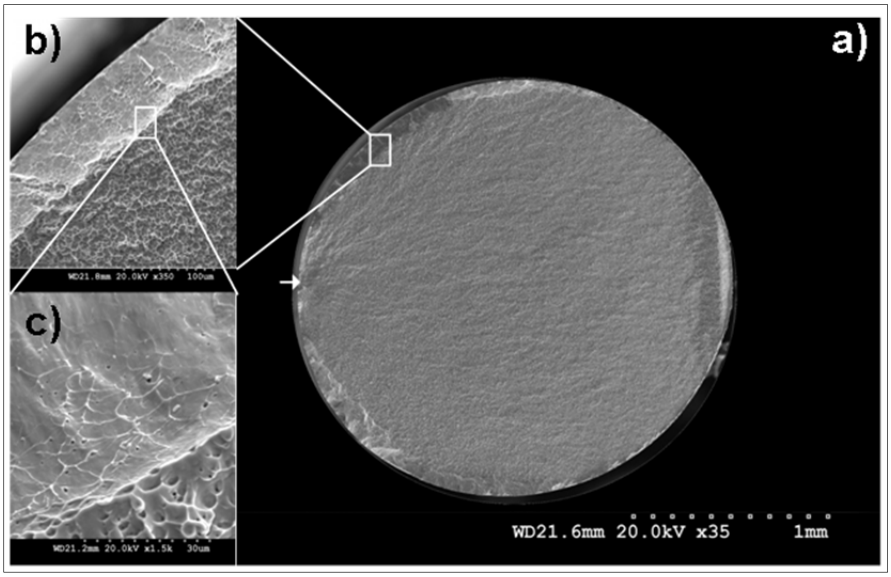

Figure 2.13 Fractography of the fatigue-tested Type I specimens
after 2% strain-controlled fatigue testing at
a) x 35, b) x 350 and c) x 1500

2.6 Discussion

There exists a large body of literature concerning the Ti-Ni SMAs sensitivity to processing conditions (Saburi et al., 1982, 1986; Miyazaki, 1990, etc). All the published information is however limited to the homogeneously deformed and heat treated materials. The authors are not aware of any comprehensive study of local thermomechanical processing of Ti-Ni SMAs and its influence on the alloy's functional properties.

The present results show that a specimen of the same composition (Ti-50.6at.% Ni) can exhibit stress-strain behaviour that varies from almost brittle (as-drawn or hardened material, ≈ 30-40% of cold work strain) to rubber-like with 80% elongation to failure (PDA : 700°C, 10 min). Between these two limit cases, almost-perfect superelastic behaviour corresponds to 400°C, 10 min furnace annealing. These phenomena are due to two concomitant processes: the higher the PDA temperature, the higher the temperature range of martensitic transformation and the lower the transformation and the true yield stresses of the material

because of stress relaxation, recovery, polygonisation and recrystallization (Todoroki and Tamura, 1987, Brailovski et al., 2004).

As seen in Figure 2.4, the hardened, unannealed, specimen behaves as a conventional metallic material because the interface movement related to martensitic transformation is hindered by a high level of strain-induced dislocation density (corresponding DSC plots are straight lines). On the other hand, the specimen annealed at 400°C shows superelastic behavior at RT due to stress-induced martensitic transformation. As can be seen from Figure 2.5b), this specimen is indeed in austenitic state at testing temperature: RT>Af. Finally, the specimen annealed at 700°C is in a mixed austenite-martensite state (Mf < RT < Af) and it manifests quazi-plastic stress-induced martensite reorientation behavior.

The fact that the phase state and therefore the mechanical behavior of the same alloy at the same testing temperature are different is logically explained by a shift to higher temperatures of the temperature range of martensitic transformation (TRMT) with increasing annealing temperature. This corresponds to what was observed by Demers et al., (2006). It can also be noticed from Figure 2.5 d) that the transformation yield stress and the true yield stress decrease when PDA temperature increases. These results are perfectly correlated with the observations made by Saburi et al. (1982, 1986).

It has been shown that furnace-annealing at 400°C (10 min) was equivalent to Joule-heating at 320°C (10 min) in terms of the resulting material behavior, but unlike furnace-heating, Joule-heating could easily be applied to a specific portion of the specimen and thus, produce localized annealing. The results obtained with the partially-annealed Type I, II and III specimens have effectively proven this point: stress-strain diagrams corresponding to the locally-annealed regions are similar to those obtained with furnace-annealing.

The temperature gradient, from the locally-heated zone towards the non-heated zone, resulted in a properties gradient. In this study, this gradient was limited to approximately five-times the diameter distance from the limits of the annealed zone (Figure 2.8).

During tensile testing, fracture systematically occurred in the transition zone between the annealed and the hardened regions. However, fatigue life of the variable stiffness specimens was found higher than that of the entirely superelastic specimens, but lower than that of the entirely hardened specimens (excepting low-strain 1% testing). Considering that fatigue life of SMAs subjected to stress-induced martensitic transformation (superelasticity) is generally lower compared with SMAs having stable either austenite or martensite structure (without superelasticity) (Humbeeck and Stalmans, 1998), it is not surprising that fatigue life of the variable stiffness specimens occupies an intermediate position.

Fractographic analysis of the specimens tested in fatigue showed that all specimens tested present a similar fracture pattern. Because of the relatively low number of cycles to failure imposed in this work, no difference could be observed between the specimens tested in terms of crack initiation, propagation and ductile rupture mechanisms.

2.7 Conclusion

It has been shown that local annealing and/or local cold work of Ti-50.6at.% Ni Ø2 mm wire allows the production of monolithic samples with variable mechanical behavior ranging from conventional elastoplastic to either superelastic or shape memory. Both the ultimate strength and the fatigue life of the specimens with variable properties (partially superelastic/partially elastoplastic) were of the same order of magnitude -or higher- than those of the entirely superelastic specimens made of the same material.

Due to the high thermal conductivity of the metallic material, a temperature gradient and therefore a properties gradient appears between the different regions of the specimens. This temperature gradient has not been thoroughly investigated in this work. However, an effective control of this gradient would help to more precisely control the gradient of properties and thus, the overall and local mechanical behaviour of spinal rods made of Ti-Ni SMA.

2.8 Acknoledgments

This work had been carried out with the financial support of the FQRNT (Fonds de Recherche du Québec – Nature et Technologies). The authors thank Mlle. P. Hydier for collaborating in the fatigue testing.

2.9 References

Bellouard, Y., Lehnert, T., Bidaux, J.E., Sidler, T., Clavel, R., Gotthardt, R., 1999. Local annealing of complex mechanical devices: a new approach for developing monolithic micro-devices, ICOMAT 98. International Conference on Martensitic Transformations, 7-11 Dec. 1998. Elsevier, Switzerland, 795-798.

Bono, C.M., Kadaba, M., Vaccaro, A.R., 2009. Posterior Pedicle Fixation-based Dynamic Stabilization Devices for the Treatment of Degenerative Diseases of the Lumbar Spine. J. Spinal. Disord. Tech. 22, 376-383.

Brailovski, V., Prokoshkin, S., Terriault, P., Trochu, F., 2003. Shape Memory Alloys: Fundamentals, Modeling and Applications. Ecole de technologie superieure, Montreal.

Brailovski, V., Khmelevskaya, I.Y., Prokoshkin, S.D. et al, 2004. Foundations of Heat and Thermomechanical Treatments and Their Effect on the Structure and Properties of Titanium Nickelide–Based Alloys. Phys. Met. Metallogr+. 97, S3-S55.

Brailovski V., Petit, Y., Mac-Thiong J-M., Driscoll M., Parent S., Labelle H., Apparatus and method for per-operative modification of medical device stiffness, U.S. Appl. US61/703388, Sept 15, 2012.

Capozzoli, J., Variable tension spine articulating rod. U.S. Appl. 20100160967, Jun 24, 2010. Dayananda, G.N., Rao, M.S., 2008. Effect of strain rate on properties of superelastic NiTi thin wires. Mater. Sci. Eng. A 486, 96-103.

Demers, V., Brailovski, V., Prokoshkin, S., Inaekyan, K., Bastarash, E., Khmelevskaya, I., Dobatkin, S., 2006. Functional properties of nanostructured Ti-50.0 at % Ni alloys. J. ASTM Int. 3, 34-43.

DeWald, C.J., Stanley, T., 2006. Instrumentation-Related Complications of Multilevel Fusions for Adult Spinal Deformity Patients Over Age 65: Surgical Considerations and Treatment Options in Patients With Poor Bone Quality. Spine. 31, pp. 144-151.

Gayet, L.E., Rideau, Y., Vertebral instrumentation rod. U.S. Patent 5,593,408, Jan 14, 1997.

Groh, J.R., Local heat treatment for improved fatigue resistance in turbine components. U.S. Patent 7,553,384, Jan 30, 2009.

Humbeeck V., Stalmans J.R., 1998. Characteristics of shape memory alloys, in: Otsuka K. and Wayman C.M., Shape Memory Materials, Cambridge University Press, pp. 149-183.

Jeon, D.M., Moore, P.D., Yang, H.J., Lee, S.K., Systems and methods for wrought nickel/titanium alloy flexible spinal rods. U.S. Appl. 2009/0194206, Feb 2, 2009.

Justis, J.R., Sherman, M.C., Superelastic spinal stabilization system and method, U.S. Patent 6,293,949, Sep 25, 2001.

Justis, J.R., Sherman, M.C., Superelastic spinal stabilization system and method. U.S. Patent 2004/0215192, May 19, 2004a.

Justis, J.R., Sherman, M.C., Superelastic spinal stabilization system and method and the methods of their manufacturing. U.S. Patent 6,761,719, Jul 13, 2004b.

Kelly, M.P., Mok, J.M., Berven, S., 2010. Dynamic Constructs for Spinal Fusion: An Evidence-Based Review. Orthop. Clin. N. Am. 41, pp. 203-215.

Luebke, N.H., Brantley, W.A., Alapati, S.B., Mitchell, J.C., Lausten, L.L., Daehn, G.S., 2005. Bending Fatigue Study of Nickel-Titanium Gates Glidden Drills. J. Endodont. 31, pp. 523-525.

Mahmud, A.S., Yinong, L., Tae-hyun, N., 2008. Gradient anneal of functionally graded NiTi. Smart Mater. Struct. 17, 015031.

Miyazaki S., 1990. Thermal and stress cycling effects and fatigue properties of Ni-Ti Alloys, in: Engineering Aspects of Shape Memory Effect, Edit. T.W. Duerig et al, Butterworth-Heinemann, London, pp. 394-413.

Nasser, R., Yadla, S., Maltenfort, M.G., Harrop, J.S., Anderson, D.G., Vaccaro, A.R., Sharan, A.D., Ratliff, J.K., 2010. Complications in spine surgery. J. Neurosurg-Spine. 13, pp. 144-157.

Otsuka, K., Wayman, C.M., 1999. Shape Memory Materials. Cambridge University Press.

Park, K.-W., Bio-flexible spinal fixation apparatus with shape memory alloy. U.S. Patent 7,727,259, Jun 1, 2010.

Park, P., Garton, H.J., Gala, V.C., Hoff, J.T., McGillicuddy, J.E., 2004. Adjacent Segment Disease after Lumbar or Lumbosacral Fusion: Review of the Literature. Spine. 29, 1938-1944.

Patterson, C.M., Veldman, M.S., Allard, R., Variable Stiffness Support Members. U.S. Appl. 20100160967, Dec 22, 2009.

Petit, D., Droulout, T., Dynamic linking element for a spinal attachment system, and spinal attachment system including said linking element. U.S. Patent 2007/0129729, Mar 2, 2005.

Qinglin, M., Yinong, L., Hong, Y., Shariat, B.S., Tae-hyun, N., 2012. Functionally graded NiTi strips prepared by laser surface anneal. Acta Mater. 60, pp. 1658-1668.

Saburi, T., Tatsumi, T., Nenno, S., 1982. Effects of heat treatment on mechanical behavior of Ti-Ni alloys. J. Phys. Colloques 43, C4-261-C264-266.

Saburi, T., Nenno, S., Nishimoto, Y., Zeniya, M., 1986. Effects of thermo-mechanical treatment on the shape memory effect and the pseudoelasticity of Ti-50.2Ni and Ti-47.5 Ni-2. 5 Fe alloys. J. Iron Steel Inst. Jpn. 72, 571.

Todoroki, T., Tamura, H., 1987. Effect of Heat Treatment after Cold Working on the Phase Transformation in TiNi Alloy. Mater. Trans. 28, 83.

Trieu, H.H., Vertebral rod system and methods of use. U.S. Appl. 2010/0222820, Sep 2, 2010.

Zylber, E., Egli, T., Thompson, R., Froehlich, M., Cicerchia, G., Dant, J.A., Viker, T.O., Ley, K.R., 2011. Spinal stabilization system with rigid and flexible elements. U.S. Appl. 20080234744, Sep 25, 2008.

CHAPITRE 3

MONOLITHIC SUPERELASTIC RODS WITH VARIABLE FLEXURAL STIFFNESS FOR SPINAL FUSION : MODELING OF THE PROCESSING-PROPERTIES RELATIONSHIP

Yann Facchinello[1,2], Vladimir Brailovski[1,2], Yvan Petit[1,2], Jean-Marc Mac-Thiong[2,3]

[1]Département de Génie Mécanique, École de technologie supérieure,

1100 Notre-Dame Ouest, Montréal, Québec, Canada H3C 1K3

[2]Centre de recherche, Hôpital du Sacré-Cœur de Montréal,

5400, boul. Gouin Ouest, Montréal, Québec, Canada H4J 1C5

[3]Département de chirurgie, Faculté de médecine, Université de Montréal,

Pavillon Roger-Gaudry, Local : S-749, Montréal, Québec, Canada H3C 3J7

Article publié dans la revue « Medical Engineering & Physics », v 36, n 11, p 1455-63, Nov. 2014

3.1 Résumé

Cet article décrit un modèle permettant de simuler l'impact du procédé de fabrication sur les propriétés mécaniques dans le cas de la fabrication de tiges à rigidité variables pour la stabilisation de la colonne vertébrale. Dans un premier temps, une base de données a été créée afin de connaitre les propriétés mécaniques correspondantes aux différentes températures de traitement thermique par effet Joule. Ensuite, un modèle thermique a été développé afin de prévoir le gradient de température présent sur une tige lors d'un traitement thermique local par effet Joule. En combinant ce gradient de température et la base de données créée précédemment, un gradient de propriétés mécaniques peut être créé le long de la tige. Après validation, deux applications sont proposées pour un tel modèle a) optimisation des paramètres (courant, durée) de chauffage et b) prédiction du comportement mécanique d'une tige à rigidité variable.

3.2 Abstract

The concept of a monolithic Ti-Ni spinal rod with variable flexural stiffness is proposed to reduce the risks associated with spinal fusion. The variable stiffness is conferred to the rod using the Joule-heating local annealing technique. The annealing temperature and the mechanical properties' distributions resulted from this thermal treatment are numerically modeled and experimentally measured. To illustrate the possible applications of such a modeling approach, two case studies are presented: a) optimization of the Joule-heating strategy to reduce annealing time, and b) modulation of the rod's overall flexural stiffness using partial annealing. A numerical model of a human spine coupled with the model of the variable flexural stiffness spinal rod developed in this work can ultimately be used to maximize the stabilization capability of spinal instrumentation, while simultaneously decreasing the risks associated with spinal fusion.

3.3 Introduction

Spinal disorders can be treated by several means including multisegmental fusion surgery. Rigid posterior instrumentations are commonly used to prevent motion of the instrumented segment and aid fusion healing [1, 2]. However, this procedure brings its own problems, including adjacent-level disc disease. Due to the abrupt stiffness variation between the instrumented and intact spinal segments, stresses are increased locally, which is commonly considered as a factor leading to disc degeneration [3]. The use of so-called dynamic stabilization systems have been proposed to lower the stress concentration at the extremities of the implant and to reduce the risk of adjacent segment degeneration [4]. Those "soft" instrumentations are however accompanied by problems such as mechanical failure of the implant or degeneration within the stabilized segment [5, 6].

An ideal implant would combine stiff and compliant properties by providing the required stiffness where a strong stabilization is needed while allowing a greater flexural compliance where motion and load-sharing capacity are more important. This complexity of properties can be obtained by different methods including the use of Ti-Ni shape memory alloys. The

mechanical properties of these metallic alloys are greatly conditioned by their thermomechanical processing as described by [7, 8, 9] and can be finely controlled by local annealing [10, 11]. In has been shown that for the same Ti-Ni alloy, the alloy's elasticity modulus can range from 30 to 60 GPa depending on the thermomechanical processing applied [12]. It has also been shown that monolithic Ti-Ni rods with variable mechanical properties could be produced using localized Joule-heating heat treatment [12]. Different sections of these rods then manifest different behavior, ranging from elastoplasticity to superelasticity and even pseudoplasticity (shape memory), each behavior corresponding to different stiffness. These technological possibilities allow multisegmental monolithic spinal rods to be designed with locally-controlled flexural stiffness, which would combine improved stabilization capacity and reduced stress concentration at the implant extremities.

The main objective of this study is to develop and validate numerical models of the Ti-Ni variable-stiffness spinal rods' processing and behavior, which could ultimately be used in human spine models to find a compromise between the static and the dynamic stabilization capacities of spinal instrumentations.

3.4 Materials and methods

Figure 3.1 illustrates the overall path followed in this study. First, a numerical model simulating localized Joule-heating on a 5.5 mm diameter rod is developed and validated by comparing experimental data with calculations. Such a model is found capable of predicting the temperature distribution on a locally-annealed rod as a function of a given electric current intensity - heating time schedule. Next, a series of Ti-Ni specimens are subjected to variable Joule-heating heat treatments and mechanically characterized by tensile testing to produce a set of annealing temperature-dependant stress-strain diagrams (material law). Each stress-strain diagram can then be assigned to a specific annealing temperature. By combining the temperature distribution of the locally-annealed rod and the material law, a numerical model capable of simulating the effect of Joule-heating annealing on the mechanical behavior of Ti-Ni variable-stiffness rods is developed and experimentally validated. The developed

numerical tools are then used for two case studies involving: a) heating strategy optimization, and b) variable-stiffness rod's flexural behavior prediction.

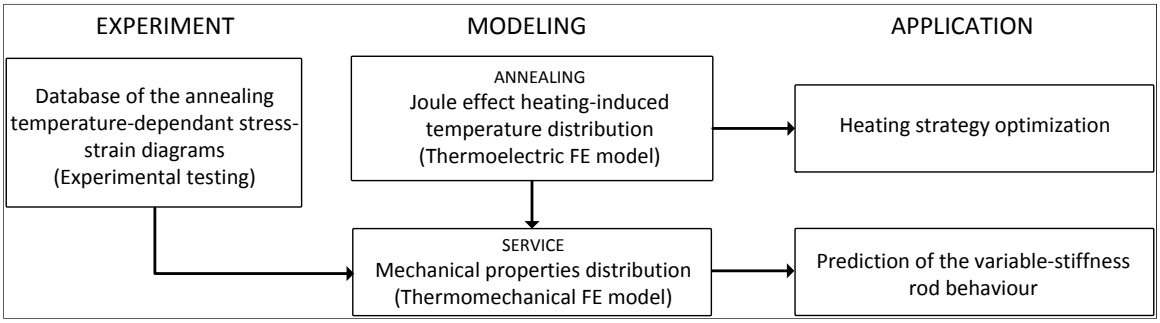

Figure 3.1 The path followed in this study

3.4.1 Material

The material is an as-drawn (cold worked strain of about 30%) Ti-55.94Ni (wt.%) 5.5 mm-diameter rod supplied by Johnson Matthey (San Jose, CA, USA).

3.4.2 Joule-heating annealing setup

Joule-heating post-deformation annealing (J-PDA) is performed on a custom-made bench (Figure 2) using an RE30-170 (Matsusada Precision, Japan) power supply capable of injecting 170 A at 30 V. Temperature is measured either by an E60 (FLIR Systems, USA) thermal imager, or by a K-type thermocouple (TT-K-36-SLE, Omega Eng. Inc, USA.).

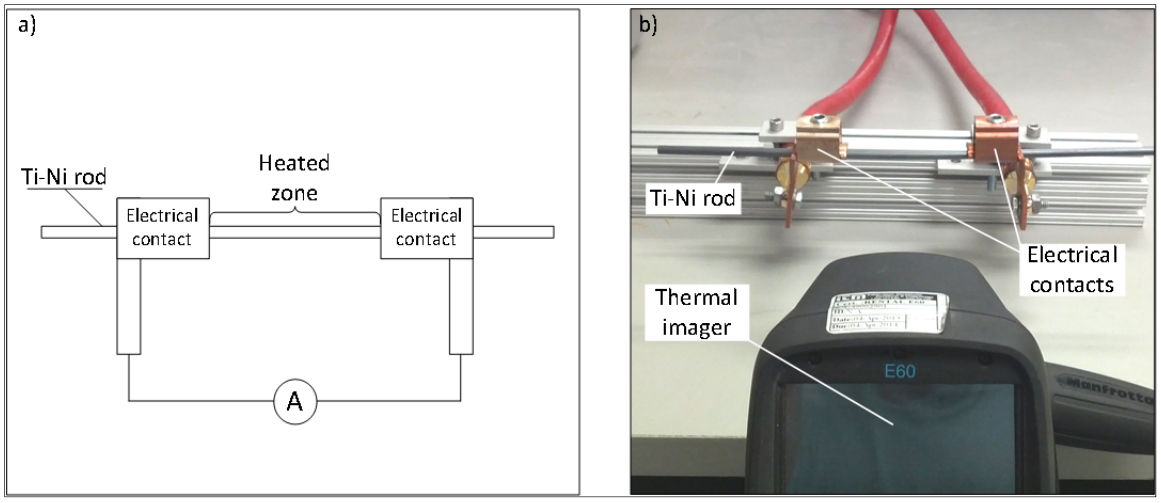

Figure 3.2 Joule-heating local annealing setup:
a) schematic representation; b) photography

3.4.3 Annealing: Joule-heating induced temperature distribution modeling and validation

Commercial ANSYS 14 finite element analysis (FEA) software is used to create the solid model of the rod and to analyze the effect of Joule-heating on the temperature distribution in the rod. The ANSYS' "Thermal-Electric" (steady-state) and "Transient Thermal" modules are used to simulate the local Joule-heating and its impact on the temperature distribution during annealing. The main inputs of the thermal-electric model are: the geometry and the electrical properties of the rod-electrical contacts assembly, the electrical current intensity, and the thermal exchange conditions with the surroundings. The output of the thermal-electric model is the volume distribution of the Joule heating-induced heat sources. These last data are used in the transient thermal model to calculate the temperature distribution in the rod-contacts assembly as a function of the heating time.

The complete model is a 25 cm long, 5.5 mm diameter rod with two electrical contacts composed of 6652 SOLID226 elements (Figure 3). The thermal convection coefficient (h) is defined by the equations provided in [13] for the horizontal cylinder (rod) (Eq 1 and Eq 2). The variables used in these equations are defined in Table 3.1 and a set of these variables is

provided in Table 3.2 for the reader's commodity. Table 3.3 presents a set of thermal model constants used in FEA.

$$h = \frac{k}{D}\left(0{,}6 + \frac{0{,}387Ra_D^{1/6}}{\left(1 + \left(\frac{0{,}559}{Pr}\right)^{9/16}\right)^{8/27}}\right)^2 \tag{3.1}$$

where Ra_D is the Rayleigh number:

$$Ra_D = \frac{g\beta(T_s - T_\infty)D^3}{\nu\alpha} \tag{3.2}$$

Table 3.1 Definition of the variables used in Eq 1 and Eq 2

Symbol	Description	Value	Unit
β	Air thermal expansion coefficient	1/ air temperature	K^{-1}
ν	Kinematic viscosity of the fluid	f(T)*	m^2/s
α	Thermal diffusivity of the fluid	f(T)*	m^2/s
k	Thermal conductivity of the fluid	f(T)*	W/(m.K)
Ts	Surface temperature of the rod	f(T)*	°C
T∞	Fluid temperature far from the object	22	°C
D	Rod diameter	5.5	mm
g	Gravitational acceleration	9.81	$m.s^{-2}$
Pr	Prandtl number	f(T)*	--
*See Table 3.2 for data's			
f(T) : Temperature-dependent value			

Table 3.2 Data adapted from Incropera and DeWitt (2002, p. 917)

Temperature (K)	**$v.10^6$ (m^2/s)**	**$k.10^3$ (W/m.K)**	**$\alpha.10^6$ (m^2/s)**	**Pr**
250	11,44	22,3	15,9	0,72
350	20,92	30	29,9	0,7
450	32,39	37,3	47,2	0,686
550	45,57	43,9	66,7	0,683
650	60,21	49,7	87,3	0,69
750	76,37	54,9	109	0,702
850	93,8	59,6	131	0,716

The electrical conductivity, specific heat and density of the alloy are provided by [8]. The emissivity values are adjusted so that the temperature values measured by the thermal imager and the thermocouple coincide. The thermal convection coefficient on the electrical contacts is defined by mapping the numerically calculated and the experimentally measured (thermal imager and thermocouple) temperatures. The thermoelectric model is validated by comparing the calculated temperature distribution with the measurements from an infrared thermal imager, as shown in Figure 3.2.

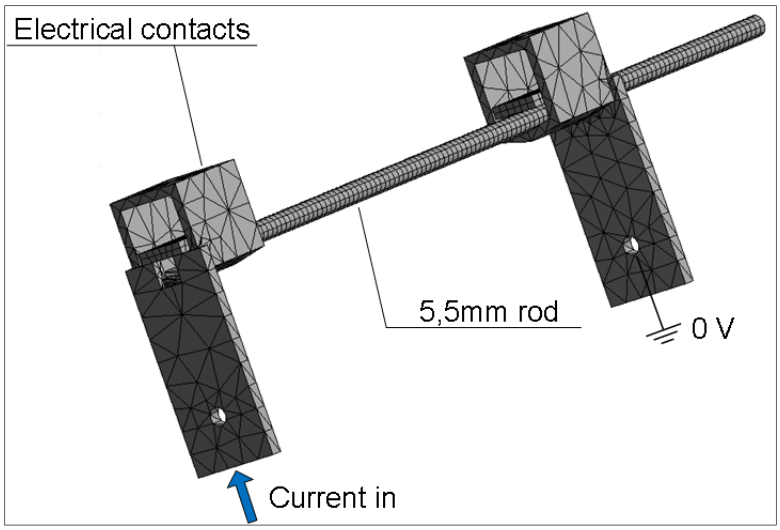

Figure 3.3 View of the thermal finite element model

Table 3.3 Parameters used for the thermal analysis

Property	Rod (Ti-Ni)*	Electr. cont. (Cu)**	Unit
Electrical conductivity, R	8.10^{-7}	$1{,}69.10^{-8}$	Ω.m
Thermal conductivity, α	15	401	W/m/°C
Convection, h	Eq 1	5***	$W/m^2/°C$
Emissivity, ε	0,97***	0,6***	--
Specific heat, c	500	385	J/kg/°C
Density, ρ	6450	8300	kg/m^3
*[8] Brailovski et al., 2003; ** ANSYS; *** experiment			

3.4.4 Mechanical behavior after Joule-heating annealing

3.4.4.1 Database of the annealing temperature-dependant stress-strain diagrams

To assess the property-modification capabilities of J-PDA, 10-minute Joule-heating of the as-drawn samples is performed to reach the following maximum steady-state temperatures on the rod: 260, 345, 430, 500 and 585°C. Evidently, this heating technique results in a certain temperature gradient along the sample, especially in the vicinity of the massive electrical contacts (heat sinks). To mitigate the effect of the uneven temperature distribution, the extremities of the specimens, which were subjected to high temperature gradients during annealing, are entirely clamped between the grips of the testing machine. This approach allows the mechanical behavior of the rod to be associated with a single processing temperature (see section 3.5.2 for more information).

Tensile testing of the specimens is realized on 25 cm long rods at room temperature using an MTS Alliance with a crosshead speed of 0.1 mm/s. Specimens are strained twice up to 6 % and released before loading to failure. Such a sequence allows the characterization of both the superelasticity-related and the conventional elastoplastic mechanical behavior of the material under study. Note that only the second –partially stabilized– loading-unloading cycle is used to define the material law utilized in the mechanical model (see the next section).

3.4.4.2 Mechanical model

The ANSYS 14 "Static Structural" module is used to build the mechanical model of the variable-stiffness cantilevered rod loaded at its free extremity by a vertical force (Figure 3.4a).

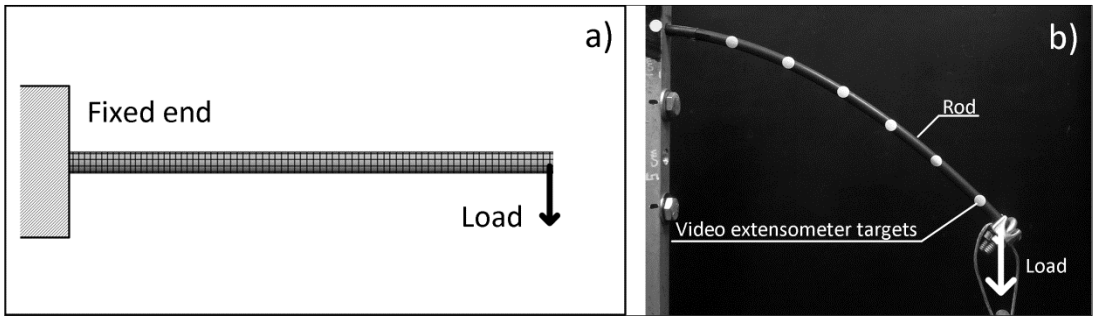

Figure 3.4 a) view of the mechanical model and its boundary conditions;
b) photography of the sample under cantilevered bending

The 25cm-long rod is meshed using 3306 SOLID186 elements. The mechanical behavior of the implant is modeled using the ANSYS SMA superelastic material law accessed via the TB (Data table) command, which requires the following set of data as the input: $\sigma_{s,t}^{AS}, \sigma_{f,t}^{AS}, \sigma_{s,t}^{SA}, \sigma_{f,t}^{SA}$, ε_L, E_{aus}, and α (see the schematic representation of the superelastic loop in Figure 3.5).

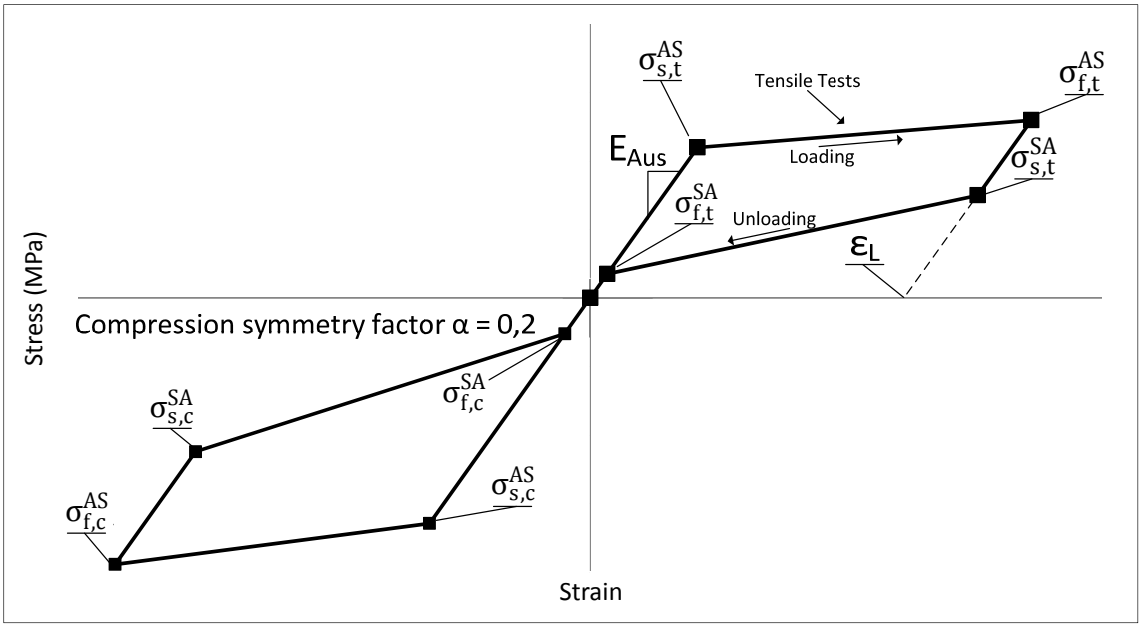

Figure 3.5 ANSYS superelastic material law and
the corresponding characteristic parameters

The constants stand for the starting and final stresses of the forward phase transformation, the starting and final stresses of the reverse phase transformation, the maximum superelastic plateau strain, and the Young's modulus of the austenite respectively in tension. The last parameter, α, measures the difference between the material responses in tension and compression, and it can be related to the initial values of austenite to martensite phase transformation in tension and compression ($\sigma_{s,t}^{AS}$, $\sigma_{s,c}^{AS}$ respectively) by the following expression:

$$\alpha = \frac{\sigma_{s,c}^{AS} - \sigma_{s,t}^{AS}}{\sigma_{s,c}^{AS} + \sigma_{s,t}^{AS}} \tag{3.3}$$

In this work, the tensile material characteristics were measured experimentally, while those in compression were calculated with α = 0.2 [14]. We are aware that such material law does not take into account the possibility for the material to be plastically deformed; its application could therefore result in unrealistically high stress values, especially under compression.

However, the level of stresses generated in our model is sufficiently low (see the next sections) to neglect the risk of plastic deformation.

To simulate the variation of material characteristics along the rod length, the correspondence between the annealing temperature distribution (thermal model) and the resulting mechanical properties is assessed using the experimentally-obtained set of stress-strain diagrams. In total, six sets of constants are then defined for the hardened state of the rod and after five annealing temperatures (260, 345, 430, 500 and 585°C). Knowing the annealing temperature of a given model's element, the mechanical model attributes to this element a set of superelastic constants corresponding to that temperature. If the element's actual temperature is situated between any two experimentally-obtained sets of data, a linear interpolation procedure is applied to create a new set of constants. This approach results in the creation of a numerical model of the variable-stiffness rod derived from the non-uniform temperature distribution caused by Joule-heating annealing.

3.4.4.3 Mechanical model validation

The mechanical model was validated by comparing the numerically predicted and experimentally measured bending profiles of a cantilevered rod loaded at its free extremity. The 25 cm long rod is loaded by a dead weight of 91 N and then partially unloaded to 47 N. This loading sequence allows for model validation under both loading and unloading. Performing both validation is relevant because the loading and unloading stress-strain paths of shape memory alloys differ (mechanical hysteresis). Bending profiles are measured using a LabVIEW-controlled video extensometer built with a GRAS-20S4M-C (Point Grey Research, Japan) video camera. A photograph of such testing is shown in Figure 3.4b).

3.5 Results

3.5.1 Joule heating-induced temperature distribution

The thermal model was validated by comparing the numerically-calculated temperature distribution with experimental measurements on a 25 cm long, 5.5 mm diameter rod with 60 mm between electrical contacts. Figure 3.6 presents: a) the simulated and experimental steady-state temperature distributions for different heating currents ranging from 80 to 150 A, and b) the simulated and experimental temperature distributions under a constant heating current of 150 A for heating times of 10 to 180s (transient state). It appears that with a 150A heating current, it takes 120s to reach the steady state.

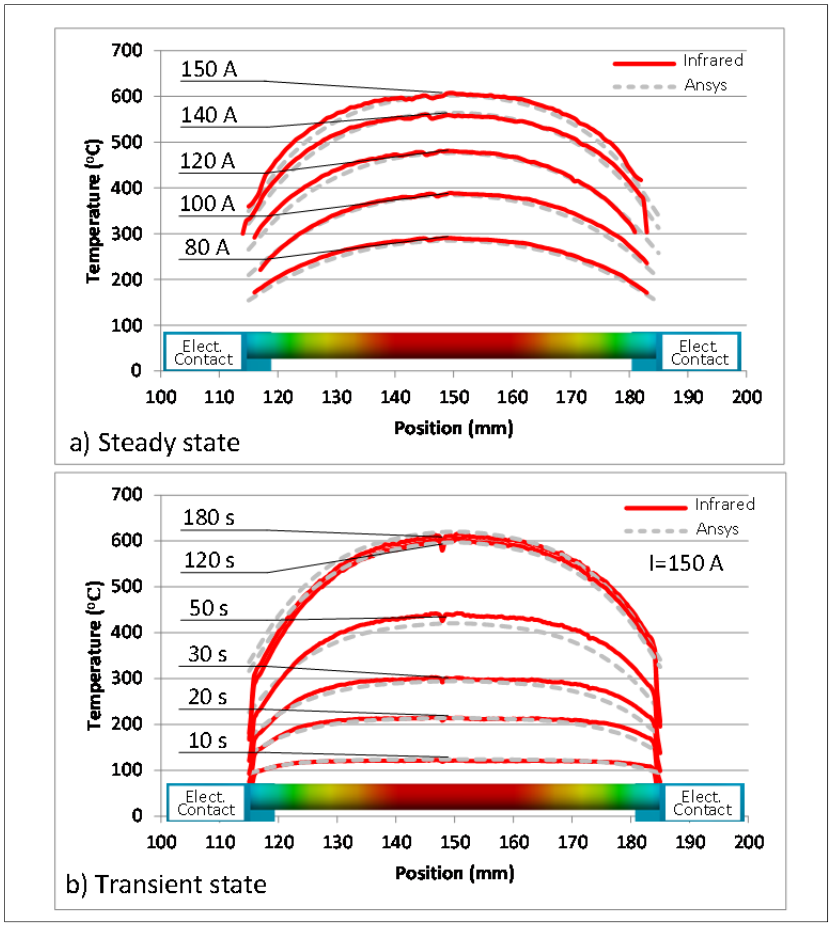

Figure 3.6 Temperature gradient between the electrical contacts for a) various heating currents in steady state and b) various heating duration at 150 A in transient state

3.5.2 Set of the annealing temperature-dependant stress-strain diagrams

In Figure 3.7, the tensile stress-strain diagrams of specimens subjected to J-PDA at various temperatures are plotted along with their ANSYS representations and characteristic parameters of the superelastic material law (430°C, 10 min). These data are collected in tabular form for the hardened (as-received) material and five annealing temperatures in Table 3.4. It appears that Joule heating annealing makes it possible to obtain radically different behavior, ranging from elastoplastic (hardened) to pseudoplastic with 30% deformation to failure (528°C). Between these two limits, 430°C Joule-heating (10 min) is considered as an optimum treatment, perfectly restoring the superelastic behavior of the hardened material.

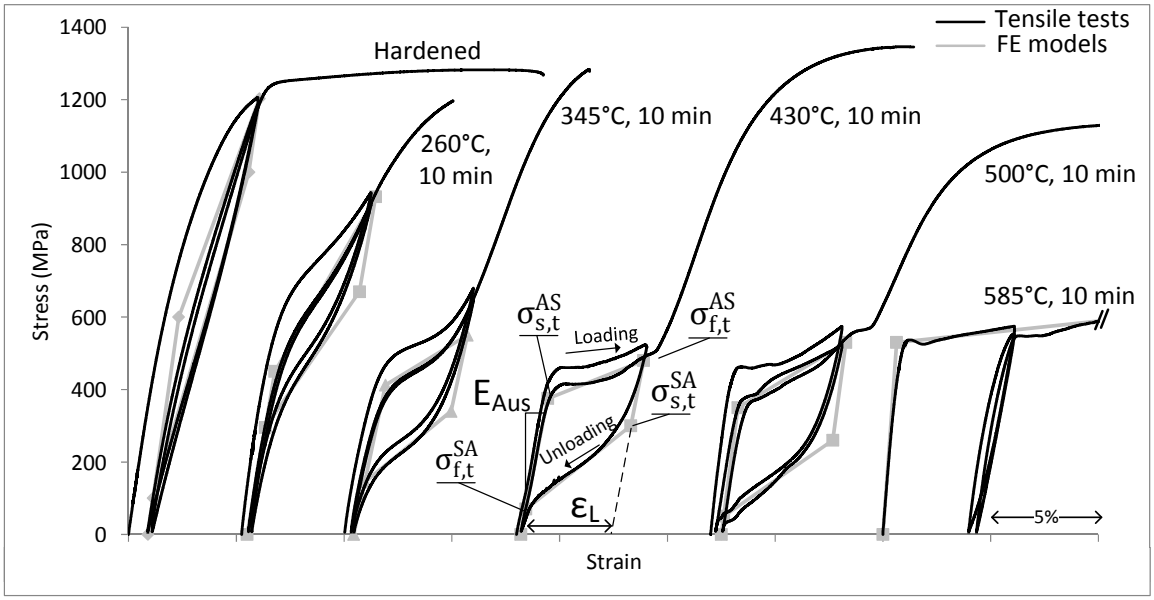

Figure 3.7 Stress-strain diagram of Ti-55,94wt%Ni annealed at different temperatures and the corresponding idealized curves for FE analysis. Characteristic constants are illustrated on the 430°C, 10 min diagram

Table 3.4 Parameters of the ANSYS TB, SMA material law

	Annealing temperature (°C)					
Model's parameters	**Hardened**	**260**	**345**	**430**	**500**	**585**
$\sigma^{AS}_{s,t}$ (MPa)	600	480	360	375	346	532
$\sigma^{AS}_{f,t}$ (MPa)	1203	900	510	480	518	683
$\sigma^{SA}_{s,t}$ (MPa)	1000	631	340	250	260	0
$\sigma^{SA}_{f,t}$ (MPa)	100	295	145	60	30	0
ε_L	0,023	0,033	0,035	0,044	0,04	0,24
E_{Aus}(GPa)	42	40	28	35	35	84
A	0,2	0,2	0,2	0,2	0,2	0,2

Joule heating results in a significant temperature gradient along the sample. However, since the extremities of the specimens are clamped into the grips of the testing machine (Figure 3.8), the tensile stress-strain diagrams shown in Figure 3.7 are associated with a single processing temperature measured in the middle of the rod.

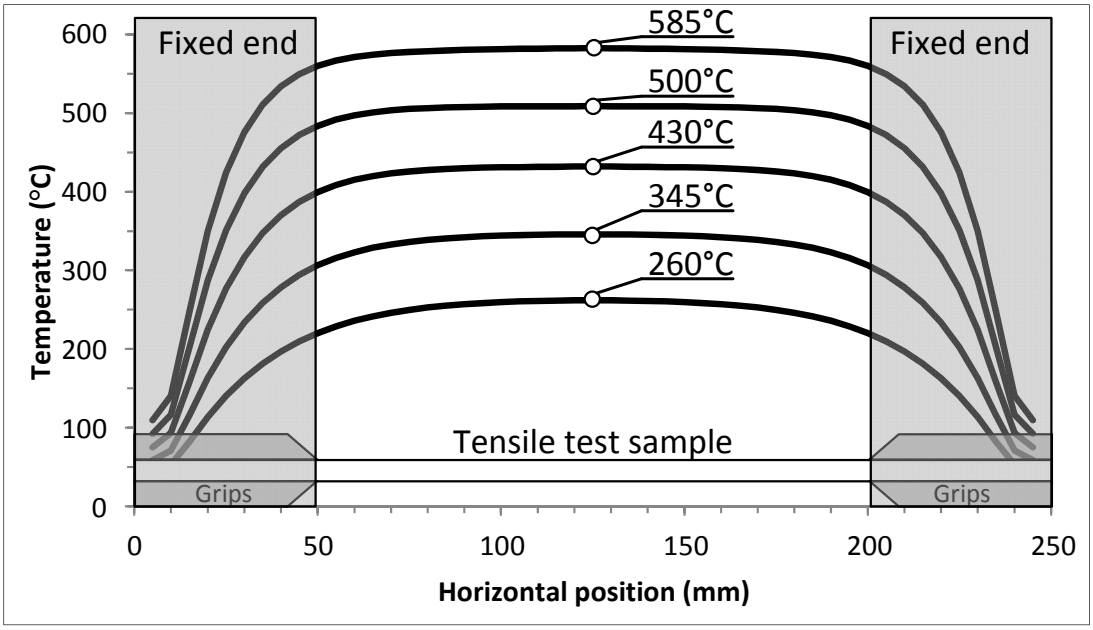

Figure 3.8 Calculated temperature distributions during annealing of the samples used to create the set of the annealing stress-strain diagrams

3.5.3 Mechanical behavior after Joule-heating annealing

Figure 3.9a compares the cantilevered bending profiles from experiments (black bold line) and from a finite element model (grey dotted line) of a Ti-Ni rod subjected on half of its length to Joule-heating annealing at a maximum temperature of 430^{o}C (see the annealing temperature distribution on top of Figure 3.9). Figure 3.9a shows that the model is capable of predicting the mechanical behavior of a heterogeneous Ti-Ni rod after local Joule-heating. Figure 3.9 b,c present the calculated stress distribution in the two cross-sections of the sample: A-A (Figure 3.9b) and B-B (Figure 3.9c). The stress distributions and the corresponding positions on the stress-strain curves of the A-A cross-section indicate that the samples were loaded to the transformation plateau and that the non-linear and hysteretic behavior of the material are fairly modeled. Furthermore, higher compressive and lower tensile stresses reflect the highly asymmetrical tension-compression behavior of Ti-Ni alloys. The B-B cross section is loaded in the elastic zone with the resulting symmetrical tension-compression stress distribution.

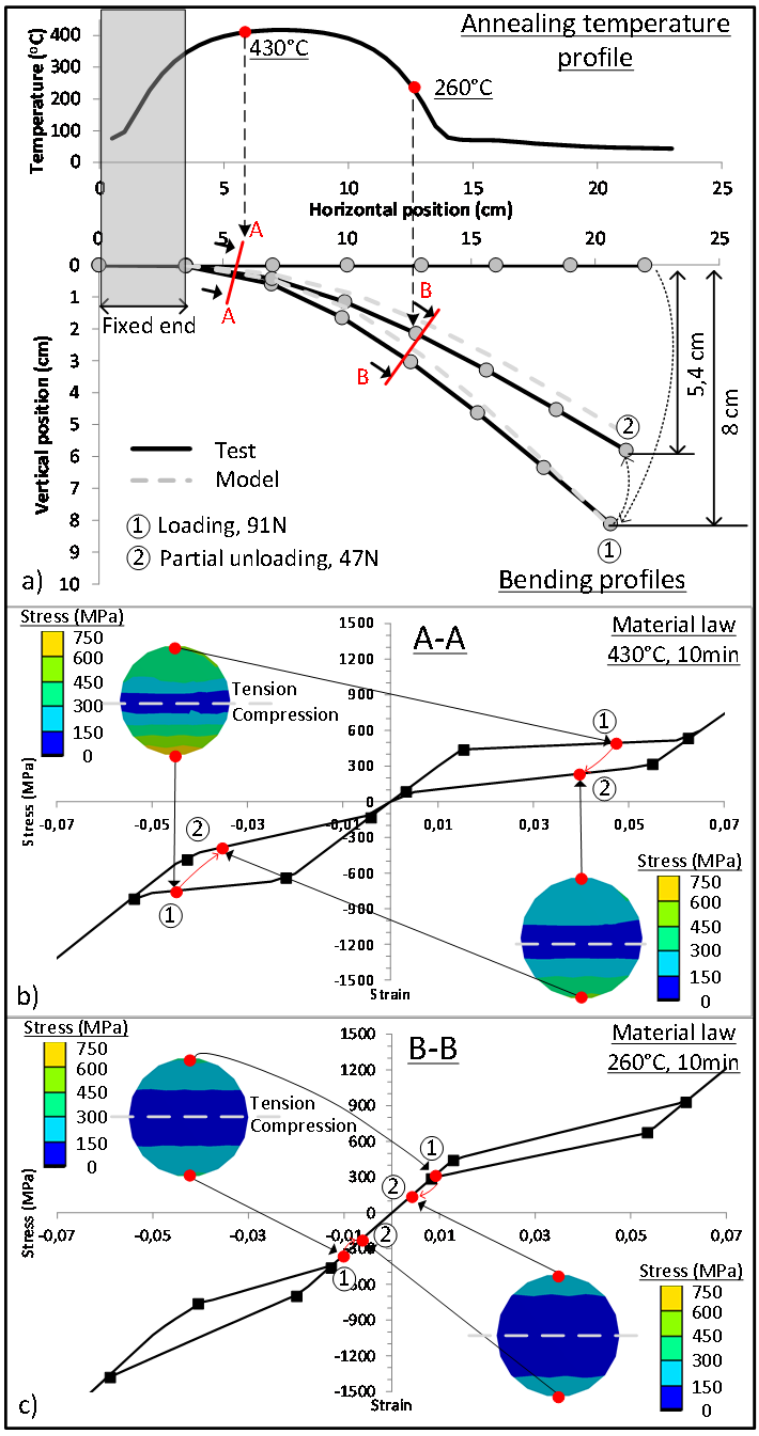

Figure 3.9 a) Temperature profile and bending profiles: (1) loading 91N, (2) – partial unloading, 47N; Stress distributions in the cross-sections A-A (b) and B-B (c) and the corresponding positions stress-strain diagrams

3.6 Models applications

3.6.1 Thermal model: testing different Joule-heating current-time schedules

The validated thermal model makes it possible to study the Joule-heating kinetic and to numerically test different heating strategies. Two paths can be considered to reach the same target temperature of 400^{o}C in the middle of the rod: A) one-step heating consisting by applying a constant current of 110 A all over the heating period, and B) two-step heating consisting of the application of a higher current (150 A) to reach the target temperature faster, followed by lowering the current to 105 A to stabilize the temperature. To illustrate this application, Figure 3.10 presents: a) the evolution of the temperature in the middle of the sample versus the heating time for various heating currents, and b) temperature profiles for two heating strategies (steady state). Figure 3.10a shows that a target temperature of about 400°C can be reached faster by applying a higher current intensity at the beginning of the heating and switching to a lower intensity when the desired temperature is reached. Such a process also affects the temperature distribution along the rod; and, in this case, allows enlarging the uniformly heated zone, as seen in Figure 3.10b.

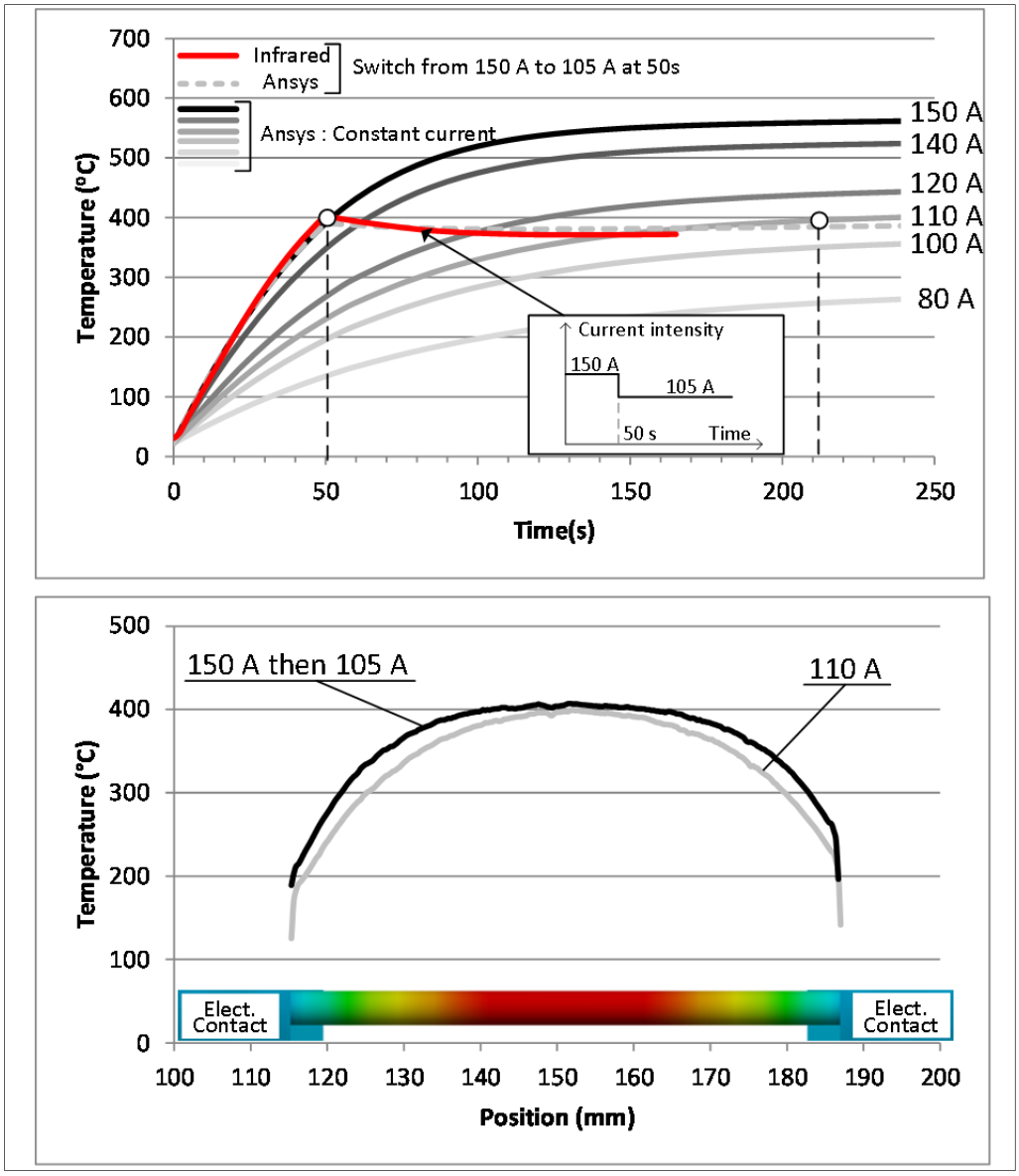

Figure 3.10 a) Temperature – time diagrams for various heating currents.
b) Experimental profiles obtained from two heating regimes:
1) 150 A for 50 s then 105 A and 2) 110 A.
Both profiles were taken as soon as the steady state was reached

3.6.2 Mechanical model: prediction of the variable-stiffness rod's flexural behavior

To illustrate the application of the mechanical model, Figure 3.11 presents a half superelastic–half hardened rod submitted to bending in two mirror-like configurations: with the superelastic part fixed and with the hardened part fixed. It can be observed that when the hardened part is fixed, the deflection is lower than when the superelastic part is fixed, due to the higher elastic modulus and absence of the transformation plateau in the first case. Since the numerically predicted bending profiles were experimentally validated (Figure 3.11a and b), it can be concluded that the model can accurately predict the flexural behavior of a heterogeneous rod. Such modeling capacity can be used in an instrumented spine model to assess the stabilization potential of variable flexural stiffness instrumentation.

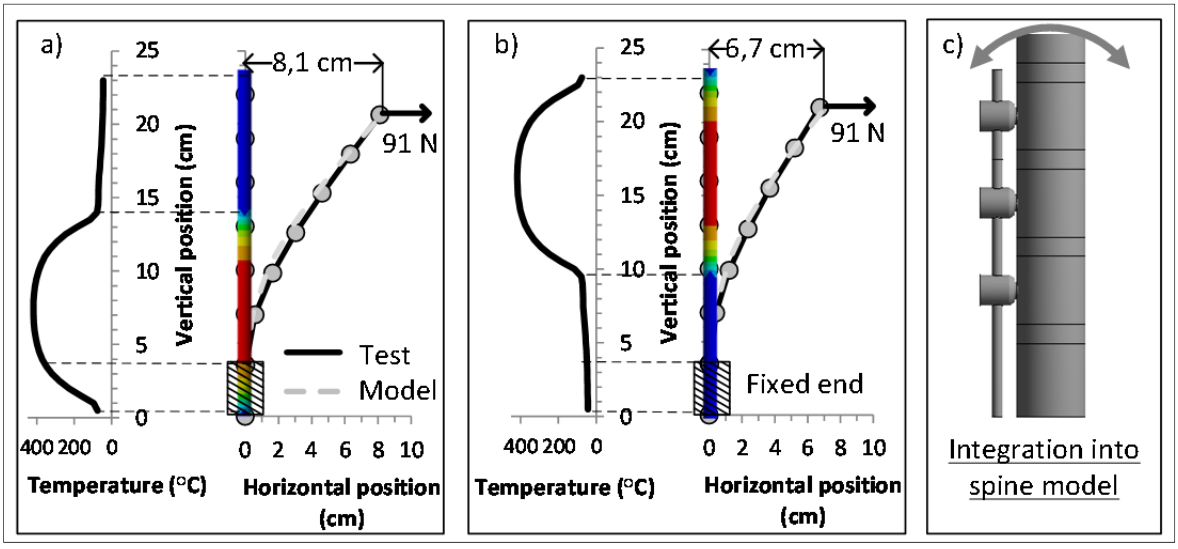

Figure 3.11 Application of the mechanical model: a,b) temperature distributions and bending profiles with a) superelastic end fixed, and b) hardened end fixed; c) Illustration of a potential integration into an instrumented model of the human spine

3.7 Discussion

Posterior dynamic stabilization has become a widely spread surgical intervention that can be performed using various types of implants [5, 15]. Most of these implants are, however, mechanically complex and not always biomimetic. Also, the optimum mechanical properties of dynamic fixation devices not yet been fully determined and the efficiency of such devices has yet to be proven [6, 16]. In this work, the use of shape memory alloy is proposed for the development of spinal stabilization rods with variable flexural stiffness.

It has been shown that Ti-Ni shape memory alloys of a given composition can exhibit different stress-strain behavior ranging from elastoplastic (hardened state) to superelastic, or rubber-like, with 30% elongation to failure (completely annealed) [17]. The tensile tests performed in this work showed that these different behaviors can be obtained with the same Ti-55.94wt.%Ni alloy subjected to Joule-heating annealing under different conditions (see Figure 7). Joule-heating at 585°C and higher leads to pseudoplastic behavior suitable for the contouring of the implant by the surgeon, while J-PDAs at temperatures between 345 and 430°C result in superelastic behavior.

A previous study showed that by utilizing local Joule-heating, a superelastic zone could be obtained within a hardened sample. Due to the temperature gradient created by the Joule-heating, a mechanical properties gradient could also be achieved [12]. By varying the annealing temperature along the rod, it is possible to obtain stiffer behaviors where strong stabilization is needed, and softer behavior where dynamic properties are more desirable. As for a classic titanium implant, the SMA rod is free of any mechanical assembly, which improves its reliability. It has been shown also that the fatigue live of heterogeneous rods is comparable to that of homogeneous rods. Such implants can also be easily tailored to a specific patient during surgery, since the annealing time required to modify the material behavior can be as short as several minutes [18].

A finite element model of a Ti-Ni rod with variable properties and its specific processing by Joule-heating have been developed, presented and validated in this work. Simulating the processing makes it possible to: 1) optimize the heating schedule and 2) predict the flexural behavior of the variable-stiffness rod. After validation of the thermal model, it was possible to study the heating speed and the temperature profile for different heating strategies. It was shown that the annealing time and temperature profile could be optimized for a given application.

The model was also used to study a half-annealed/ half-hardened rod under bending load. The stress distribution in the A-A cross section (superelastic zone) in Figure 9b shows that under loading above the first "yield point", strains as high as 6% can be achieved with only a small stress increase. This behavior appears to be suitable for a spine implant because in the case of large patient motion, the load applied to the pedicle screws would not increase nearly as much as it would with a classic elastic implant. Under unloading, the stress is considerably lowered but does not fall to zero. This again limits the pullout force applied on the pedicle screws, while maintaining a certain level of stability.

To determine if such an implant is suitable for spine stabilization, a finite element analysis is necessary to compare the classic rigid instrumentation with the proposed new instrumentation. The model presented in this paper could be implemented in a spine model to study its efficiency. That process would also make it possible to determine the optimal geometry and configuration of the implant (superelastic zone vs hardened zone).

3.8 Conclusion

A finite element model that can simulate the gradient of mechanical properties obtained after local Joule-heating of a Ti-55.94wt.%Ni rod has been developed. The processing model has been presented and validated by comparison with experimental data. The results of the simulation were combined with the experimental material characterization to define the mechanical properties' gradient. The model was loaded by cantilevered bending and the

results compared with experimental data for both a homogeneous sample and for a rod with variable properties. This study showed that the model is capable of predicting the mechanical behavior of a Ti-Ni rod with variable properties. It could also be useful to optimize the heating process of the rod. Such a model could be used within a spine model to assess the stabilization capability and to define an optimum stiffness profile of this new type of implant.

3.9 Acknowledgments

This work had been carried out with the financial support of the FQRNT (*Fonds de Recherche du Québec – Nature et Technologies*).

3.10 References

[1] Kotani Y, Cunningham BW, Cappuccino A, Kaneda K, McAfee PC, The role of spinal instrumentation in augmenting lumbar posterolateral fusion, Spine (Phila Pa 1976), 1996, 21, 278-87.

[2] Lorenz M, Zindrick M, Schwaegler P, Vrbos L, Collatz MA, Behal R, et al., A comparison of single-level fusions with and without hardware, Spine (Phila Pa 1976), 1991, 16, 455-8.

[3] DeWald CJ, Stanley T., Instrumentation-Related Complications of Multilevel Fusions for Adult Spinal Deformity Patients Over Age 65: Surgical Considerations and Treatment Options in Patients With Poor Bone Quality, Spine, 2006, 31, 144-51.

[4] Bono CM, Kadaba M, Vaccaro AR., Posterior Pedicle Fixation-based Dynamic Stabilization Devices for the Treatment of Degenerative Diseases of the Lumbar Spine, Journal of Spinal Disorders & Techniques, 2009, 22, 376-83.

[5] Barrey CY, Ponnappan RK, Song J, Vaccaro AR. Biomechanical Evaluation of Pedicle Screw-Based Dynamic Stabilization Devices for the Lumbar Spine: A Systematic Review, SAS Journal, 2008, 2, 159-70.

[6] Kelly MP, Mok JM, Berven S., Dynamic Constructs for Spinal Fusion: An Evidence-Based Review, Orthopedic Clinics of North America, 2010, 41, 203-15.

[7] Brailovski V, Khmelevskaya IY, Prokoshkin SD, Pushin VG, Ryklina EP, Z. VR., Foundations of Heat and Thermomechanical Treatments and Their Effect on the Structure and Properties of Titanium Nickelide–Based Alloys, The Physics of Metals and Metallography, 2004, 97, 3-55.

[8] Brailovski V, Prokoshkin S, Terriault P, Trochu F., Shape Memory Alloys: Fundamentals, Modeling and Applications; Ecole de Technologie Superieure; 2003.

[9] Otsuka, K., Wayman, C.M., Shape Memory Materials. Cambridge University Press. 1999.

[10] Groh JR., Local heat treatment for improved fatigue resistance in turbine components. European Patent Application. United States, 2007.

[11] Mahmud AS, Yinong L, Tae-hyun N., Gradient anneal of functionally graded NiTi. Smart Materials and Structures, 2008, 17, 015031.1-5.

[12] Facchinello Y, Brailovski V, Inaekyan K, Petit Y, Mac-Thiong J-M., Manufacturing of monolithic superelastic rods with variable properties for spinal correction: Feasibility study, Journal of the Mechanical Behavior of Biomedical Materials, 2013, 22, 1-11.

[13] Incropera FP, DeWitt DP.; Fundamentals of heat and mass transfer; John Wiley & Sons; 5th edition; 2002, 554-5.

[14] Orgeas L, Favier D., Non-symmetric tension-compression behaviour of NiTi alloy, International Conference on Martensitic Transformation ICOMAT 95, 20-25 Aug 1995. C8 ed. France: Editions de Physique; 1995. 605-10.

[15] Erbulut DU, Zafarparandeh I, Ozer AF, Goel VK., Biomechanics of Posterior Dynamic Stabilization Systems, Advances in Orthopedics, 2013, 2013, 6.

[16] Lee MJ, Lindsey JD, Bransford RJ., Pedicle screw-based posterior dynamic stabilization in the lumbar spine, Journal of the American Academy of Orthopaedic Surgeons, 2010, 18, 581-8.

[17] Demers V, Brailovski V, Prokoshkin SD, Inaekyan KE., Optimization of the cold rolling processing for continuous manufacturing of nanostructured Ti–Ni shape memory alloys, Journal of Materials Processing Technology, 2009, 209, 3096-105.

[18] Brailovski V, Petit Y, Mac-Thiong J-M, Driscoll M, Parent S, Labelle H. Apparatus and Method for Per-operative Modification of Medical Device Stiffness. U.S. Appl. US61/703388, 2012.

CHAPITRE 4

BIOMECHANICAL ASSESSMENT OF THE STABILIZATION CAPACITY OF Ti-Ni MONOLITHIC SPINAL RODS WITH DIFFERENT FLEXURAL STIFFNESS AND ANCHORING ARRANGEMENT.

Yann Facchinello[1,2], Vladimir Brailovski[1,2], Yvan Petit[1,2],Martin Brummund[1,2],
Jaëlle Tremblay[3], Jean-Marc Mac-Thiong[2,4]
[1]Département de Génie Mécanique, École de technologie supérieure,
1100 Notre-Dame Ouest, Montréal, Québec, Canada H3C 1K3
[2]Centre de recherche, Hôpital du Sacré-Cœur de Montréal,
5400, boul. Gouin Ouest, Montréal, Québec, Canada H4J 1C5
[3]Zimmer CAS, auparavant avec Centre de recherche, Hôpital du Sacré-Cœur de Montréal
[4]Département de chirurgie, Faculté de médecine, Université de Montréal,
Pavillon Roger-Gaudry, Local : S-749, Montréal, Québec, Canada H3C 3J7

Article publié dans la revue « Clinical biomechanics » en septembre 2015.
doi:10.1016/j.clinbiomech.2015.09.011

4.1 Résumé

Cet article présente les résultats obtenus lors de l'étude biomécanique sur spécimens porcins menée afin d'identifier les éventuels bénéfices liés à l'utilisation des tiges aux propriétés variables. Les essais ont été réalisés sur des segments lombaires (L1-L6). Trois types de tiges (Ti, Ti-Ni superélastique et Ti-Ni variables) ont été implantés sur six segments vertébraux. Deux configurations d'ancrage ont été testées : vis pédiculaires uniquement ou alors, vis pédiculaires combinées à deux crochets transverses à l'extrémité de l'instrumentation. Les spécimens intacts et instrumentés ont été chargés en déplacement contrôlé (18°) selon trois directions : flexion, extension et inflexion latérale. Les détails concernant le montage expérimental sont présentés en Annexe II. La rigidité des spécimens, les rotations vertébrales, les efforts sur les ancrages ainsi que la pression intradiscale du disque

instrumenté supérieur ont été enregistrés lors des mouvements. Ces tests ont permis de constater que l'utilisation de tiges variables et de crochets transverses permet de créer une transition de mobilité entre la zone stabilisée et le segment intact. De plus, l'extrémité souple de la tige variable permet de réduire considérablement les efforts appliqués sur les processus transverses par les crochets comparativement aux tiges de titane.

4.2 Abstract

In vitro biomechanical tests were conducted on porcine spine segments (L1-L6) to assess the stabilization capacity of Ti-Ni spinal rods with variable flexural stiffness. Dual-rod fusion constructs containing three kinds of rods (Ti, Ti-Ni superelastic and Ti-Ni half stiff – half superelastic) were implanted using two anchor arrangements: pedicle screws at all levels or pedicle screws at all levels except for upper instrumented vertebra, in which case pedicle screws were replaced with transverse process hooks. Specimens were loaded in forward flexion, extension and lateral bending before and after implantation of the fusion constructs. The effects of different rods on vertebra mobility, intradiscal pressures and forces on the anchors were evaluated. The rod properties had a moderate impact on the biomechanics of the instrumented spine when only pedicle screws were used. However, this effect was amplified when transverse process hooks were used as proximal anchors. Combining transverse hooks and softer (Ti-Ni superelastic and Ti-Ni half stiff – half superelastic) rods provided more motion at the UIV level and applied less force on the anchors, potentially improving the load sharing capacity of the instrumentation.

4.3 Introduction

Spinal fusion is a common treatment to relieve chronic back pain, instability or neurological injury. Strong and rigid posterior constructs are used to prevent fixation failure and to provide the stability needed for fusion (Kotani et al., 1996; Lorenz et al., 1991). However, because of an abrupt variation in stiffness between the instrumented and the intact spinal segments, the range of motion between the end of the construct and the adjacent segment

changes suddenly, which leads to high stress concentration in the transition zone, to the adjacent segment degeneration, proximal junctional kyphosis (PJK) or even fractures (DeWald and Stanley 2006, Hassanzadeh et al., 2013; Helgeson et al., 2010).

So-called dynamic stabilization systems (DSS) have been proposed to provide more motion at the upper instrumented vertebra (UIV) level and to reduce the risk of adjacent segment degeneration. However, DSS are often mechanically complex, bulky and frequently associated with inadequate stability or persistent PJK (Bono et al., 2009). For example, (Li et al., 2013) reported on two-year follow-up of 36 patients who underwent surgery using the Isobar TTL Semi-Rigid Rod System. The system did not show superior results compared to traditional fusion constructs, as 14 patients showed signs of PJK despite the use of DSS.
An ideal implant should combine high stabilization capacity where fusion is needed, with a gradual transition between the instrumented and intact spine segments to reduce stress on the adjacent segment, while maintaining a low level of force on the anchors.

Such a transition could be obtained by modifying the rod stiffness or by changing the anchor arrangement. For example, (Bruner et al., 2010) performed an in vitro study to compare titanium and composite rods. They showed that customizing the bending compliance of a dynamic rod according to specific patient needs allows a certain improvement in the load sharing capacity of instrumentation. However, an abrupt change in mobility between the instrumented and the intact spine segments is still problematic even for rods with significantly different flexural stiffness, such as titanium (Young's modulus E=110 GPa) or PEEK (E=3,6 GPa) , when they are anchored with pedicle screws (Gornet et al., 2011). On the other hand, (Thawrani et al., 2014) showed in an in vitro study that transverse process hooks at the upper instrumented vertebrae are effective for creating a gradual transition and relieve the stress on the adjacent segment.

Considering the above, the main objective of this study was to evaluate the effect of the flexural stiffness of the rod, combined with the use of different anchoring techniques at the

proximal end of the instrumentation on the load sharing capacity of the dual-rod spinal instrumentation.

A variation of the rod's flexural stiffness was obtained using Ti-Ni shape memory alloys. The mechanical properties of these alloys are strongly processing-dependent, and can be controlled by local annealing. Previous studies have shown that radically different mechanical properties could be obtained on monolithic Ti-Ni rods using local Joule-effect annealing. For example, a ten-minute annealing of Ti-Ni rods has allowed a variation of mechanical properties from elasto-plastic (Young's modulus E=50 GPa) to superelastic (E=36 GPa) or pseudoplastic (E=83 GPa) (Facchinello et al., 2013). Using this technology, it was possible to produce 5.5 mm diameter spinal rods with variable flexural stiffness (Facchinello et al., 2014a).

The different anchoring techniques at the proximal end of the instrumentation used in this study were either pedicle screws or transverse process hooks.

To summarize, this paper presents the results obtained by in vitro testing of Ti-Ni rods with variable flexural stiffness anchored to a porcine spine specimen with pedicle screws or transverse process hooks, which are compared with conventional Ti rods of the same size.

4.4 Materials and methods

The biomechanical testing was conducted on six lumbar porcine spine models (L1-L6, 6-8 months, about 220 lbs).

4.4.1 Specimen preparation and fixation

Upon reception of fresh spines, soft tissues were dissected, while ensuring that the ligaments, intervertebral discs and bones were preserved intact. On the same day, holes were free-hand drilled in the L5, L4 and L3 vertebrae for subsequent pedicle screw insertion. The specimens were then stored frozen in plastic bags at -20 °C. Prior to testing, the specimens were thawed for 24 hours at 4 °C as recommended (Tremblay et al., 2015b). A saline solution was used to keep the specimen hydrated throughout the experiment.

The dual rods were then implanted using two anchoring strategies: fixed using pedicle screws (PS) (6.5x45mm, Ti, Medtronic) at all levels (L3, L4 and L5) or, instead of pedicle screws, the proximal ends of the rods were anchored using transverse process hooks (TPH) (Extended body, Ti, Medtronic). Polyester resin (Bondo, St. Paul, MN) was used to fix the end vertebrae to the testing apparatus. An aluminum bloc was used to solidly fix the caudal end of the rods. Such configuration was used to simulate an extended segment of dual-rod instrumentation. Figure 4.1 shows pictures of the specimens.

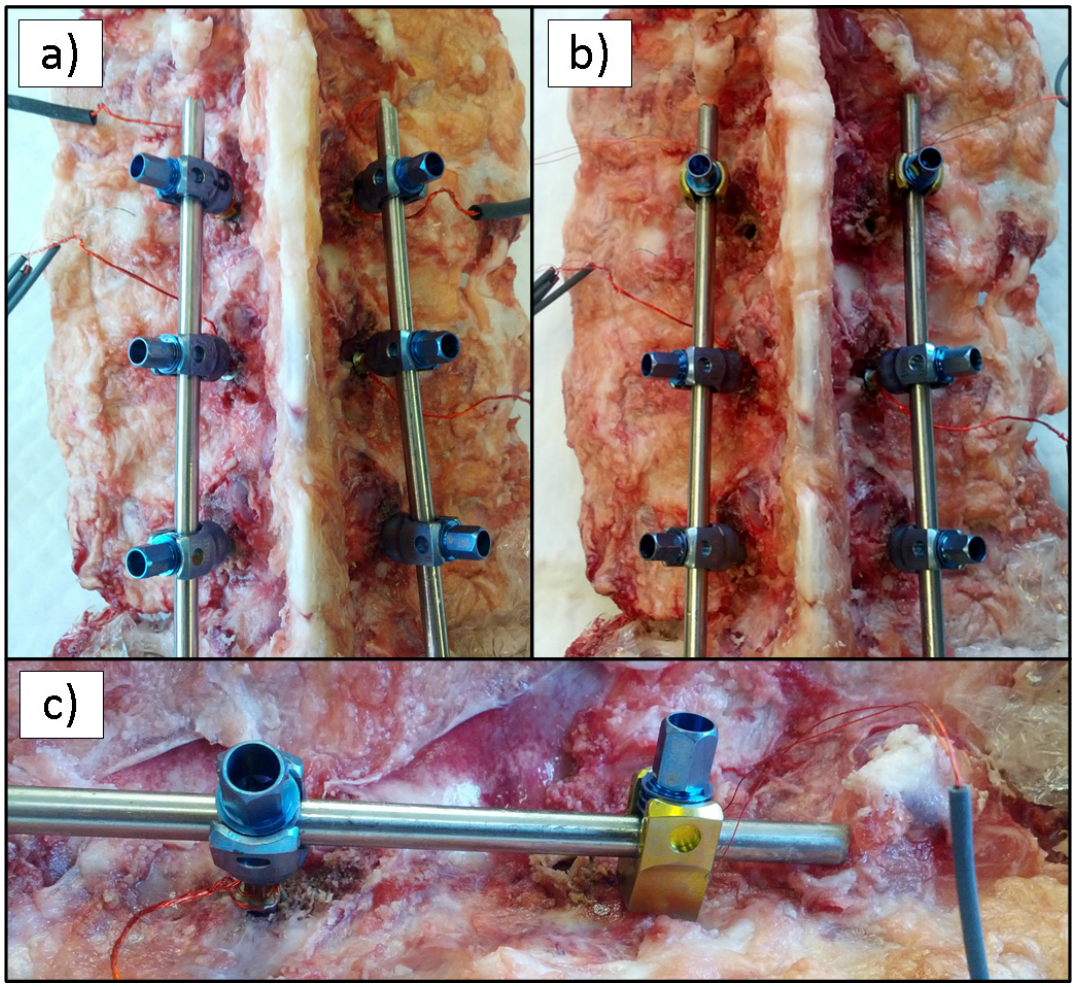

Figure 4.1 Pictures of an instrumented specimen with a) all pedicle screws, b) pedicle screws and transverse process hooks at the upper instrumented vertebra, and c) sideview of a pedicle screw and a transverse hook on a specimen.

4.4.2 Spinal rods

Three different 5.5 mm diameter rods were used: Titanium (Ti), Ti-Ni superelastic (SE) and Ti-Ni half pseudoplasic-half superelastic (VAR) (Figure 4.2). Titanium rods (Ti-6Al-4V, ELI) provided by Fort Wayne Metals (IN, USA) exhibit mechanical properties close to commercial titanium implants with a Young's modulus of 86 GPa (Figure 4.2a,b).

Ti-55.94wt.%Ni rods (Johnson Mattey Medical, PA, USA) were used as completely superelastic (SE) rods (E= 36 GPa) (Figure 4.2a,b), or as variable stiffness (VAR) rods (Figure 4.2b). To obtain the VAR rods, the SE rods were Joule-effect annealed (585°C, 10 min) on the half of their length (Facchinello et al., 2013; Facchinello et al., 2014a). This partial annealing transforms a compliant (E=36 GPa) SE material into a high-stiffness (E=83 GPa) pseudoplastic material (Ti-Ni (Mart)) (Figure 4.2a). Following this processing, the VAR rods contained superelastic and pseudoplastic parts of equal lengths with a gradual transition between the two (Figure 4.2b).

For the installation, the superelastic part of the VAR rods was always oriented towards the intact segment of the construct to reduce stress concentration in the adjacent segments of the spine (Figure 4.2c), in conformity with our calculations (Facchinello et al., 2014b).

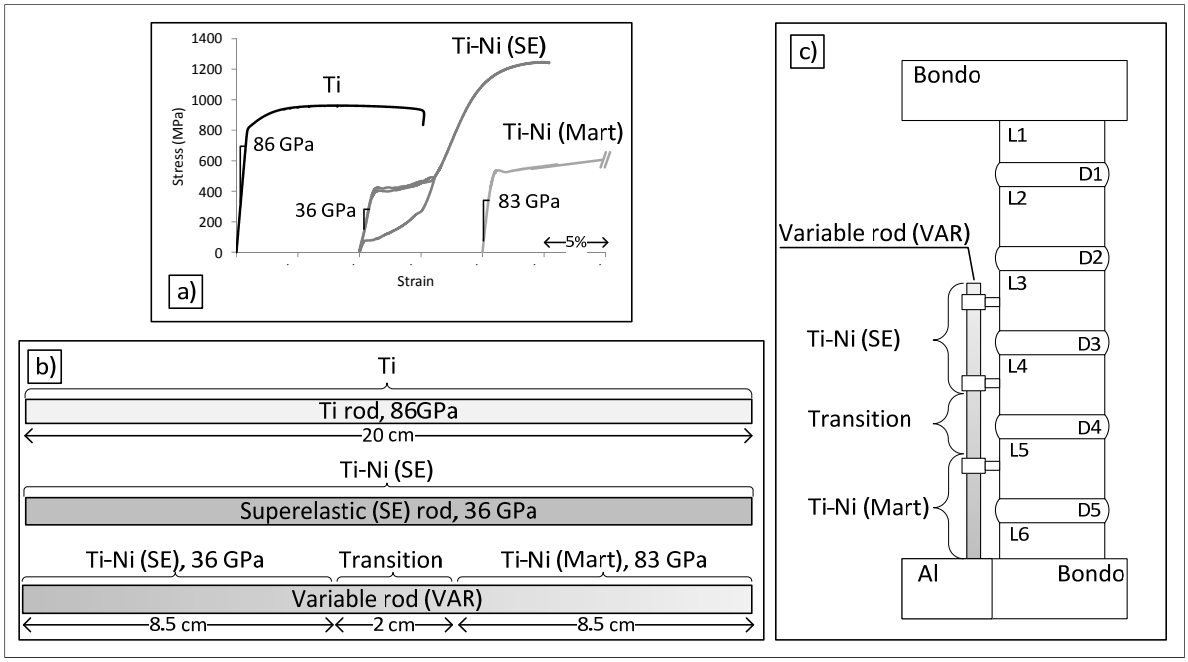

Figure 4.2 Mechanical behaviour (tension) of the different rods' constituents; b) Ti, SE and VAR rods' identification, and c) position of the VAR rods on porcine specimens

4.4.3 Biomechanical testing setup

Non-instrumented and instrumented specimens were tested under displacement-controlled forward flexion (FE), extension (EX) and lateral bending (LB) modes, using an MTS 858 Minibionix II (MN, USA: 15kN, 150 Nm). The order of the tested motions (FE, EX or LB) was randomized (Table 4.1). The maximum rotation of the distal end of the construct for all the testing modes corresponded to 18°, which is slightly inferior to the range of motion measured by (Wilke et al., 2011) under pure moment loading (7.5 Nm). This precaution was taken to decrease the risk of specimen damage during testing. Loading rate was 1°/s. During all tests, a follower load of 400 N was applied using a cable deadweight system to simulate spine loading conditions when surrounding muscles are kept intact (Panjabi, 2007; Patwardhan et al., 2003; Patwardhan et al., 1999; Wilke et al., 1998). The cables were guided along the spine segment through the eyelets attached to the side of each free vertebra (see Figure 4.3a) and e)). A 400N value corresponds to the middle of the preload range studied by (Patwardhan et al., 2003), and this value is recommended by (Goel et al., 2006). Axial

rotation tests were not performed in this study since this motion was not considered to be a significant PJK risk factor (Thawrani et al., 2014).

Note that the use of a custom translation table presented in Figure 4.3 allows an almost frictionless translation of the caudal end of the specimen, thus resulting in the application of a pure bending moment during testing. It has been shown that these loading conditions acceptably simulate in vivo motions (Wilke et al., 2001). The results of a detailed validation of the testing bench and the testing procedure can be found in (Tremblay et al., 2015a)

To improve repeatability, each specimen was tested with all the configurations without being removed from the test bench. Preliminary experiments (Facchinello et al., 2015) had shown that a 10-cycle stabilization routine was sufficient to obtain reproducible behavior. They had also shown that removing and repositioning the same rods did not significantly affect the vertebrae positions: a maximum 0.3° rotation was observed at the end of this stabilization routine.

Table 4.1 Testing sequence (1,2,3…21) applied to each specimen (A,B,C…F) with the corresponding loading modes (flexion, extension, bending), and instrumentation arrangements (rods and anchors)

	Flexion							Extension							Lateral bending						
Specimen	Non-instr.	Screw			Hook			Non-instr.	Screw			Hook			Non-instr.	Screw			Hook		
		Ti	SE	VAR	Ti	SE	VAR		Ti	SE	VAR	Ti	SE	VAR		Ti	SE	VAR	Ti	SE	VAR
A	1	2	3	4	5	6	7	8	9	10	11	12	13	14	15	16	17	18	19	20	21
B	1	2	3	4	5	6	7	8	9	10	11	12	13	14	15	16	17	18	19	20	21
C	15	16	17	18	19	20	21	1	2	3	4	5	6	7	8	9	10	11	12	13	14
D	15	16	17	18	19	20	21	1	2	3	4	5	6	7	8	9	10	11	12	13	14
E	8	9	10	11	12	13	14	15	16	17	18	19	20	21	1	2	3	4	5	6	7
F	8	9	10	11	12	13	14	15	16	17	18	19	20	21	1	2	3	4	5	6	7

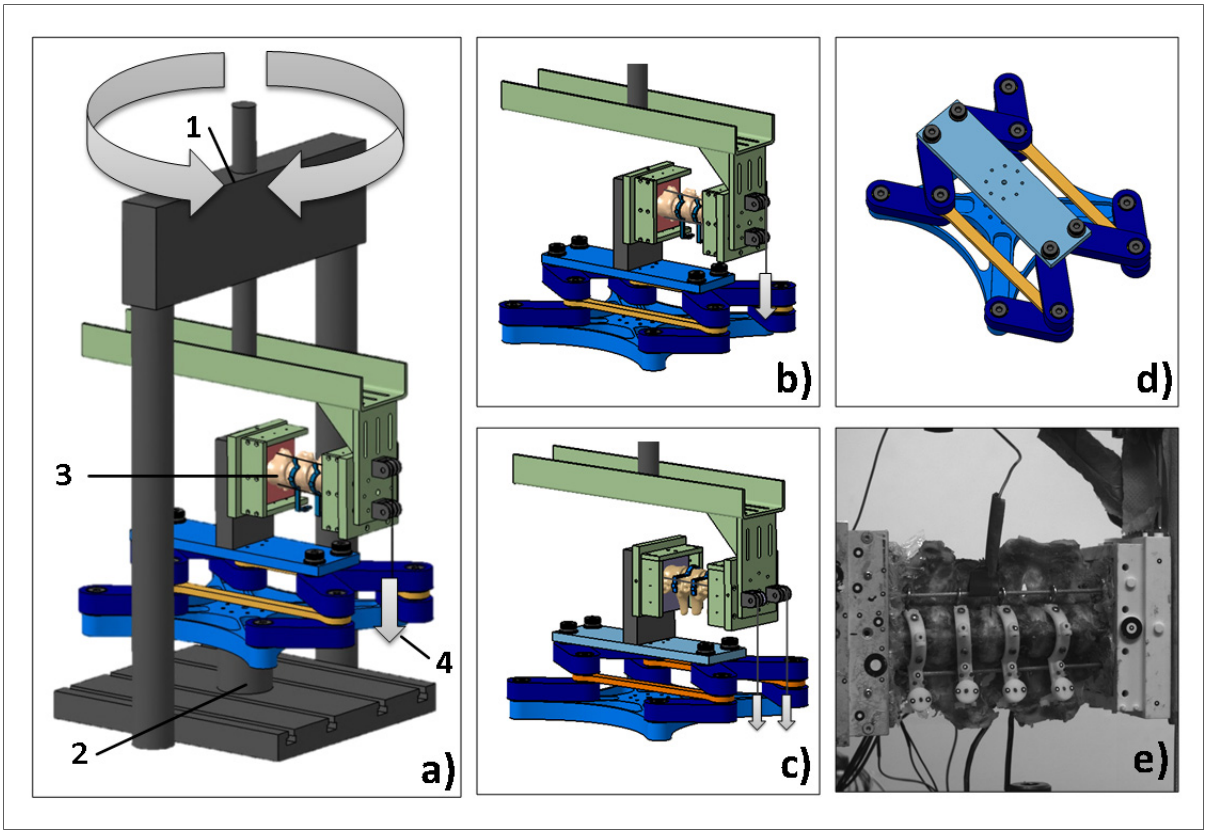

Figure 4.3 a) Spinal testing apparatus used to apply continuous loading with (1) axial and torsional actuators, (2) load cell, (3) specimen, and (4) follower-load. Specimen can be loaded in flexion-extension (b) and lateral bending (c). Translation table (d) and specimen with markers installed (e), ready for flexion-extension loading

4.4.4 Measurements

The following metrics were used to characterise the specimens under forward flexion, extension and lateral bending testing modes: a) stiffness of the construct; b) intervertebral rotations; c) forces on the upper anchors, and d) intervertebral disc pressure. The construct stiffness was defined as a ratio of the bending moment measured at the maximum imposed rotation to the amplitude of this rotation (18°). Bending moments were recorded using the load cell of the test system. Intervertebral rotations were defined as the difference of rotation between two adjacent vertebrae during the motion and were evaluated by filming rigid markers attached to the vertebral bodies with an Aramis video camera system (GOM, Germany) (Figure 4.3e). ProAnalyst software (Xcitex, MA, USA) and a custom Matlab

(MathWork, MA, USA) program were used to calculate the Euler angles from the markers positions following the roll, pitch and yaw convention. Rotations of the markers were defined as the difference of orientation of the markers' coordinate system between the neutral and peak displacement loadings. Relative rotations of pairs of markers attached to pairs of adjacent vertebrae were finally used to evaluate the intervertebral rotations.

Bending moments applied to the upper pedicle screws were measured using strain gages as described in (Freeman et al., 2012). For the installation of the strain gages, four flat surfaces were machined on each screw close to its polyaxial head (Figure 4.3a). Using two pairs of gages allows the measurement of the bending moment in two planes. Prior to testing, each pair of gages was calibrated in bending up to a moment of 1.5 N.m.

Transverse hooks were also equipped with strain gages, but due to their geometry, only one strain gage was attached to the upper surface of a hook (Figure 4.3b), which does not allow a distinction between bending moments and axial forces. Consequently, a direct comparison could not be made between bending moments on the screws and forces on the hooks. The signal recorded with the instrumented hooks was used for the comparative measurement of forces applied to the anchors by different types of rods. Figure 4.4 shows pictures of the instrumented anchors.

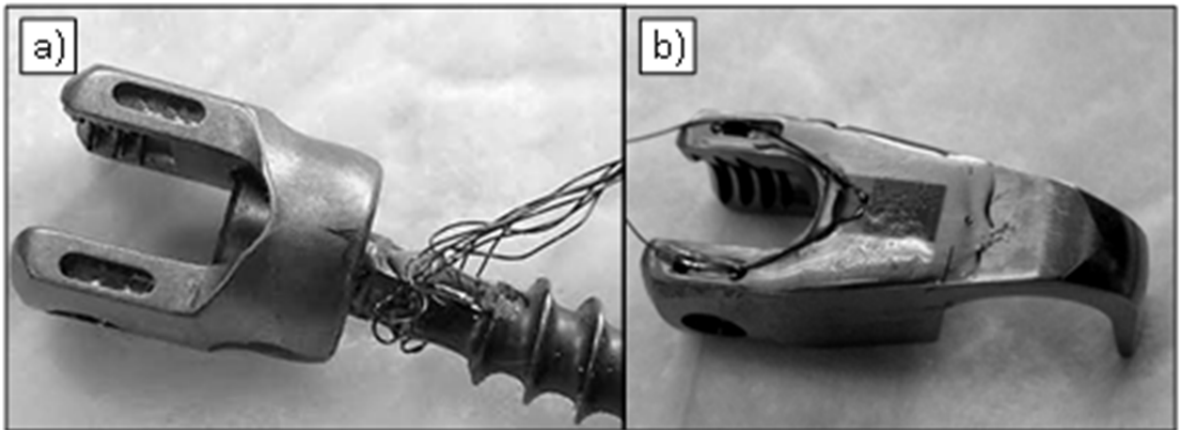

Figure 4.4 Pictures of a) an instrumented pedicle screw and
b) instrumented transverse hook

Intervertebral disc pressures are measured at the highest instrumented level (D3, Figure 4.2c) using Gaeltec needle pressure transducers (Gaeltec Devices Ltd, Scotland) capable of measuring pressures up to 3 MPa. A needle is inserted from the anterolateral position and care is taken to position its sensing area in the middle of the nucleus. Figure 4.4 gives an example of D3 pressure measurement in a non-instrumented specimen during two-step loading and involves the application of a follower load (200 N, then 400 N) continued by a forward flexion movement. The pressure increase recorded during the follower load application (200N then 400N) is used to ensure that the pressure sensor signal is proportional to the followed load applied. The intradiscal pressure variation during motion is evaluated as the difference in D3-intradiscal pressure measured before and after the motion, as designated by ΔP in Figure 4.5.

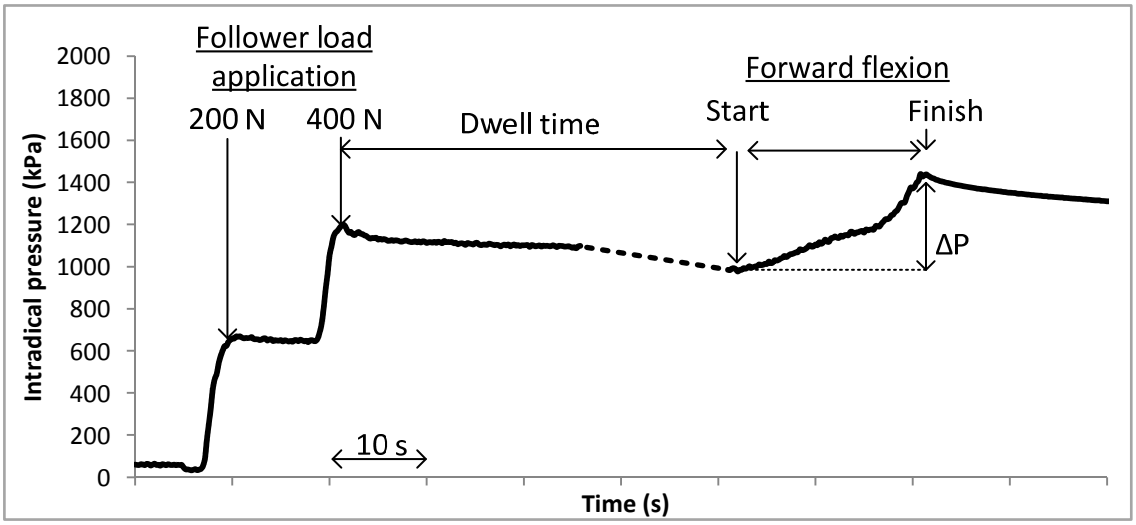

Figure 4.5 D3-Intradiscal pressure measurements on an intact (non-instrumented) specimen during application of follower load and forward flexion. ΔP mark shows the pressure variation caused by flexion

4.4.5 Statistical analysis

T-tests (Excel with Analysis ToolPak, Microsoft Corporation) were used to compare all configurations with the reference case (pedicle screws + Ti rods). Statistical tests were applied to the following metrics: intervertebral rotation (L4-L3 and L3-L2), construct stiffness, forces on anchors (screws only) and intradiscal pressure. Other comparisons were also performed and are mentioned in the discussion. The Holm-Bonferroni correction was used to manage the type I error. The significance level was set to $\alpha=0.05$.

4.5 Results

4.5.1 Forward flexion

The results obtained under forward flexion testing mode are presented in Figure 4.6.

The normalized construct stiffness is expressed as a fraction of the stiffness of the all-screw anchored Ti-rod constructs, with the latter assumed to be 100%. The forces on the UIV

anchors (screws or transverse hooks) were also measured. For each type of anchor, the signal obtained with the Ti rod was considered as the reference (100%). Signals recorded with SE and VAR rods were then expressed as a percentage of what was obtained with the Ti rods. Finally, the intradiscal pressure variation was recorded.

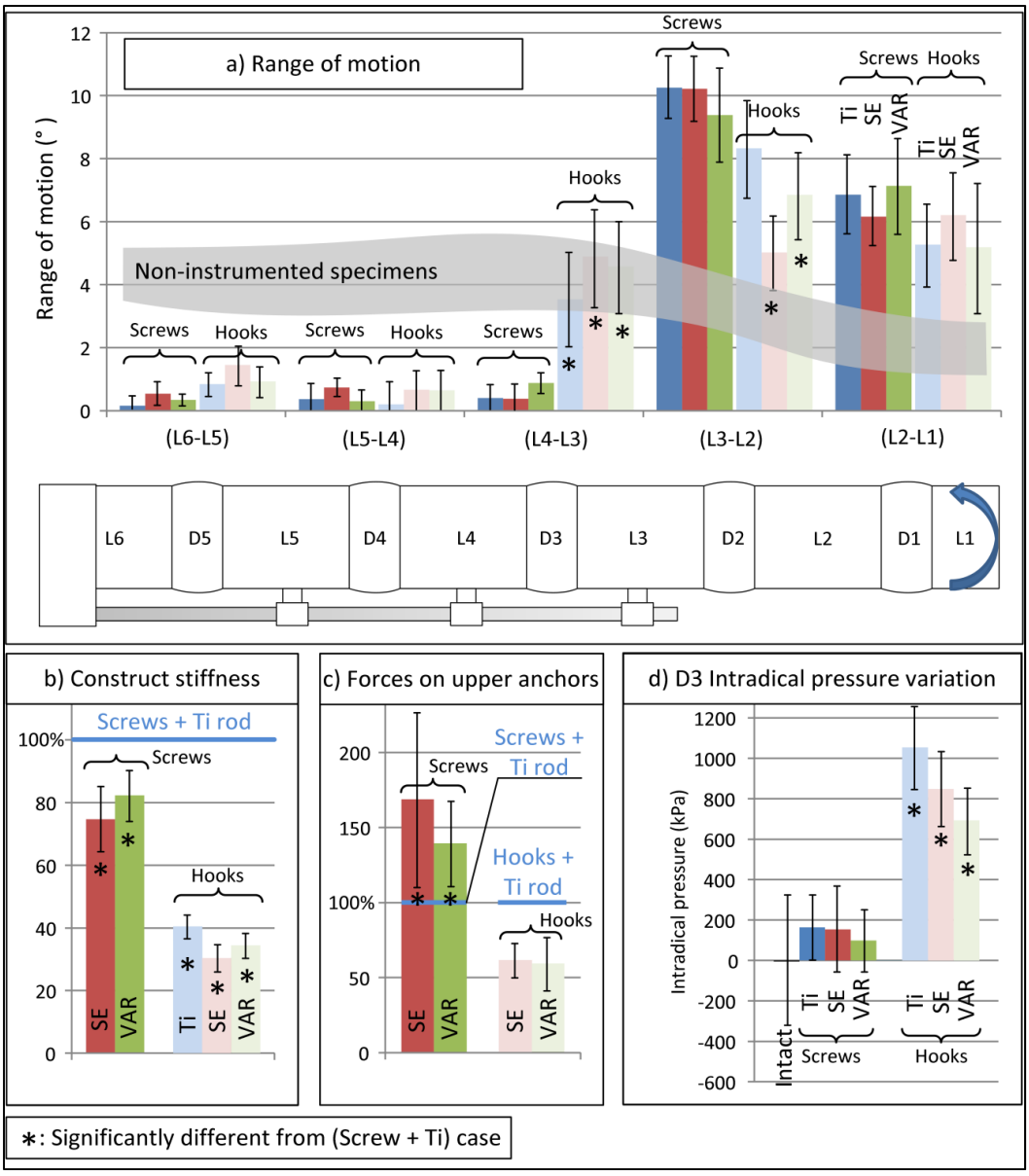

Figure 4.6 Forward flexion: a) range of motion, b) specimen stiffness compared to the Ti rods - PS configuration, c) forces on the upper anchors compared to the Ti rods configuration, and d) D3 pressure variation caused by motion.
Mean values and standard deviations

It was observed that in forward flexion, the Ti rods-pedicle screws configuration confers the highest stiffness to the construct (Figure 4.6b), thus decreasing the mobility of the instrumented part of the construct (Figure 4.6a). No significant differences in the intervertebral rotations (Figure 4.6a) and D3 pressure variations (Figure 4.6d) between the all-screw anchored Ti, SE and VAR rods were observed. However, when stiff Ti rods are replaced by softer SE or VAR rods in the all-screw anchored constructs, bending moments on the upper anchors increased (Figure 4.6c).

Replacing the upper screw anchors with transverse hooks significantly decreased the stiffness of all the constructs (Figure 4.6b), thus amplifying the motion of the upper instrumented L4-L3 segments (Figure 4.6a). This was accompanied by significantly higher D3 disc pressure variations. When combined with transverse hooks, the use of softer rods (SE and VAR) resulted in lower anchor forces compared to Ti rods (Figure 4.6c).

4.5.2 Extension

During extension movement, the combination of pedicle screws and titanium rods provided the highest stiffness (Figure 4.7b) and, therefore, the lowest mobility to the construct (Figure 4.7a). With this anchor configuration, the softer SE and VAR rods allowed more mobility at the upper instrumented segment, although not significant (L4-L3) (Figure 4.7a). The use of transverse hooks at the upper instrumented level decreased the construct stiffness (Figure 4.7b) and the D3 intradiscal pressure variation (Figure 4.7d), but did not significantly change the mobility of all the constructs except with the VAR rods (Figure 4.7a). Moreover, a combination of softer rods (SE and VAR) and hook anchors decreased the upper anchor forces and, thus, the forces applied on transverse processes, compared to the Ti rods - instrumented constructs (Figure 4.7c).

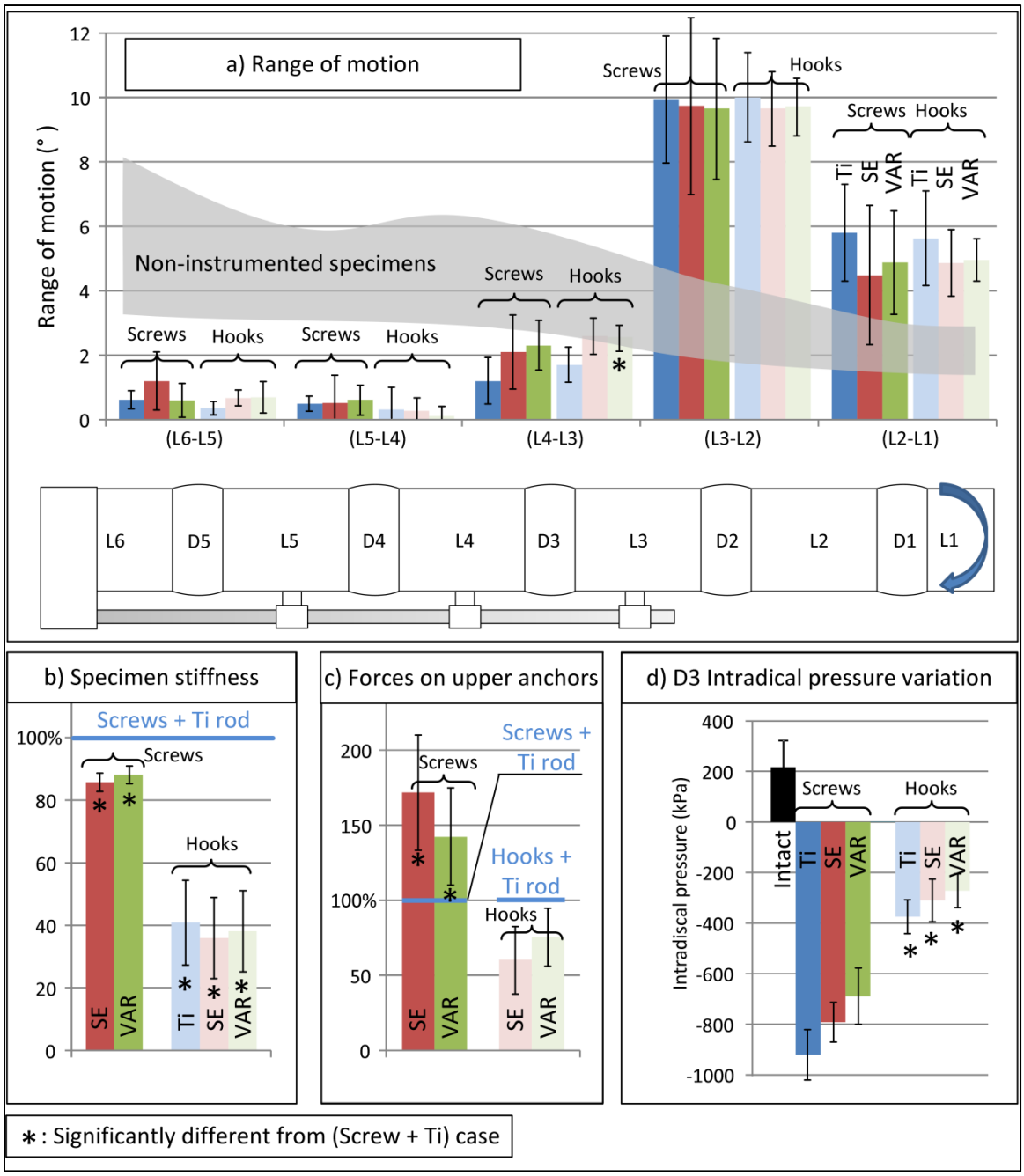

Figure 4.7 Extension testing: a) range of motion, b) specimen stiffness, c) forces on the upper anchors, and d) D3 pressure variation caused by motion. Mean values and standard deviations

4.5.3 Lateral bending

In lateral bending, the stiffness of all-screw anchored constructs decreased when Ti rods are replaced by their SE and VAR counterparts (Figure 4.8b), but the mobility of the constructs was not significantly affected by this replacement (Figure 4.8a). On the contrary, the softer the rods, the higher the anchor forces (Figure 4.8c).

Similarly to the forward flexion mode, the replacement of the upper screw anchors by transverse hooks reduced the stiffness of the instrumented construct (Figure 4.8a) and allowed greater mobility of the last instrumented segment when combined with softer rods (L4-L3) (Figure 4.8a). The adjacent segment (L3-L2) was then subjected to less motion, thus unloading the D2 disc. Once again, the use of VAR rods lowered the forces applied on the hook anchors (Figure 4.8c). In lateral bending, the pressure measurements were not repeatable as they were strongly dependent on the sensor position (Figure 4.8d).

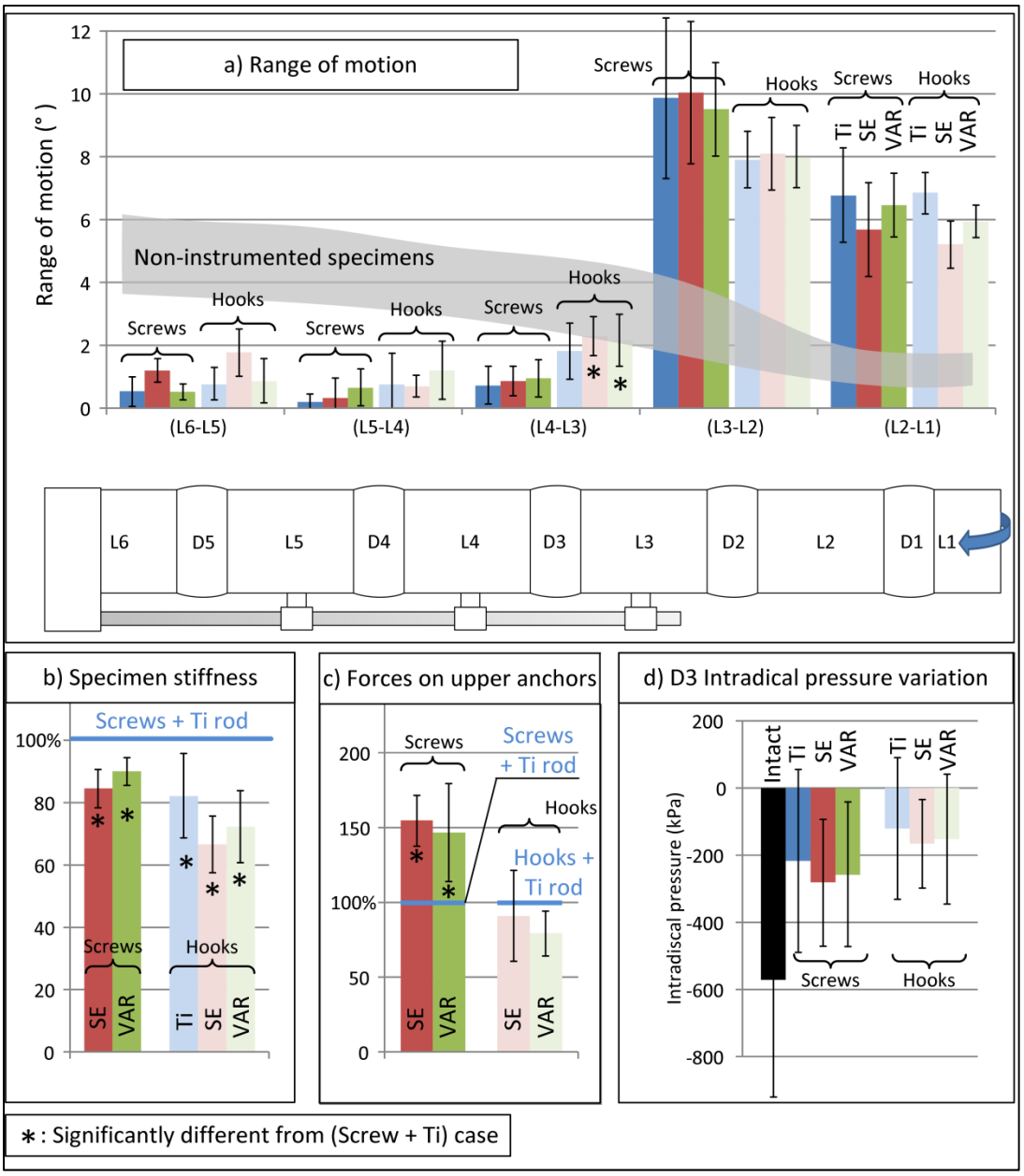

Figure 4.8 Lateral bending: a) range of motion, b) stiffness of the constructs, c) forces on the upper anchors, and d) pressure variations during motion. Mean values and standard deviations

4.6 Summary on relative mobility for different configurations

Figure 4.9a,b,c compares the mobility of the screws-Ti rods configuration and the hooks-VAR rods configuration expressed as a percentage of the mobility recorded in the non-instrumented configuration. This comparison shows that a combination of VAR rods and transverse hook anchors produces a more gradual transition between the stabilized and the intact segments than does a combination of Ti rods with screws, thus reducing the mobility of the adjacent segment.

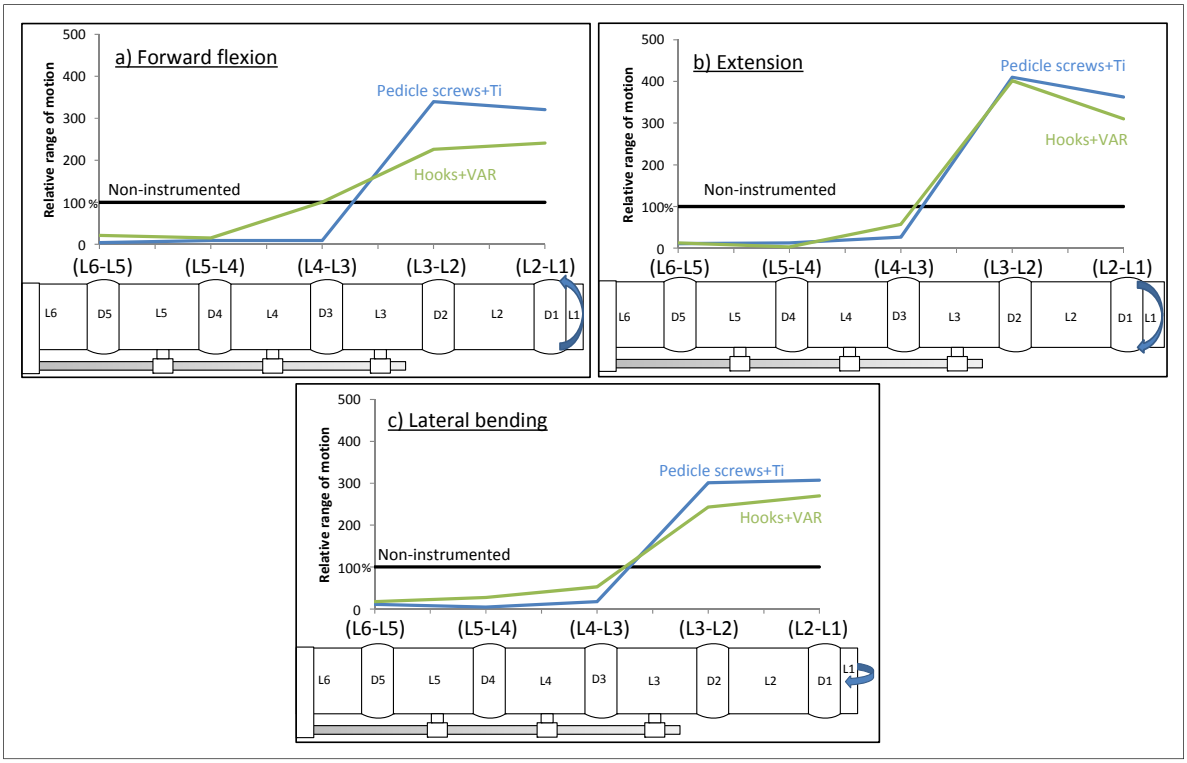

Figure 4.9 Average mobility profiles relative to the intact specimen for a) forward flexion motion, b) extension and c) lateral bending

4.7 Discussion

The rod materials and the anchor configurations used to stabilize lumbar porcine spine segments were found to affect the biomechanics of the constructs under displacement-controlled forward flexion, extension and lateral bending movements.

Statistical tests have shown that when pedicle screws are used, the rod stiffness ranging from 36 GPa (SE) to 36+86 GPa (VAR) to 86 GPa (Ti) affects the overall construct stiffness, but not the mobility of the construct.

Furthermore, transverse process hooks at the proximal end of the construct increase the mobility of the UIV for all rods in flexion, for VAR rods in extension and for SE/VAR rods in lateral bending. For all the motions, the overall stiffness of the constructs with hooks as upper anchors is lower than that with pedicle screws. In flexion and extension, forces applied on hooks in the SE/VAR rods-instrumented constructs are lower than those applied on their Ti rods-instrumented counterparts.

The observed phenomena can be explained by the hypothesis that the transverse process hooks allow the end-vertebra to rotate in respect to the spinal rods (Figure 4.10a), which, in turn, results in a greater ROM in flexion and extension. In lateral bending however, the hooks push against transverse processes, thus offering larger resistance to their relative movement.

During flexion with the all-screw anchoring configuration, the D3 pressure increases within the same range that was observed in the non-instrumented specimens. When transverse hooks are used, larger movements of L3 generate significantly higher D3 pressure surge than what was recorded with the all-screw configuration. These observations are consistent with those made by (Weinhoffer et al., 1995). This phenomenon can be explained by disc compression, since the rotation axis of the vertebra is shifted towards the instrumentation (Figure 4.10b) and (Lee and Langrana, 1984). In extension, the pressure drops significantly, especially when pedicle screws are used, indicating the disc distraction (Figure 4.10c). The same phenomenon was recorded by (Adams et al., 2000; Swanson et al., 2003)

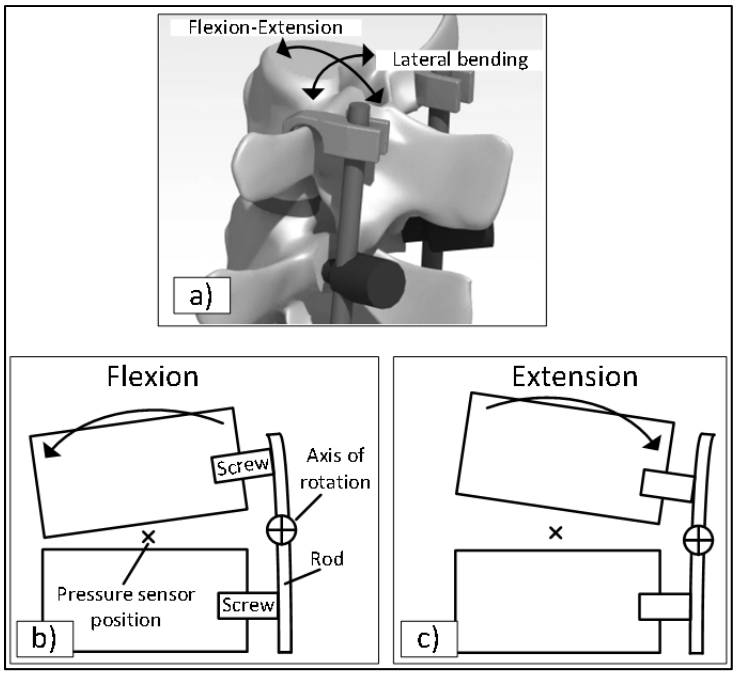

Figure 4.10 a) Illustration of transverse process hooks as upper anchors and motion of a pair of instrumented vertebrae after posterior instrumentation for b) forward flexion and c) extension

It appears also that the spinal rods used in this study combined with transverse process hooks at the upper instrumented vertebrae smoothers the transition between the stabilized and the intact segments, and this observation is in line with that of (Thawrani et al., 2014).

Even though the difference between rods with variable properties (VAR) and completely SE rods is not statistically significant, the VAR rods occupy an intermediate position between their SE and Ti counterparts. They combine the strong stabilization capacity of Ti rods at L6-L5 level with the load-sharing capacity of SE rods at L4-L3 level. Note that at the lowest instrumented level L6-L5, mean ROM of VAR rods is consistently lower than mean ROM of SE rods, for all the motions tested, which is consistent with the VAR rods being stiffer than the SE rods at this level.

The objective of our work was to evaluate the capacity of variable rods combined with transverse process hooks to reduce the sudden change in ROM at the proximal end of the

construct, which may prevent PJK. Several in vitro studies have been recently published regarding the use of dynamic stabilization systems and their influence on the biomechanics of a spine segment (Dhillon et al., 2009; Gornet et al., 2011; Schilling et al., 2010; Schilling et al., 2011). Moderate to weak changes in vertebrae motion have been reported regardless of the rod material when pedicle screws are used as anchors. However, (Thawrani et al., 2014) observed significant changes in mobility when replacing the pedicle screws with transverse hooks at the UIV using stiff Co-Cr rods.

Keeping all these observations in mind, it can also be supposed that VAR rods-transverse hooks configuration could be promising if the fixation is extended to an unfused (index) level (Hudson et al., 2011). Such instrumentation consists of a combination of rigid instrumentation in the zone of fusion with a more permissive fixation at the extremity of the implant. This is believed to create a transition between the stiff, fused segment and the intact spine. The softer ends of the rods could also limit the forces applied on the transverse processes. This is off-label use of the instrumentation, but several clinical studies are under way with promising results, even though screw loosening seems to be a frequent complication in these cases (Matthew B. Maserati et al., 2010, Hudson et al., 2011).

In other studies, it has also been highlighted that PJK occurrence seems to be strongly dependent on the alignment of the upper instrumented vertebra. The use of an transverse process hooks at the UIV may improve this alignment (Chen et al., 2011, Anderson et al., 2009; Hassanzadeh et al., 2013).

One of the strongest limitations of this study is the use of porcine spine models, which do not possess the same lumbar curvature as the humans. However, porcine spines are considered appropriate to study spinal implants (Busscher et al., 2010). This study represents also the post-operative state of the spine and does not take into consideration the initial deformity, the bone fusion or the disc degeneration that can develop over time.

Another limitation comes from using the same specimen with different instrumentations. Even though all the precautions were taken to preserve the specimens' integrity during each series of testing, there is still a risk of specimen damage which may affect the results obtained. Also during testing, the fixation arrangement order was not randomized. The all-screw fixation was always tested before the hook which may have altered the behaviour of the specimens.

This study was limited to the measurement of the D3 disc pressure only. Pressure in the adjacent disc (D2) could not be recorded because of repetitive sensor failure, given large amplitude of the adjacent disc movement during testing. Fiber optic pressure sensor might be better for this application. The lack of reliable pressure measurement during lateral bending is also problematic.

Note also that Joule-effect thermal treatment used to produce VAR rods may affect their biocompatibility by altering the surface composition. To keep an appropriate level of biocompatibility, surface treatment such as electro- or mechanical polishing could be applied on these rods after Joule effect thermal treatment (Zhu et al., 2003).

As further work, the results presented in this study will be used to validate a numerical model still under development. The simulation will be used to try different anchor configurations and to optimize the stiffness profile of the rod.

4.8 Conclusion

The effect of the flexural stiffness of spinal rods on the biomechanics of instrumented spine segments (constructs) was investigated using lumbar porcine spine specimens. The rod's stiffness has a slight-to-moderate effect on the construct mobility, when pedicle screws are used as anchors. This is especially visible in forward flexion. Replacing upper screw anchors with transverse process hooks amplifies the effect of the rod material. The variable-stiffness

(half superelastic-half pseudoplastic) rods, combined with upper hook anchors provide the most gradual transition between the instruments and the intact segments among all the instrumentations studied in this work.

4.9 Funding

This work was carried out with financial support from the FQRNT (Fonds de Recherche du Québec–Nature et Technologies) and the CFI (Canadian Foundation for Innovation).

4.10 Acknowledgments

The authors acknowledge the assistance of Hanneke V. W., MD in pedicle screw implantation and express their gratitude to Michel D. and Serge P. for collaborating in pedicle screw instrumentation. Pedicle screws and transverse process hooks were provided free of charge by Medtronic.

4.11 Conflict of interest

Nothing to declare.

4.12 References

Adams, M.A., May, S., Freeman, B.J., Morrison, H.P., Dolan, P., 2000. Effects of backward bending on lumbar intervertebral discs. Relevance to physical therapy treatments for low back pain. Spine (Phila Pa 1976) 25, 431-437; discussion 438.

Anderson, A.L., McIff, T.E., Asher, M.A., Burton, D.C., Glattes, R.C., 2009. The effect of posterior thoracic spine anatomical structures on motion segment flexion stiffness. Spine (Phila Pa 1976) 34, 441-446.

Bono, C.M., Kadaba, M., Vaccaro, A.R., 2009. Posterior Pedicle Fixation-based Dynamic Stabilization Devices for the Treatment of Degenerative Diseases of the Lumbar Spine. Journal of Spinal Disorders & Techniques 22, 376-383 310.1097/BSD.1090b1013e31817c36489.

Bruner, H.J., Guan, Y., Yoganandan, N., Pintar, F.A., Maiman, D.J., Slivka, M.A., 2010. Biomechanics of polyaryletherketone rod composites and titanium rods for posterior lumbosacral instrumentation. Presented at the 2010 Joint Spine Section Meeting. Laboratory investigation. Journal of neurosurgery. Spine 13, 766-772.

Busscher, I., Ploegmakers, J.J., Verkerke, G.J., Veldhuizen, A.G., 2010. Comparative anatomical dimensions of the complete human and porcine spine. European spine journal : official publication of the European Spine Society, the European Spinal Deformity Society, and the European Section of the Cervical Spine Research Society 19, 1104-1114.

Chen, H., Charles, Y.P., Bogorin, I., Steib, J.-P., 2011. Influence of 2 Different Dynamic Stabilization Systems on Sagittal Spinopelvic Alignment. Journal of Spinal Disorders & Techniques 24, 37-43.

DeWald, C.J., Stanley, T., 2006. Instrumentation-Related Complications of Multilevel Fusions for Adult Spinal Deformity Patients Over Age 65: Surgical Considerations and Treatment Options in Patients With Poor Bone Quality. Spine 31, S144-S151 110.1097/1001.brs.0000236893.0000265878.0000236839.

Dhillon, B.K., Fraysur, K., Sedacki, K., Ammerman, M., Kelly, B.P., DiAngelo, D.J., 2009. Biomechanical Testing of Posterior Lumbar Stabilization Systems, 25th Southern Biomedical Engineering Conference (IFMBE 2009), 15-17 May 2009. Springer-Verlag, Berlin, Germany, pp. 213-218.

Facchinello, Y., Brailovski, V., Inaekyan, K., Petit, Y., Mac-Thiong, J.-M., 2013. Manufacturing of monolithic superelastic rods with variable properties for spinal correction: Feasibility study. Journal of the Mechanical Behavior of Biomedical Materials 22, 1-11.

Facchinello, Y., Brailovski, V., Petit, Y., Brummund, M., Tremblay, J., Mac-Thiong, J.M., 2015. In-vitro assessment of the stabilization capacity of monolithic spinal rods with variable flexural stiffness: Methodology and Examples, Submitted to : 37th Annual International Conference of the IEEE Engineering in Medicine and Biology Society, Milan, Italia.

Facchinello, Y., Brailovski, V., Petit, Y., Mac-Thiong, J.M., 2014a. Monolithic superelastic rods with variable flexural stiffness for spinal fusion: Modeling of the processing-properties relationship. Medical Engineering & Physics 36, 1455-1463.

Facchinello, Y., Brailovski, V., Petit, Y., Mac-Thiong, J.M., 2014b. Monolithic superelastic rods with variable flexural stiffness for spinal fusion: Simplified finite element analysis of an instrumented spine segment. Conf Proc IEEE Eng Med Biol Soc 2014, 6605-6608.

Freeman, A.L., Fahim, M.S., Bechtold, J.E., 2012. Validation of an improved method to calculate the orientation and magnitude of pedicle screw bending moments. J Biomech Eng 134, 104502-104502.

Goel, V.K., Panjabi, M.M., Patwardhan, A.G., Dooris, A.P., Serhan, H., 2006. Test protocols for evaluation of spinal implants. The Journal of bone and joint surgery. American volume 88 Suppl 2, 103-109.

Gornet, M.F., Chan, F.W., Coleman, J.C., Murrell, B., Nockels, R.P., Taylor, B.A., Lanman, T.H., Ochoa, J.A., 2011. Biomechanical assessment of a PEEK rod system for semi-rigid fixation of lumbar fusion constructs. J Biomech Eng 133, 081009.

Hassanzadeh, H., Gupta, S., Jain, A., El Dafrawy, M.H., Skolasky, R.L., Kebaish, K.M., 2013. Type of Anchor at the Proximal Fusion Level Has a Significant Effect on the Incidence of Proximal Junctional Kyphosis and Outcome in Adults After Long Posterior Spinal Fusion. Spine Deformity 1, 299-305.

Helgeson, M.D., Shah, S.A., Newton, P.O., Clements, D.H., 3rd, Betz, R.R., Marks, M.C., Bastrom, T., 2010. Evaluation of proximal junctional kyphosis in adolescent idiopathic scoliosis following pedicle screw, hook, or hybrid instrumentation. Spine (Phila Pa 1976) 35, 177-181.

Hudson, W.R.S., Gee, J.E., Billys, J.B., Castellvi, A.E., 2011. Hybrid dynamic stabilization with posterior spinal fusion in the lumbar spine. SAS Journal 5, 36-43.

Kotani, Y., Cunningham, B.W., Cappuccino, A., Kaneda, K., McAfee, P.C., 1996. The role of spinal instrumentation in augmenting lumbar posterolateral fusion. Spine (Phila Pa 1976) 21, 278-287.

Lee, C.K., Langrana, N.A., 1984. Lumbosacral spinal fusion. A biomechanical study. Spine (Phila Pa 1976) 9, 574-581.

Li, Z., Li, F., Yu, S., Ma, H., Chen, Z., Zhang, H., Fu, Q., 2013. Two-year follow-up results of the Isobar TTL Semi-Rigid Rod System for the treatment of lumbar degenerative disease. Journal of Clinical Neuroscience 20, 394-399.

Lorenz, M., Zindrick, M., Schwaegler, P., Vrbos, L., Collatz, M.A., Behal, R., Cram, R., 1991. A comparison of single-level fusions with and without hardware. Spine (Phila Pa 1976) 16, S455-458.

Matthew B. Maserati, Matthew J. Tormenti, David M. Panczykowski, Christopher M. Bonfield, Peter C. Gerszten, 2010. The use of a hybrid dynamic stabilization and fusion system in the lumbar spine: preliminary experience. Neurosurgical focus 28, E2.

Panjabi, M.M., 2007. Hybrid multidirectional test method to evaluate spinal adjacent-level effects. Clinical Biomechanics 22, 257-265.

Patwardhan, A.G., Havey, R.M., Carandang, G., Simonds, J., Voronov, L.I., Ghanayem, A.J., Meade, K.P., Gavin, T.M., Paxinos, O., 2003. Effect of compressive follower preload on the flexion–extension response of the human lumbar spine. Journal of Orthopaedic Research 21, 540-546.

Patwardhan, A.G., Havey, R.M., Meade, K.P., Lee, B., Dunlap, B., 1999. A follower load increases the load-carrying capacity of the lumbar spine in compression. Spine (Phila Pa 1976) 24, 1003-1009.

Schilling, C., Krüger, S., Beger, J., Grupp, T.M., Blömer, W., 2010. In-vitro Flexibility Characteristics of Dynamic Pedicle Screw Systems, in: Dössel, O., Schlegel, W. (Eds.), World Congress on Medical Physics and Biomedical Engineering, September 7 - 12, 2009, Munich, Germany. Springer Berlin Heidelberg, pp. 441-444.

Schilling, C., Kruger, S., Grupp, T.M., Duda, G.N., Blomer, W., Rohlmann, A., 2011. The effect of design parameters of dynamic pedicle screw systems on kinematics and load bearing: an in vitro study. European spine journal : official publication of the European Spine Society, the European Spinal Deformity Society, and the European Section of the Cervical Spine Research Society 20, 297-307.

Swanson, K.E., Lindsey, D.P., Hsu, K.Y., Zucherman, J.F., Yerby, S.A., 2003. The effects of an interspinous implant on intervertebral disc pressures. Spine (Phila Pa 1976) 28, 26-32.

Thawrani, D.P., Glos, D.L., Coombs, M.T., Bylski-Austrow, D.I., Sturm, P.F., 2014. Transverse Process Hooks at Upper Instrumented Vertebra Provide More Gradual Motion Transition than Pedicle Screws. Spine 39, E826-832.

Tremblay, J., Mac-Thiong, J.-M., Brailovski, V., Petit, Y., 2015a. Braided tubular superelastic cables provide improved spinal stability compared to multifilament sublaminar cables. Proceedings of the Institution of Mechanical Engineers, Part H: Journal of Engineering in Medicine [ePub ahead of print].

Tremblay, J., Mac-Thiong, J.-M., Brailovski, V., Petit, Y., 2015b. Factors affecting intradiscal pressure measurement during in vitro biomechanical tests. Scoliosis 10, O19.

Weinhoffer, S.L., Guyer, R.D., Herbert, M., Griffith, S.L., 1995. Intradiscal pressure measurements above an instrumented fusion. A cadaveric study. Spine (Phila Pa 1976) 20, 526-531.

Wilke, H.J., Geppert, J., Kienle, A., 2011. Biomechanical in vitro evaluation of the complete porcine spine in comparison with data of the human spine. European spine journal : official publication of the European Spine Society, the European Spinal Deformity Society, and the European Section of the Cervical Spine Research Society 20, 1859-1868.

Wilke, H.J., Rohlmann, A., Neller, S., Schultheiss, M., Bergmann, G., Graichen, F., Claes, L.E., 2001. Is it possible to simulate physiologic loading conditions by applying pure moments? A comparison of in vivo and in vitro load components in an internal fixator. Spine (Phila Pa 1976) 26, 636-642.

Wilke, H.J., Wenger, K., Claes, L., 1998. Testing criteria for spinal implants: recommendations for the standardization of in vitro stability testing of spinal implants. European spine journal : official publication of the European Spine Society, the European Spinal Deformity Society, and the European Section of the Cervical Spine Research Society 7, 148-154.

Zhu, L., Trepanier, C., Pelton, A.R., Fino, J., 2003. Oxidation of nitinol and its effect on corrosion resistance, Medical Device Materials - Proceedings of the Materials and Processes for Medical Devices Conference 2003, September 8, 2003 - September 10, 2003. ASM International, Anaheim, CA., United states, pp. 156-161.

DISCUSSION GÉNÉRALE

L'objectif de ce projet était de proposer une instrumentation monolithique aux propriétés variables pour la stabilisation de la colonne vertébrale pouvant potentiellement résoudre les problèmes observés aux segments adjacents. Les travaux ont été présentés dans trois articles de revues et deux de conférences inclus intégralement dans les chapitres 2, 3, 4 et annexe I et II.

Dans le premier article, la technologie de fabrication de tiges aux propriétés variables a été développée et décrite. Deux méthodes ont été testées : recuits locaux et écrouissage local. Les deux méthodes ont prouvé leurs efficacités. Il a été démontré que des recuits de 10 minutes permettaient de modifier localement les propriétés mécaniques de fils (Ø 2 mm) en alliage à mémoire de forme Ti-Ni. Il a été constaté qu'un gradient de propriétés mécaniques résultait du gradient de température apparaissant lors du recuit. Les essais de fatigue en flexion rotative ont permis de constater que les échantillons hétérogènes présentaient une durée de vie comparable à celle des échantillons homogènes. L'écrouissage local permet également de modifier localement les propriétés des tiges. Cependant, le changement de section de la tige dans la zone déformée semble problématique pour l'application visée. Le chauffage local a donc été choisi pour la fabrication des tiges.

Dans le deuxième article, la technologie de chauffage par effet Joule a été appliquée avec succès sur des tiges de 5.5mm de diamètre en alliage Ti-55.94wt.%Ni. Afin d'optimiser les paramètres de chauffage ainsi que de prévoir le profil de rigidité de la tige, un modèle numérique a été développé. Ce modèle permet de calculer un profil de température selon les paramètres de chauffage et de prévoir l'impact de ce profil de température sur le profil de propriétés mécaniques obtenu. Une optimisation du profil de température et donc des propriétés mécaniques est également possible. Ce modèle de tiges aux propriétés variables devrait par la suite être implanté dans un modèle de colonne vertébrale afin d'optimiser le profil de rigidité des tiges.

Afin de prédire les bénéfices potentiels des tiges variables, un modèle simplifié de colonne vertébrale a été développé et est décrit dans l'annexe I. Ce modèle a permis de montrer que l'utilisation de vis pédiculaires comme ancrages empêche la flexion des tiges et annule l'effet des variations de rigidité. Il a cependant été observé que l'utilisation de câbles ou de crochets à l'extrémité de l'instrumentation permet d'amplifier l'effet des tiges aux propriétés variables.

Afin de vérifier cette hypothèse, des tests biomécaniques ont été réalisés sur spécimens porcins. Les résultats obtenus lors de cette étude sont présentés dans le troisième article tandis que la méthodologie expérimentale suivie lors de ces essais est décrite et validée dans l'annexe II. Lors de cette étude, les tiges aux propriétés variables ont été comparées aux tiges en titane conventionelles et à des tiges entièrement superélastiques. De plus, les tiges ont été ancrées aux spécimens via des vis pédiculaires uniquement ou par une combinaison de vis et de crochets transverses. Cette étude a montré que l'utilisation des tiges variables couplées à des crochets transverses en fin d'instrumentation permettait de créer une zone de transition entre la zone de fusion rigide et la zone intacte. Il a également été constaté que les tiges variables permettaient d'abaisser significativement les forces appliquées sur les crochets comparés aux tiges en titane. La variation de la rigidité des tiges ne parvient donc pas à elle seule à créer une transition entre la zone instrumentée et la zone intacte. Il apparait nécessaire de modifier les ancrages pour que l'utilisation des tiges variables présente un avantage.

<u>Contributions scientifiques</u>

- Développement de la technique de fabrication des tiges aux propriétés mécaniques variables
    - -Étude de faisabilité sur des fils de Ø2mm
    - -Application de cette technique sur des tiges standards Ø5,5mm

- Développement et validation d'un modèle numérique permettant de prédire l'effet d'un recuit sur les propriétés mécaniques du matériau
    - -Simulation du procédé de fabrication
    - -Simulation des propriétés variables

- Élaboration d'une méthodologie expérimentale pour l'étude in vitro
    - -Étude simultanée de la mobilité, de la pression intradiscale, de la rigidité et des efforts appliqués sur les ancrages

- Les résultats de cette étude ont servi à la validation d'un modèle numérique de colonne instrumentée

CONCLUSION

L'objectif de ce projet était de développer la technologie de fabrication de tiges monolithiques aux propriétés mécaniques variables pour la stabilisation de la colonne vertébrale et d'identifier leurs éventuels bénéfices comparés aux tiges rigides classiques. Il était également question de déterminer si l'utilisation de crochets transverses à l'extrémité de l'instrumentation permettait d'amplifier l'effet des tiges variables sur le comportement d'un segment instrumenté.

Les travaux effectués dans le cadre de cette thèse ont montré que la technique des recuits locaux par effet Joule était efficace pour fabriquer de telles tiges en alliage Ti-Ni. Les tests biomécaniques effectués sur spécimens porcins ont montré que l'impact de la rigidité de la tige est très limité lorsque des vis pédiculaires sont utilisées comme ancrage ce qui confirme les données déjà publiées à ce sujet (Gornet et al, 2011b). En revanche, il a été trouvé que l'effet de la rigidité de la tige est amplifié par l'utilisation de crochets transverses à l'extrémité de l'instrumentation. Une instrumentation combinant tiges variables et crochets à l'extrémité permet donc de réduire l'hypermobilité du segment adjacent tout en assurant la stabilité nécessaire pour la fusion.

Dans cette configuration, la partie rigide des tiges combinée à des vis pédiculaires permet d'assurer une stabilité proche de celle de tiges de titane. La fin de l'instrumentation est stabilisée à l'aide de crochets transverses et de la section souple des tiges. Dans cette zone, le mouvement permis par les crochets et par la section souple permet de favoriser l'alignement du segment adjacent et de limiter les efforts appliqués par les crochets sur les processus transverses. Selon la même configuration, une instrumentation hybride combinant une zone de fusion et une zone stabilisée avec préservation de mouvement pourrait également être envisagée. Il faudrait cependant être prudent avec l'effet du frottement répété du crochet sur les processus transverses.

Les résultats obtenus lors de ces travaux ouvrent également la voie vers des instrumentations combinant des implants dynamiques, des vis pédiculaires et des crochets transverses. L'utilisation de crochets transverses pourrait en effet amplifier l'influence des implants dynamiques déjà disponibles sur le marché. Pour tester de telles configurations, la méthodologie expérimentale développée lors de ces travaux parait adaptée. En particulier, il semble important d'évaluer les forces appliquées par les crochets sur les vertèbres puisque le risque de fracture osseuse à cet endroit est important avec l'utilisation des crochets.

RECOMMANDATIONS

Les recommandations suivantes peuvent être formulées pour la suite de ce projet :

- lors de cette étude, aucune optimisation du profil de rigidité des implants ou de la configuration des ancrages n'a été tentée. Pour cela, le développement d'un modèle numérique de colonne validé serait nécessaire. L'optimisation numérique de l'instrumentation serait par la suite possible. Un tel implant optimisé pourrait enfin être fabriqué et testé *in-vitro* pour vérifier ses capacités de stabilisation;

- l'utilisation d'autres matériaux pour la fabrication des tiges pourrait être envisagée. Les matériaux composites semblent par exemple être de bon candidat grâce à leurs propriétés mécaniques facilement modifiables;

- enfin, des géométries d'implant différentes des tiges pourraient être imaginées, fabriquées puis testées *in-vitro*.

ANNEXE I

MONOLITHIC SUPERELASTIC RODS WITH VARIABLE FLEXURAL STIFFNESS: SIMPLIFIED FINITE ELEMENT ANALYSIS OF AN INSTRUMENTED SPINE SEGMENT

Yann Facchinello[1,2], Vladimir Brailovski[1,2], Yvan Petit[1,2], Jean-Marc Mac-Thiong[2,3]

[1]Département de Génie Mécanique, École de technologie supérieure,

1100 Notre-Dame Ouest, Montréal, Québec, Canada H3C 1K3

[2]Centre de recherche, Hôpital du Sacré-Cœur de Montréal,

5400, boul. Gouin Ouest, Montreal, Québec, Canada H4J 1C5,

[3]Département de chirurgie, Faculté de médecine, Université de Montréal,

Pavillon Roger-Gaudry, Local : S-749, Montréal, Québec, Canada H3C 3J7

Cet article a été présenté à la conférence :

36TH ANNUAL INTERNATIONAL CONFERENCE OF THE

IEEE Engineering in Medicine and Biology Society

Chicago, USA, 26-30 Aout 2015

Résumé

Afin de prédire l'effet de la variation de la rigidité des tiges sur le comportement d'un segment de colonne, un modèle simplifié a été développé. Ce modèle comporte six vertèbres et cinq disques qui ont été instrumentés à l'aide d'une tige de titane, de Ti-Ni superélastique ou d'une tige à rigidité variable. La tige est ancrée à la colonne à l'aide de vis pédiculaires. L'extrémité de la tige est attachée via une vis ou alors à l'aide d'un câble. Ce modèle a été chargé en déplacement contrôlé selon trois mouvements : flexion, extension et inflexion latérale. Les calculs ont montrés que l'effet de la rigidité de la tige est très limité lorsque des vis pédiculaires sont utilisées comme ancrage. L'utilisation d'un câble à l'extrémité de la tige semble être efficace pour débloquer les mouvements.

Abstract

Rigid instrumentations have been widely used for spinal fusion but they come with complications, such as adjacent disc degeneration. Dynamic instrumentations have been tested but their efficiency (stabilization capability) and reliability (mechanical integrity of the implant) have yet to be proven. A monolithic Ti-Ni spinal rod with variable flexural stiffness is proposed to reduce the risks associated with spinal fusion while maintaining adequate stabilization. This publication presents a simplified numerical model capable of evaluating the eventual benefits of a Ti-Ni spinal rod with variable flexural stiffness.

Methods: A simplified instrumented spine segment model composed of six vertebrae and five discs has been developed. Two types of spinal rods were evaluated: Classic Ti instrumentation and Ti-Ni rods with variable stiffness. Both instrumentations were tested using two anchor configurations: pedicle screws only or a screws-cable combination.

Findings and discussion: The all-screws configuration does not allow much motion with either classic Ti or variable Ti-Ni rods. The combination of a Ti rod with screws-cable anchoring allows more motion and, therefore, lower adjacent disk pressure, but puts extremely high stresses on the rod and anchors. The combination of the variable Ti-Ni rod and screws-cable anchoring leads to a significant decrease in adjacent disk pressure, without increasing stresses and pullout forces in the spinal instrumentation.

Introduction

Spinal disorders can be treated by several means including fusion surgery. Rigid posterior instrumentations are commonly used to prevent motion of the instrumented segment and to aid fusion healing [1,2]. Due to the abrupt stiffness variation between the instrumented and intact spinal segments, stresses are increased locally, which leads to adjacent disc degeneration [3]. Dynamic stabilization systems (DSS) have been proposed to lower the stress the risk of adjacent segment degeneration [4]. Clinical studies have shown that “soft” instrumentations are not risk-free: problems related to these implants’ loosening, their mechanical failure and poor fusion rate have been reported [5].

An ideal implant would combine static and dynamic properties with the required stiffness where a strong stabilization is needed and more flexible behavior where dynamic properties and load-sharing capacity are important. This combination of properties can be obtained by different methods including the use of Ti-Ni shape memory alloys. The mechanical properties of these alloys are conditioned by their thermomechanical processing [6] and can be controlled by local annealing [7,8].

Our previous study showed that monolithic Ti-Ni rods with variable mechanical properties can be produced using localized Joule-heating heat treatment [9]. Different sections of these rods manifest different behavior, ranging from elastoplasticity (martensitic) to superelasticity (annealed). These technological possibilities allow monolithic spinal rods to be designed with variable flexural stiffness, which would combine stabilization capacity with reduced stress concentration at the implant extremities.

To conduct a preliminary evaluation of the biomechanical implications related to the use of such spinal rods, a simplified numerical model of an instrumented spine segment was developed. The results of this preliminary study are presented in this publication.

Materials and methods

A simplified three-dimensional (3D) finite-element model of a spine segment was developed using Ansys 14 commercial software. The model presented in Figure-A I-1 is composed of six vertebrae separated by five discs. The main inputs: the geometry and mechanical properties of the spine (vertebrae, discs), the geometry and mechanical properties of the rod, the configuration of the anchor system, and the mechanical load applied to the spine segment. The vertebrae are modeled as homogeneous solids, whereas the discs are composed of annulus fibrosus and nucleus.

The spine segment is instrumented with two types of a 3 mm-diameter 90 mm-long rod: a) homogeneous (Ti), and b) half elastic-half superelastic (Ti-Ni) (Figure-A I-1a,b). Note that a smaller, than standard, diameter rod was used in the model to accentuate the effect of variable stiffness on the behavior of the instrumented segment. The Ti rod represents a conventional titanium implant, while the Ti-Ni rod is a novel instrumentation. The rods are attached to the spine using one of two anchors configurations: all-screws (three Ø6mm pedicle screws, Figure-A I-1a) or screws-cable (two Ø6mm pedicle screws and one Ø2mm cable, Figure-A I-1b); all fixation components are made of Ti. The mechanical properties of the model components are collected in Table- A I-1. The complete model is meshed with 26453 SOLID186 elements and loaded in forward flexion, lateral bending and axial rotation with imposed rotations of the end-vertebra (V1) of 45°, 45° and 30°, respectively. Figure-A I-2 shows a compilation of the results.

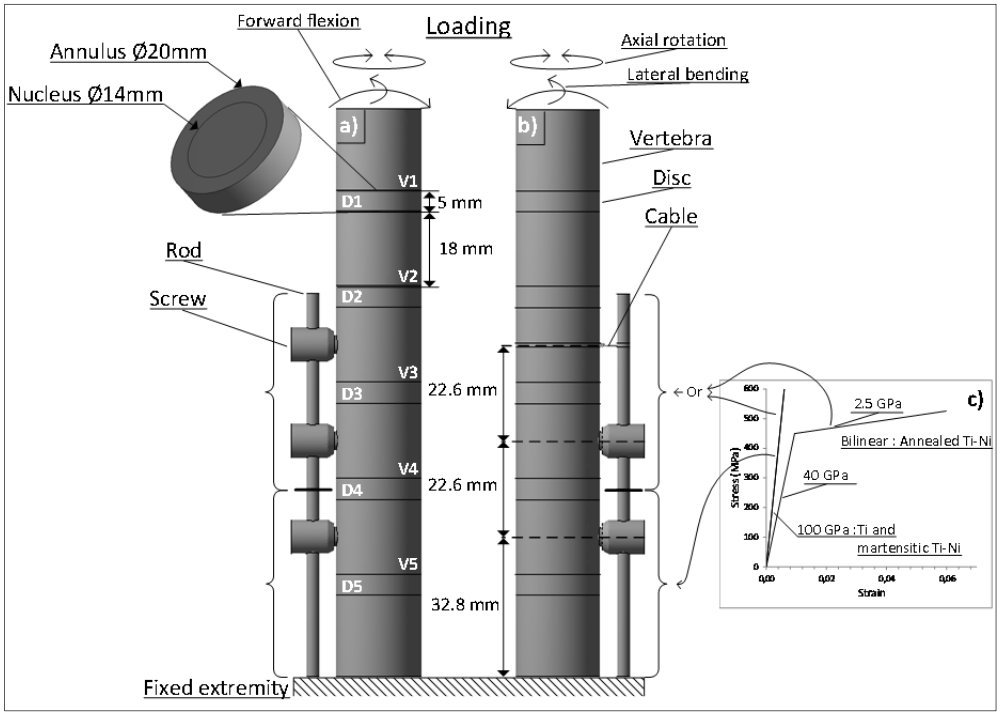

Figure-A I-1 The model's schematic: a) all-screw and b) screws-cable anchoring; c) Stress-strain plots of half elastic-half superleastic (bilinear) and elastic (linear) components.

Table-A I-1 Materials characteristics
used in the model

Material	Young's Moduli, GPa	Poisson's ratio
Vertebrae*	0,374	0,3
Discs:** -Annulus fibrosus -Nucleus	 0,03 0,001	 0,45 0,49
Rods: a) Ti b) Ti-Ni: elastic/superelastic	100 Figure 1c	0,3
Screws, cable (Ti)	100	0.3
*El Masri et al., [10]; **Castellvi et al., [11]		

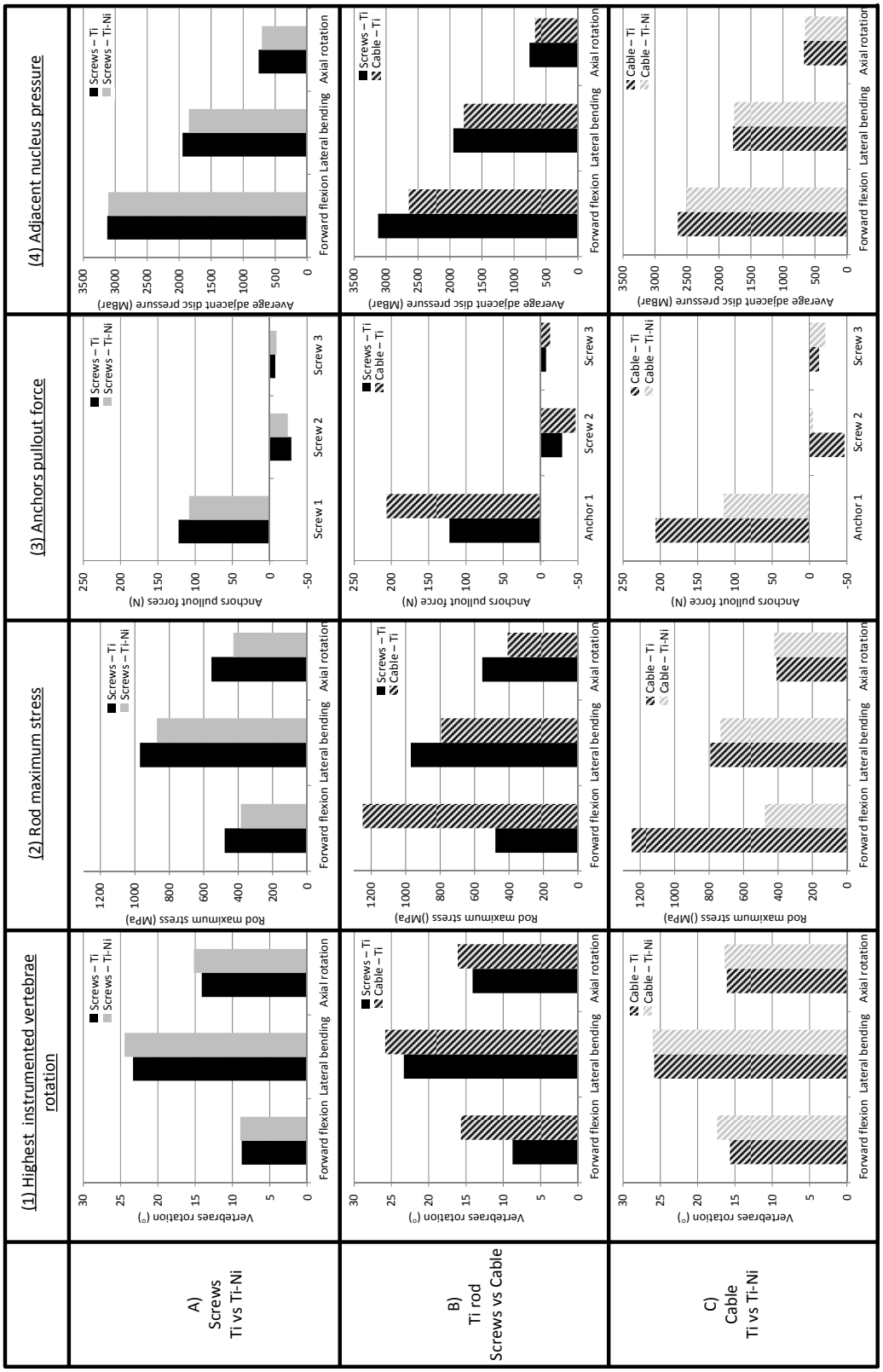

Figure-A I-2 Compilation of the results obtained with the model

Results and discussion

Figure-A I-2 presents: (1) the rotation of the top-instrumented vertebra (V3); (2) the maximum stress in the rod; (3) the anchors' pullout force and (4) the average nucleus pressure in the adjacent disc (D2). These four parameters are considered for three motions (forward flexion, lateral bending and rotation) and under three comparative configurations: A) All-screws anchoring: Ti rod vs Ti-Ni rod; B) Ti rod: all-screws vs screws-cable anchoring; and (C) Screws-cable anchoring: Ti rod vs Ti-Ni rod. Note that the pullout forces were only considered for forward flexion, as these values were very weak in lateral bending and rotation.

Case (A) All-screws anchoring: When using only pedicle screws, the impact of the Ti-Ni rod with variable stiffness compared to the homogeneous Ti rod, can be rated as being "moderate-to-weak": The variable-stiffness "softer" implant allows a slightly greater motion of the top-instrumented vertebra, especially in lateral bending (+5%) and axial rotation (+7.8%), which leads to a slightly lower (-5.2 and -6.7%) adjacent disc pressure. The lower pressure output is combined with even lower rod stresses (-10 and -22%). These moderate differences between the homogeneous and heterogeneous rods are due to the all-screws anchoring, which does not allow the top-instrumented vertebra much flexibility of movement, irrespective of the flexural stiffness of the spinal instrumentation.

Case (B) Ti rod: To offer more flexibility to the upper part of the instrumented segment, the highest screw is replaced by less rigid anchor, such as a cable, and this configuration is first tested with the homogeneous implant. It can be seen that the screw-to-cable replacement increases the motion of the top-instrumented vertebra especially in forward flexion (+78%), thus decreasing the adjacent disc pressure (-15%). These benefits are, however, obtained at the expense of extremely high stresses in all of the instrumentation components (rod, screws, cables), potentially leading to instrumentation failure.

Case (C) Screws-cable anchoring: The replacement of the constant-stiffness Ti rod by the variable-stiffness Ti-Ni rod, while keeping the screws-cable anchoring, significantly lowers the stresses and pullout forces, and also reduces the adjacent disc pressure because of the higher mobility of the top-instrumented vertebra.

Using the Ti-Ni rods and screw-cable anchoring (Case C) allows a 20% decrease in adjacent disk pressure (forward flexion), compared to the Ti rods and all-screw anchoring (Case A), without increasing stresses and pullout forces in the spinal instrumentation.

Conclusion

This paper proposes a simplified finite element analysis of an instrumented spine segment to assess the eventual biomechanical benefits of variable flexural stiffness Ti-Ni rods. It was shown that the use of a “softer” Ti-Ni rod changes the behaviors of the spine in lateral bending and rotation but not in forward flexion. It was possible to enhance the effects of such rods in all three motions by replacing the highest screw by a cable. With this anchor configuration, the heterogeneous Ti-Ni rod makes it possible to lower the adjacent disc pressure, the stress on the rod and the pullout force applied on the anchors.

To enhance the effect of the Ti-Ni rod in lateral bending and axial rotation, the cable could be replaced by a spinal hook. Further work should lead to the development of a more detailed spine model and its experimental validation. Fusion of the vertebrae should also be considered to improve the model’s accuracy. Finally, the mechanical properties gradient of the spinal rod will be optimized to provide to the spine an adequate stabilization, while decreasing the risk of adjacent disk degeneration.

Acknowledgment

The authors express their gratitude to V. Fong-Magnan for collaborating in the model development. This research was funded by the Fonds Québecois de Recherche en Nature et Technologies (FRQNT).

References

[1] Y. Kotani, B. W. Cunningham, A. Cappuccino, K. Kaneda, and P. C. McAfee, "The role of spinal instrumentation in augmenting lumbar posterolateral fusion," Spine, vol. 21, pp. 278-87, Feb. 1996.

[2] M. Lorenz, M. Zindrick, P. Schwaegler, L. Vrbos, M. A. Collatz, R. Behal, and R. Cram., "A comparison of single-level fusions with and without hardware," Spine, vol. 16, pp. S455-8, Aug. 1991.

[3] C. J. DeWald and T. Stanley, "Instrumentation-Related Complications of Multilevel Fusions for Adult Spinal Deformity Patients Over Age 65: Surgical Considerations and Treatment Options in Patients With Poor Bone Quality," Spine, vol. 31, pp. S144-S151, Sept. 2006.

[4] C. M. Bono, M. Kadaba, and A. R. Vaccaro, "Posterior Pedicle Fixation-based Dynamic Stabilization Devices for the Treatment of Degenerative Diseases of the Lumbar Spine," J. Spinal Disord. Tech., vol. 22, pp. 376-383, Jul. 2009.

[5] M. P. Kelly, J. M. Mok, and S. Berven, "Dynamic Constructs for Spinal Fusion: An Evidence-Based Review," Orthop. Clin. of N. Am., vol. 41, pp. 203-215, Apr. 2010.

[6] V. Brailovski, I. Y. Khmelevskaya, S. D. Prokoshkin, V. G. Pushin, E. P. Ryklina, and R. Z. Valiev, "Foundations of Heat and Thermomechanical Treatments and Their Effect on the Structure and Properties of Titanium Nickelide–Based Alloys," Phys. Met. Metallogr+., vol. 97, pp. S3-S55, 2004.

[7] J. R. Groh, "Local heat treatment for improved fatigue resistance in turbine components," United States Patent, 2007

[8] A. S. Mahmud, L. Yinong, and N. Tae-hyun, "Gradient anneal of functionally graded NiTi," Smart Mater. Struct., vol. 17, p. 015031 (5 pp.), Jan. 2008.

[9] Y. Facchinello, V. Brailovski, K. Inaekyan, Y. Petit, and J.-M. Mac-Thiong, "Manufacturing of monolithic superelastic rods with variable properties for spinal correction: Feasibility study," J. Mech. Behav. Biomed, vol. 22, pp. 1-11, Jun. 2013.

[10] F. El Masri, E. Sapin de Brosses, K. Rhissassi, W. Skalli, and D. Mitton, "Apparent Young's modulus of vertebral cortico-cancellous bone specimens," Comput. Method. Biomec., vol. 15, pp. 23-28, Jul. 2011.

[11] A. E. Castellvi, H. Huang, T. Vestgaarden, S. Saigal, D. H. Clabeaux, and D. Pienkowski, "Stress Reduction in Adjacent Level Discs via Dynamic Instrumentation: A Finite Element Analysis," SAS J., vol. 1, pp. 74-81, Jun. 2007.

ANNEXE II

IN-VITRO ASSESSMENT OF THE STABILIZATION CAPACITY OF MONOLITHIC SPINAL RODS WITH VARIABLE FLEXURAL STIFFNESS : METHOLOGY AND EXAMPLE

Yann Facchinello[1,2], Vladimir Brailovski[1,2], Yvan Petit[1,2],Martin Brummund[1,2],
Jaëlle Tremblay[3], Jean-Marc Mac-Thiong[2,4]
[1]Département de Génie Mécanique, École de technologie supérieure,
1100 Notre-Dame Ouest, Montréal, Québec, Canada H3C 1K3
[2]Centre de recherche, Hôpital du Sacré-Cœur de Montréal,
5400, boul. Gouin Ouest, Montreal, Québec, Canada H4J 1C5
[3]Zimmer CAS, auparavant avec Centre de recherche, Hôpital du Sacré-Cœur de Montréal
[4]Département de chirurgie, Faculté de médecine, Université de Montréal,
Pavillon Roger-Gaudry, Local : S-749, Montréal, Québec, Canada H3C 3J7

Cet article a été accepté pour présentation à la conférence :
37TH ANNUAL INTERNATIONAL CONFERENCE OF THE
IEEE Engineering in Medicine and Biology Society
MiCo - Milano Conference Center - Milan, Italy, August 25-29 2015

Résumé

Cet article de conférence décrit en détail la méthodologie expérimentale utilisée pour les essais biomécaniques. Cette méthodologie a été développée afin d'identifier les effets des tiges aux propriétés variables comparées aux tiges classiques de titane. Pour cela, les tests ont été effectués sur spécimens porcins (L1-L6). Chaque spécimen a été chargé selon trois mouvements en déplacement contrôlé : flexion, extension et inflexion latérale. Les spécimens ont été testés à l'état non instrumenté et instrumenté avec trois types de tiges : titane, superélastique et 50% rigide-50% superélastique. Ces tiges ont été fixées aux spécimens selon deux configurations soit des vis pédiculaires uniquement ou alors des vis pédiculaires

associées à deux crochets transverses à l'extrémité de l'instrumentation. Lors de ces essais, les rotations des vertèbres, les moments de flexion appliqués sur les spécimens, les forces sur les ancrages ainsi que certaines pressions intradiscales ont été mesurées. Le présent article présente la validation de la méthodologie ainsi qu'un exemple de résultats obtenus lors d'essais préliminaires.

Abstract

The concept of a monolithic Ti-Ni spinal rod with variable flexural stiffness is proposed to reduce the risks associated with spinal fusion. The variable stiffness is conferred to the rod using the Joule-heating local annealing technique. To assess the stabilization capacity of such a spinal rod, *in-vitro* experiments on porcine spine models are carried out. This paper describes the methodology followed to evaluate the effect of Ti-Ni rods and to compare their performance to that of conventional titanium rods. A validation of the methodology and the examples of results obtained are also presented.

Introduction

Spinal disorders can be treated by several means including fusion surgery. Rigid posterior instrumentations are commonly used to prevent motion of the instrumented segment and thereby to promote fusion healing [1,2]. Due to the abrupt stiffness variation between the instrumented and the intact spinal segments, stresses are increased locally, which leads to adjacent disc degeneration [3]. Dynamic stabilization systems (DSS) have been used to lower the stress concentration at the extremities of the implant and to reduce the risk of adjacent segment degeneration [4]. The efficiency of DSS is commonly evaluated by means of biomechanical experiments prior to clinical testing. Clinical studies have shown that DSS are not without their complications, such as mechanical failure of the implant or degeneration within the stabilized segment [5,6]. An ideal implant would combine static and dynamic properties with the required stiffness where a strong stabilization is needed and more flexible behaviour where dynamic properties and load-sharing capacity are important.

This complex of properties can be obtained by different methods including the use of shape memory alloys. The mechanical properties of these alloys are conditioned by their thermomechanical processing [7] and can be controlled by local annealing [8,9]. Our previous study showed that monolithic Ti-Ni rods with variable mechanical properties could be produced using localized Joule-heating heat treatment [10]. Different sections of these rods then manifest different behavior, ranging from elastoplasticity (martensitic) to superelasticity (annealed). These technological possibilities allow monolithic spinal rods to be designed with variable flexural stiffness, which can combine stabilization capacity and reduced stress concentration at the implant extremities.

To assess the stabilization capability of such rods, a simplified finite element model was developed and tested in [11]. It was found that using only pedicle screws-based fixation, the impact of the proposed rods is relatively modest, and that this impact can be amplified when the upper pedicle screw is replaced by a cable or a transverse hook to allow the extremity of the rod to flex significantly, thus improving load sharing between the instrumented and the intact spine segments.

This paper describes an original *in-vitro* testing methodology developed to comparatively assess the stabilisation capacity of spinal rods and, therefore, to validate the preliminary calculations and the detailed numerical model of an instrumented spine (under development).

Materials and methods

The biomechanical testing is conducted on a lumbar porcine spine model (L1-L6, 6-8 month, about 220 lbs). The lumbar spines segments are stored frozen at -20°C. Prior to instrumentation and testing, specimens are thawed for 24 hours at 4°C.

Specimen preparation and fixation

Upon reception of the fresh spines, soft tissues are dissected, taking care to preserve the ligaments, intervertebral discs and bone intact. On the same day, holes are drilled in L5, L4 and L3 for pedicle screws insertion using the free-hand technique, and dual rods are implanted using pedicle screws (6.5*45mm, Ti, Medtronic). The cephalad end of the construct is anchored with either two pedicle screws or two transverse process hooks (Extended body large, Ti, Medtronic). Polyester resin (Bondo, St. Paul, MN) is used to fix the end vertebrae into the testing apparatus. An aluminum bloc is used to solidly fix the caudal end of the rods. Such configuration simulates an extended segment of dual-rod instrumentation. Care is taken to keep the specimen hydrated with saline solution throughout the experiment.

Implant description

Spinal specimens are instrumented using three 5.5 mm diameter rods (Figure 1): a) titanium (Ti), b) Ti-Ni superelastic (SE), and c) Ti-Ni with variable stiffness (VAR). Titanium rods (Ti-6Al-4V, ELI) provided by Fort Wayne Metals (IN, USA) exhibit mechanical properties comparable to those of commercial titanium rods). Ti-55.94at%Ni rods supplied by Johnson Mattey (CA, USA) are used either as entirely superelastic rods or as variable-stiffness rods (VAR). The latter are half-length martensitic (Mart) - half-length superelastic (SE) produced by partial annealing of the superelastic rods [10]. The stress-strain diagrams of the different rods are shown in Figure1a, and their elastic modulus distributions, in Figure 1b. When fixed to the spine segment, the superelastic part of the VAR rods are oriented towards the non-instrumented end of the construct (Figure-A II-1c) to reduce stress concentration in the adjacent disc [11].

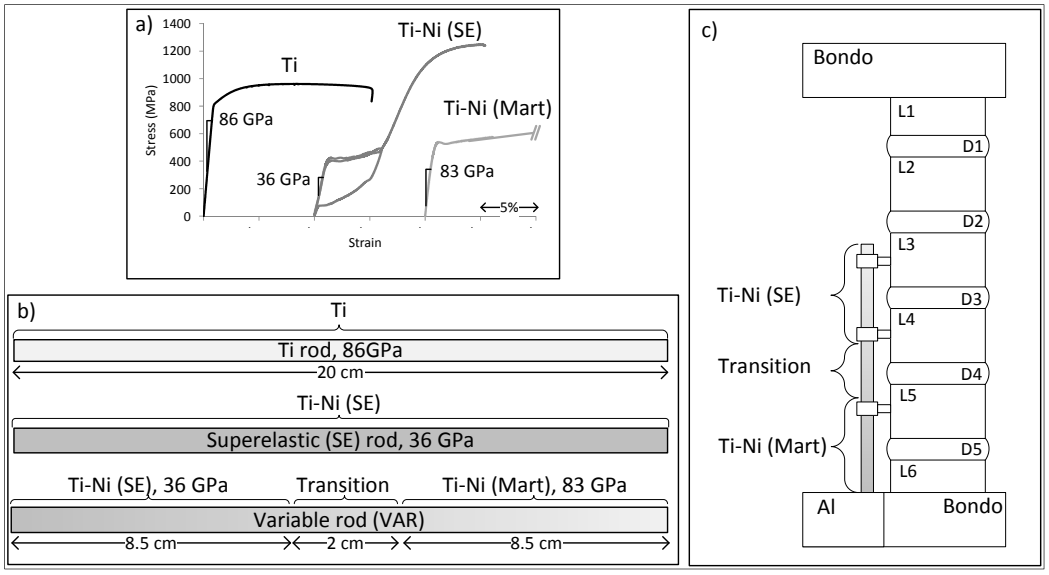

Figure-A II-1 a) Stress-strain diagrams of the different rod materials;
b) Elastic modulus distribution in the rods,
and c) Position of the the variable-stiffness rod on a spine segment

Biomechanical experiment design

An MTS 858 Minibionix II (MN, USA) is used to load the specimen in flexion, extension and lateral bending (20°, 1°/s, displacement-controlled mode). The MTS is equipped with a custom-built translation table (Figure-A II-2). Such a table allows free translation of the caudal end of the specimen, which results in the application of pure bending moment. A follower load of 400 N is applied to the specimen throughout all the tests. Axial rotation tests are not performed in this study since this motion is not considered a significant risk factor for adjacent segment disease [12]. Each specimen is tested with different instrumentations without being removed from the test bench, allowing for the testing repeatability.

Measurement

Vertebrae rotations are measured by filming rigid markers attached to the vertebral bodies using an Aramis video cameras system (GOM, Germany). ProAnalyst software (Xcitex, MA, USA) and a custom Matlab (MathWork, MA, USA) program are used to evaluate the Euler

angles following the roll, pitch and yaw convention. Rotations of the vertebrae are defined as the difference in orientation between the neutral position and the peak bending motion. Mechanical loads applied to the specimen are measured using a test system load cell (15kN, 150 N.m).

The bending moments in the four upper pedicle screws are measured by strain gages (see [13] for a detailed description). Each instrumented screw is calibrated in bending up to 2 Nm. Transverse hooks are also equipped with strain gages, but due to their geometry, only one strain gage can be attached to the upper surface of a hook, which does not allow making a distinction between bending moments and axial forces. The measured signal, however, is used in this study for relative measurement of stresses applied on the hook under different experimental conditions.

Intervertebral disc pressures are measured at the highest instrumented and adjacent levels using Gaeltec needle pressure transducers (Gaeltec Devices Ltd, Scotland) capable of measuring pressures up to 3 MPa. Care is taken to position the sensing area of the needle in the middle of the nucleus and to preserve this position during testing.

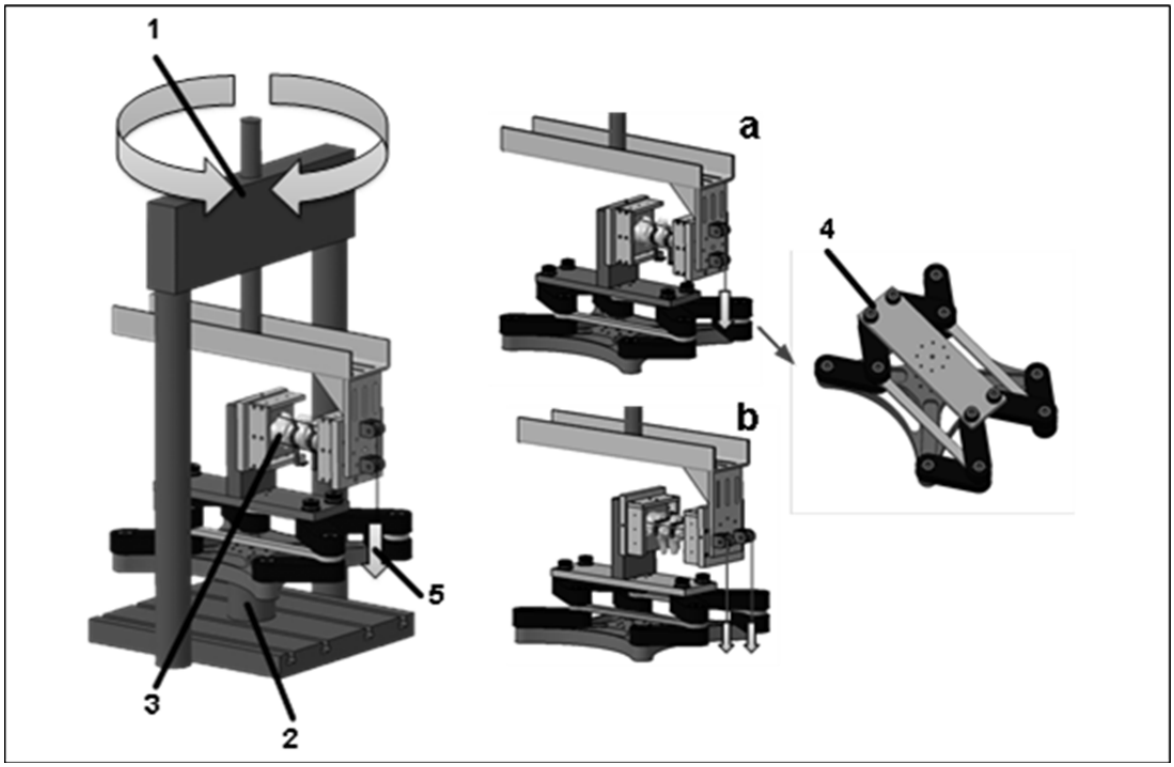

Figure-A II-2 Spinal testing apparatus used to apply loading in: a) flexion-extension and b) lateral bending. The testing apparatus is composed of: 1) MTS 858 MiniBionix II with axial and torsional actuators, 2) load cell, 3) specimen, 4) translation table, 5) follower-load application (deadweight)

Validation of the experimental procedure

To obtain stable measurements, each specimen is loaded repeatedly until two reproducible cycles are obtained. To ensure that the specimen will be in the same pretest position after the replacement of the rods, this operation is made with the follower load applied to the specimen. Additionally, rods are replaced one at a time so that the specimen is kept straight by one rod while the other one is being replaced. Furthermore, the first stabilization cycle is made without form tightening of the set screws on the anchors to allow the polyaxial head of the screws to be set into position. Figure-A II-3 shows the vertebrae angular positions during (a) stabilization cycling, and (b) rod removal, reinstallation and stabilization cycling (points 1, 2 and 3 respectively). All rotations are relative to the pretest installation position. The results indicate that a 10-cycle stabilization routine is sufficient to obtain reproducible

behaviour. Furthermore, the removal and repositioning of the same rods do not significantly affect the vertebrae positions: a maximum 0.3° rotation is observed at the end of this stabilization routine.

Example of results and discussion

As examples of the experimental data, Figure-A II-4 shows a set of results for forward flexion. It can be seen that, regardless of the anchor configuration, Ti rods confer the highest stability to the instrumented specimen (Figure-A II-4b) and cause the highest D3 intradiscal pressure (Figure-A II-4c) during forward flexion, compared to their SE and VAR counterparts. The most compliant rods, the SE type, allow the greatest vertebrae rotations with the consequent lowest D3 intradiscal pressure. The VAR rods are not distinguishable from the SE rods when used with only screw anchors, but appear to lower the D3 intradiscal pressure when used with transverse hooks at the top extremity of the construct.

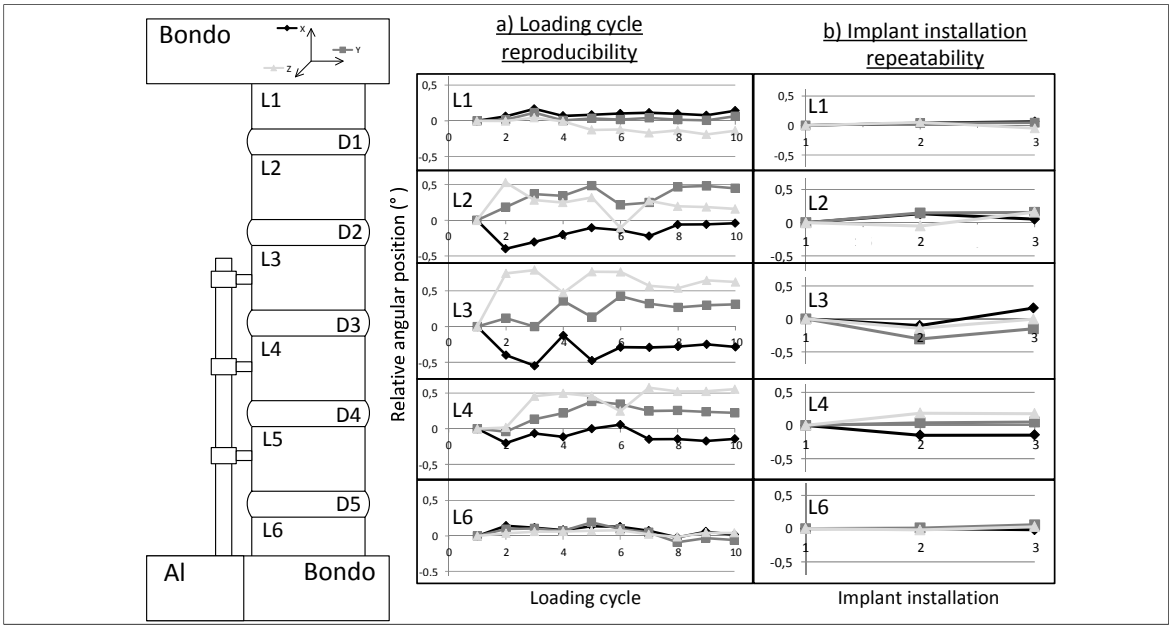

Figure-A II-3 Validation of the experimental procedure. Rotations are relative to the pretest position: a) Relative angular positions of the vertebrae during a 10-cycle stabilization procedure (30° forward flexion), and b) Relative angular positions of the vertebrae after the rod removal (1), reinstallation (2) and a 10-cycle stabilization routine (3)

As predicted by the simulations, the replacement of upper pedicle screws by transverse hooks facilitates the rod flexion, but leads to higher D3 intradiscal pressure. The rod stiffness variability (SE towards VAR towards Ti) appears to be significant enough to modify the spine behaviour and intradiscal pressure, with the effect being more pronounced in the case of hook anchors. It can be observed for the VAR rods that the specimen stability in the higher-stiffness zone is close to that for the Ti rods. On the other hand, the combination of a lower stiffness zone with transverse hook anchoring near the top extremity of the construct allow for better motion distribution. Finally, compared to the stiffest Ti rods, the use of compliant rods (SE and VAR) decreases the stress on the hook anchors, but increases the stress on the end-screw anchors. These properties mean that a combination of variable-stiffness rods with high-mobility anchors may prevent fracture in the last instrumented vertebrae, while simultaneously ensuring the stability required for the instrumented spine.

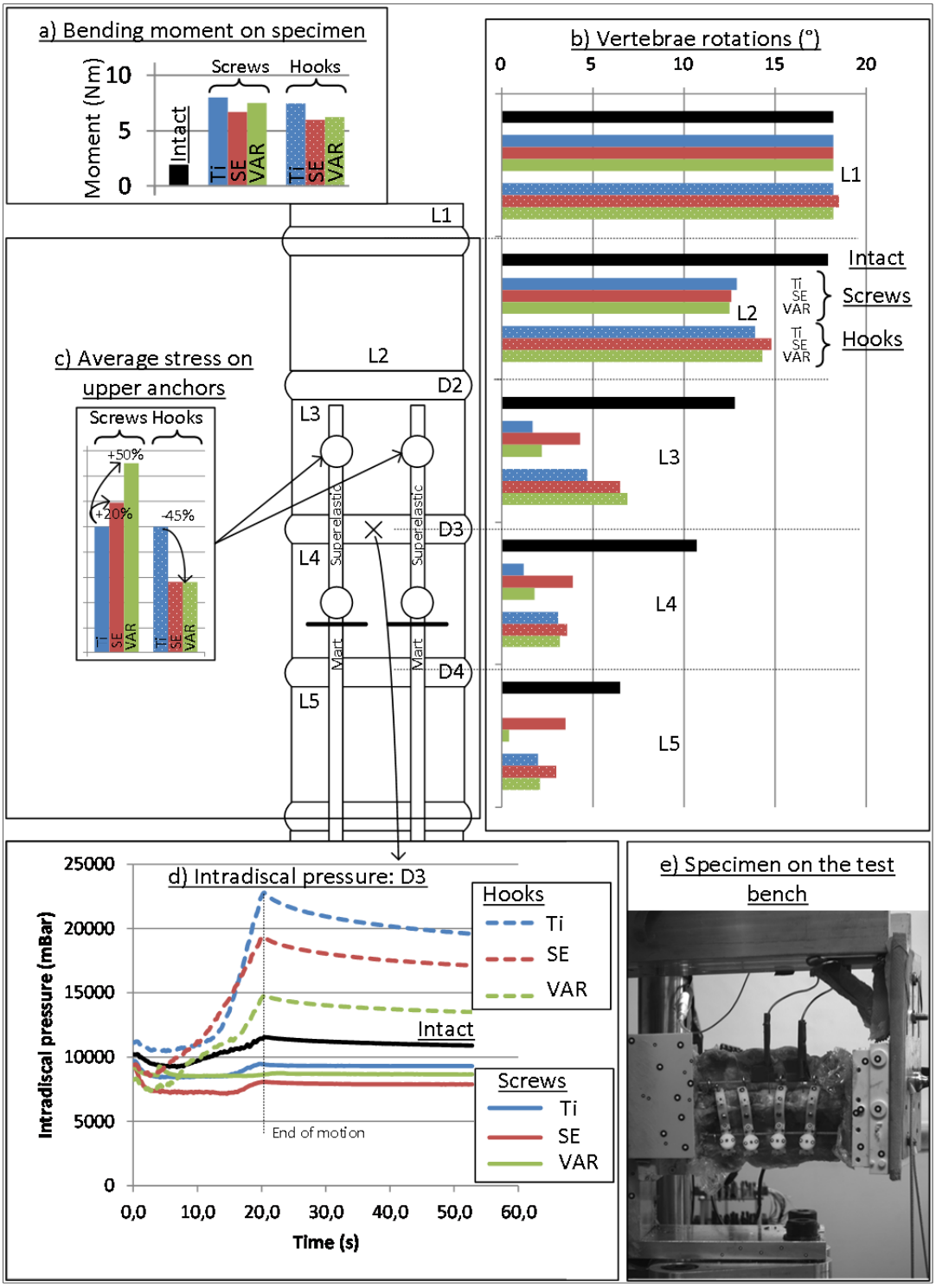

Figure-A II-4 Set of results obtained for forward flexion, 20°.
a) Bending moment on the specimen, b) Vertebrae rotation,
c) Stress on upper anchors relative to what was obtained with the titanium rod,
d) Intradiscal pressure and e) Picture of a specimen installed in the testing apparatus

Conclusion

This paper proposes an experimental methodology for *in-vitro* evaluation of the eventual benefits of monolithic spinal Ti-Ni rods with variable flexural stiffness. By measuring the vertebrae rotations, the moments applied to the specimens, the stresses on the anchors and the intradiscal pressures, this methodology is able to detect the effect of the spinal rods' properties on the instrumented spine mobility and stresses. Based on the results presented in this paper, variable-stiffness rods appear to have a positive impact on the studied parameters. Further work will include other motions such as extension and lateral bending, as well as the testing of a series of instrumented and non-instrumented specimens, to better assess the statistical significance of our findings.

Acknowledgment

The authors express their gratitude to M. Drouin and S. Plamondon for their collaboration in the pedicle screws instrumentation.

References

[1] Y. Kotani, B. W. Cunningham, A. Cappuccino, K. Kaneda, and P. C. McAfee, "The role of spinal instrumentation in augmenting lumbar posterolateral fusion," Spine, vol. 21, pp. 278-87, Feb 1996.

[2] M. Lorenz, M. Zindrick, P. Schwaegler, L. Vrbos, M. A. Collatz, R. Behal, et al., "A comparison of single-level fusions with and without hardware," Spine, vol. 16, pp. S455-8, Aug 1991.

[3] C. J. DeWald and T. Stanley, "Instrumentation-Related Complications of Multilevel Fusions for Adult Spinal Deformity Patients Over Age 65: Surgical Considerations and Treatment Options in Patients With Poor Bone Quality," Spine, vol. 31, pp. S144-S151

[4] C. M. Bono, M. Kadaba, and A. R. Vaccaro, "Posterior Pedicle Fixation-based Dynamic Stabilization Devices for the Treatment of Degenerative Diseases of the Lumbar Spine," J Spinal. Disord. Tech., vol. 22, pp. 376-383, 2009.

[5] C. Y. Barrey, R. K. Ponnappan, J. Song, and A. R. Vaccaro, "Biomechanical Evaluation of Pedicle Screw-Based Dynamic Stabilization Devices for the Lumbar Spine: A Systematic Review," SAS Journal, vol. 2, pp. 159-170, 2008.

[6] M. P. Kelly, J. M. Mok, and S. Berven, "Dynamic Constructs for Spinal Fusion: An Evidence-Based Review," Orthop. Clin. N. Am., vol. 41, pp. 203-215, 2010.

[7] V. Brailovski, I. Y. Khmelevskaya, S. D. Prokoshkin, V. G. Pushin, E. P. Ryklina, and V. R. Z., "Foundations of Heat and Thermomechanical Treatments and Their Effect on the Structure and Properties of Titanium Nickelide–Based Alloys," Phys Met Metallogr+, vol. 97, pp. S3-S55, 2004.

[8] J. R. Groh, "Local heat treatment for improved fatigue resistance in turbine components," U.S. Patent 20100043924, 2007.

[9] A. S. Mahmud, L. Yinong, and N. Tae-hyun, "Gradient anneal of functionally graded NiTi," Smart. Mater. Struct., vol. 17, p. 015031, 2008.

[10] Y. Facchinello, V. Brailovski, K. Inaekyan, Y. Petit, and J.-M. Mac-Thiong, "Manufacturing of monolithic superelastic rods with variable properties for spinal correction: Feasibility study," J. Mech. Behav. Biomed., vol. 22, pp. 1-11, 2013.

[11] Y. Facchinello, V. Brailovski, Y. Petit, and J. M. Mac-Thiong, "Monolithic superelastic rods with variable flexural stiffness for spinal fusion: Simplified finite element analysis of an instrumented spine segment," in Conf. Proc. IEEE Eng. Med. Biol. Soc., Chicago, 2014 pp. 6605-8.

[12] D. P. Thawrani, D. L. Glos, M. T. Coombs, D. I. Bylski-Austrow, and P. F. Sturm, "Transverse Process Hooks at Upper Instrumented Vertebra Provide More Gradual Motion Transition than Pedicle Screws," Spine, 2014.

[13] A. L. Freeman, M. S. Fahim, and J. E. Bechtold, "Validation of an improved method to calculate the orientation and magnitude of pedicle screw bending moments," J. Biomech. Eng., vol. 134, pp. 104502

LISTE DE RÉFÉRENCES BIBLIOGRAPHIQUES

Alphatec Spine. 2015. *Alphatec Spine*. En ligne. < http://www.alphatecspine.com/products/thoracolumbar/isobar.asp > Consulté le 12 mai 2015.

AO Foundation. 2015. *AO Foundation*. En ligne. < https://www2.aofoundation.org/ > Consulté le 28 mai 2015.

Bellouard, Y., T. Lehnert, J. E. Bidaux, T. Sidler, R. Clavel et R. Gotthardt. 1999. « Local annealing of complex mechanical devices: a new approach for developing monolithic micro-devices ». In *ICOMAT 98. International Conference on Martensitic Transformations, 7-11 Dec. 1998*. (Switzerland) Vol. A273-275, p. 795-8. Coll. « Mater. Sci. Eng. A, Struct. Mater., Prop. Microstruct. Process. (Switzerland) »: Elsevier.

Bono, Christopher M., et Casey K. Lee. 2004. « Critical Analysis of Trends in Fusion for Degenerative Disc Disease Over the Past 20 Years: Influence of Technique on Fusion Rate and Clinical Outcome ». *Spine,* vol. 29, n^{o} 4, p. 455-463.

Bothmann, M., E. Kast, G. J. Boldt et J. Oberle. 2008. « Dynesys fixation for lumbar spine degeneration ». *Neurosurg Rev,* vol. 31, n^{o} 2, p. 189-96.

Brailovski, V., S. Prokoshkin, P. Terriault et F. Trochu. 2003. *Shape Memory Alloys: Fundamentals, Modeling and Applications*. Ecole de Technologie Superieure.

Cahill, P. J., W. Wang, J. Asghar, R. Booker, R. R. Betz, C. Ramsey et G. Baran. 2012. « The use of a transition rod may prevent proximal junctional kyphosis in the thoracic spine after scoliosis surgery: a finite element analysis ». *Spine (Phila Pa 1976),* vol. 37, n^{o} 12, p. E687-95.

Castellvi, Antonio E., H. Hao, D. Pienkowski, S. Saigal et S. Clabeaux. 2004. « Dynamic Semi-rigidity and Prevention of Adjacent Disc Degeneration in the Lumbar Spine ». In *International ARGOS Meeting*. (Paris).

Castellvi, Antonio E., Hao Huang, Tov Vestgaarden, Sunil Saigal, Deborah H. Clabeaux et David Pienkowski. 2007. « Stress Reduction in Adjacent Level Discs via Dynamic Instrumentation: A Finite Element Analysis ». *SAS Journal,* vol. 1, n^{o} 2, p. 74-81.

Cheh, Gene, Keith H. Bridwell, Lawrence G. Lenke, Jacob M. Buchowski, Michael D. Daubs, Yongjung Kim et Christy Baldus. 2007. « Adjacent Segment Disease FollowingLumbar/Thoracolumbar Fusion With Pedicle Screw Instrumentation: A Minimum 5-Year Follow-up ». *Spine,* vol. 32, n^{o} 20, p. 2253-2257.

Chiu, Yen-Chun, Shih-Chieh Yang, Shang-Won Yu et Yuan-Kun Tu. 2011. « Pedicle screw breakage in a vertebral body: A rare complication in a dynamic stabilization device ». *Formosan Journal of Musculoskeletal Disorders,* vol. 2, n° 4, p. 143-146.

Chou, Wen-Ying, Chien-Jen Hsu, Wei-Ning Chang et Chi-Yin Wong. 2002. « Adjacent segment degeneration after lumbar spinal posterolateral fusion with instrumentation in elderly patients ». *Arch Orthop Trauma Surg,* vol. 122, n° 1, p. 39-43.

Dekutoski, M. B., M. J. Schendel, J. W. Ogilvie, J. M. Olsewski, L. J. Wallace et J. L. Lewis. 1994. « Comparison of in vivo and in vitro adjacent segment motion after lumbar fusion ». *Spine (Phila Pa 1976),* vol. 19, n° 15, p. 1745-51.

Drexel, Masao J., Guna S. Selvaduray et Alan R. Peltan. 2008. « The effects of cold work and heat treatment on the properties of nitinol wire ». In *International Conference on Shape Memory and Superelastic Technologies, SMST-2006, May 7, 2006 - May 11, 2006*. (Pacific Grove, CA, United states), p. 447-454. Coll. « SMST-2006 - Proceedings of the International Conference on Shape Memory and Superelastic Technologies »: ASM International.

Freeman, A. L., M. S. Fahim et J. E. Bechtold. 2012. « Validation of an improved method to calculate the orientation and magnitude of pedicle screw bending moments ». *J Biomech Eng,* vol. 134, n° 10, p. 104502-104502.

Ghiselli, G., J. C. Wang, N. N. Bhatia, W. K. Hsu et E. G. Dawson. 2004. « Adjacent segment degeneration in the lumbar spine ». *J Bone Joint Surg Am,* vol. 86-A, n° 7, p. 1497-503.

Gibson, J. N., et G. Waddell. 2005. « Surgery for degenerative lumbar spondylosis ». *Cochrane Database Syst Rev,* vol. CD001352.

Gillet, P. 2003. « The fate of the adjacent motion segments after lumbar fusion ». *J Spinal Disord Tech,* vol. 16, n° 4, p. 338-45.

Gornet, M. F., F. W. Chan, J. C. Coleman, B. Murrell, R. P. Nockels, B. A. Taylor, T. H. Lanman et J. A. Ochoa. 2011a. « Biomechanical assessment of a PEEK rod system for semi-rigid fixation of lumbar fusion constructs ». *J Biomech Eng,* vol. 133, n° 8, p. 081009.

Gornet, Matthew F., Frank W. Chan, John C. Coleman, Brian Murrell, Russ P. Nockels, Brett A. Taylor, Todd H. Lanman et Jorge A. Ochoa. 2011b. « Biomechanical Assessment of a PEEK Rod System for Semi-Rigid Fixation of Lumbar Fusion Constructs ». *Journal of Biomechanical Engineering,* vol. 133, n° 8, p. 081009-081009.

Hassanzadeh, Hamid, Sachin Gupta, Amit Jain, Mostafa H. El Dafrawy, Richard L. Skolasky et Khaled M. Kebaish. 2013. « Type of Anchor at the Proximal Fusion Level Has a Significant Effect on the Incidence of Proximal Junctional Kyphosis and Outcome in Adults After Long Posterior Spinal Fusion ». *Spine Deformity,* vol. 1, n° 4, p. 299-305.

Helgeson, M. D., S. A. Shah, P. O. Newton, D. H. Clements, 3rd, R. R. Betz, M. C. Marks et T. Bastrom. 2010. « Evaluation of proximal junctional kyphosis in adolescent idiopathic scoliosis following pedicle screw, hook, or hybrid instrumentation ». *Spine (Phila Pa 1976),* vol. 35, n° 2, p. 177-81.

Highsmith, J. M., L. M. Tumialan et G. E. Rodts, Jr. 2007. « Flexible rods and the case for dynamic stabilization ». *Neurosurg Focus,* vol. 22, n° 1, p. E11.

Hongo, Michio, Ralph E. Gay, Kristin D. Zhao, Brice Ilharreborde, Paul M. Huddleston, Lawrence J. Berglund, Kai-Nan An et Chunfeng Zhao. 2009. « Junction kinematics between proximal mobile and distal fused lumbar segments: biomechanical analysis of pedicle and hook constructs ». *The Spine Journal,* vol. 9, n° 10, p. 846-853.

Hudson, William R. S., John Eric Gee, James B. Billys et Antonio E. Castellvi. 2011. « Hybrid dynamic stabilization with posterior spinal fusion in the lumbar spine ». *SAS Journal,* vol. 5, n° 2, p. 36-43.

Kelly, Michael P., James M. Mok et Sigurd Berven. 2010. « Dynamic Constructs for Spinal Fusion: An Evidence-Based Review ». *Orthopedic Clinics of North America,* vol. 41, n° 2, p. 203-215.

Ko, C. C., H. W. Tsai, W. C. Huang, J. C. Wu, Y. C. Chen, Y. H. Shih, H. C. Chen, C. L. Wu et H. Cheng. 2010. « Screw loosening in the Dynesys stabilization system: radiographic evidence and effect on outcomes ». *Neurosurg Focus,* vol. 28, n° 6, p. E10.

Lee, M. J., J. D. Lindsey et R. J. Bransford. 2010. « Pedicle screw-based posterior dynamic stabilization in the lumbar spine ». *J Am Acad Orthop Surg,* vol. 18, n° 10, p. 581-8.

Li, Zhonghai, Fengning Li, Shunzhi Yu, Hui Ma, Zhaohui Chen, Hailong Zhang et Qiang Fu. 2013. « Two-year follow-up results of the Isobar TTL Semi-Rigid Rod System for the treatment of lumbar degenerative disease ». *Journal of Clinical Neuroscience,* vol. 20, n° 3, p. 394-399.

Lyerly Neurosurgery.[s.d.]. *Lyerly Neurosurgery*. En ligne.
< http://www.lyerlyneuro.com/spinal-fusion.html >
Consulté le 26 mai 2015.

Mahmud, A. S., Liu Yinong et Nam Tae-hyun. 2008. « Gradient anneal of functionally graded NiTi ». *Smart Materials and Structures,* vol. 17, n° 1, p. 015031 (5 pp.).

Maserati, M. B., M. J. Tormenti, D. M. Panczykowski, C. M. Bonfield et P. C. Gerszten. 2010. « The use of a hybrid dynamic stabilization and fusion system in the lumbar spine: preliminary experience ». *Neurosurg Focus,* vol. 28, n° 6, p. E2.

ORlive. 2007. *ORlive*. En ligne.
< http://www.or-live.com/medtronicspinal/1856/ >
Consulté le 15 mai 2013.

Nockels, R. P. 2005. « Dynamic stabilization in the surgical management of painful lumbar spinal disorders ». *Spine (Phila Pa 1976),* vol. 30, n° 16 Suppl, p. S68-72.

Ormond, D. R., L. Albert, Jr. et K. Das. 2012. « Polyetheretherketone (PEEK) Rods in Lumbar Spine Degenerative Disease: A Case Series ». *J Spinal Disord Tech*.

Medtronic. 2010. *Medtronic*. En ligne.
< https://www.medtronic.com/patients/scoliosis/device/our-spinal-system/ >
Consulté le 12 mai 2013.

Panjabi, Manohar M. 2007. « Hybrid multidirectional test method to evaluate spinal adjacent-level effects ». *Clinical Biomechanics,* vol. 22, n° 3, p. 257-265.

Schaeren, S., I. Broger et B. Jeanneret. 2008. « Minimum four-year follow-up of spinal stenosis with degenerative spondylolisthesis treated with decompression and dynamic stabilization ». *Spine (Phila Pa 1976),* vol. 33, n° 18, p. E636-42.

Schwarzenbach, O., N. Rohrbach et U. Berlemann. 2010. « Segment-by-segment stabilization for degenerative disc disease: a hybrid technique ». *Eur Spine J,* vol. 19, n° 6, p. 1010-20.

Scient'X. 2010. « Degenerative module with top-loading inner set screw : Surgical technique guide ». En ligne. 32 p. http://implantesclp.com/uploads/pdf/ISOBAR_TTL_IN.pdf. Consulté le 26 mai 2015.

Thawrani, Dinesh P, David L Glos, Matthew T Coombs, Donita I Bylski-Austrow et Peter F Sturm. 2014. « Transverse Process Hooks at Upper Instrumented Vertebra Provide More Gradual Motion Transition than Pedicle Screws ». *Spine (Phila Pa 1976),* vol. 39, n° 14, p. E826-832.

Van Laar, Wilbert, Rinse J. Meester, Theo H. Smit et Barend J. van Royen. 2007. « A biomechanical analysis of the self-retaining pedicle hook device in posterior spinal fixation ». *European Spine Journal,* vol. 16, n° 8, p. 1209-1214.

Wu, J. C., W. C. Huang, H. W. Tsai, C. C. Ko, C. L. Wu, T. H. Tu et H. Cheng. 2011. « Pedicle screw loosening in dynamic stabilization: incidence, risk, and outcome in 126 patients ». *Neurosurg Focus,* vol. 31, n^{o} 4, p. E9.

Wurgler-Hauri, C. C., A. Kalbarczyk, M. Wiesli, H. Landolt et J. Fandino. 2008. « Dynamic neutralization of the lumbar spine after microsurgical decompression in acquired lumbar spinal stenosis and segmental instability ». *Spine (Phila Pa 1976),* vol. 33, n^{o} 3, p. E66-72.

Zimmer. 2015. *Zimmer*. En ligne. < http://www.zimmer.com/medical-professionals/products/spine/dynesys-dynamic-stabilization-system.html > Consulté le 28 mai 2015.